MODULE FOR SIMULATING COMPOSITION EFFECTS ON SECONDARY

ORGANIC AEROSOL PARTITIONING AND ITS EVALUATION IN THE

SOUTHEASTERN UNITED STATES

By

Xinlian Chang

Dissertation

Submitted to the Faculty of the

Graduate School of Vanderbilt University

in partial fulfillment of the requirements

for the degree of

DOCTOR OF PHILOSOPHY

In

Environmental Engineering

December, 2006

Nashville, Tennessee

Approved:

Professor James H. Clarke

Professor Frank M. Bowman

Professor Karl B. Schnelle, Jr.

Professor D. Greg Walker

Professor Alan R. Bowers

To my parents, especially to my mother, for always loving and encouraging me

Lanxiu Ran and Delong Chang

To my sisters and brothers for the many years of understanding and support

Shuilian, Cuilian, Xinling and Lijun Chang

To my lovely son, the most beautiful part of my life

Evan Du

And most importantly to my beloved husband, without your support I would have never

done this

Yuqi Du

ACKNOWLEDGMENTS

TABLE OF CONTENTS

vi

APPENDIX

LIST OF TABLES

LIST OF FIGURES

xi

GLOSSARY OF TERMS

ALK5   long alkanes

AORGA   anthropogenic SOA

AORGB   biogenic SOA

ARO1   high-yield aromatics like toluene

ARO2   low-yield aromatics like xylene

BC   boundary condition

BCON   boundary conditions processor within CMAQ

BHM   North Birmingham, AL

CACM   Caltech atmospheric chemistry mechanism

CB4   chemical mechanism with organic representation based on carbon

                bond type

CCTM   the chemical-transport model processor within CMAQ

CF   Cornelia Fort, Nashville, TN

CMAQ   community multi-scale air quality modeling system

CRES   aromatics like cresol

CTR   Centreville, AL

DI   Dickson, TN

$EC_{2.5}$ elemental carbon in $PM_{2.5}$

EPA   Environmental Protection Agency

EURAD/MADE   the comprehensive European Air Pollution and Dispersion/Modal

                Aerosol Dynamics Model for Europe

G/P	gas/particle
GRSM	Great Smoky Mountains National Park, TN
HC	hydrocarbons
HEN	Hendersonville, TN
IC	initial condition
ICON	initial conditions processor within CMAQ
IMPROVE	the Interagency Monitoring of Protected Visual Environments
ISORROPIA	thermodynamic equilibrium model for multiphase multicomponent inorganic aerosols
JST	Jefferson Street, Atlanta, GA
LAVO	Lassen Volcanic National Park
LWC	liquid water content
MACA	Mammoth Cave Nation Park, KY
MB	mean bias
MCIP	meteorology-chemistry interface processor within CMAQ
ME	mean error
MFB	mean fractional bias
MFE	mean fractional error
MM5	Pennsylvania State University (PSU) /NCAR Mesoscale Modeling System Geration 5
MNB	mean normalized bias
MNE	mean normalized error
MW	molecular weight

NEI99	national emission inventory for 1999
NMB	normalized mean bias
NME	normalized mean error
NMVOC	non-methane volatile organic compounds
OA	organic aerosol
$OC_{2.5}$	organic carbon in $PM_{2.5}$
OC_{pri}	primary organic carbon
OC_{sec}	secondary organic carbon
OLE2	internal alkenes
PINN	Pinnacles National Monument
PM	particulate matter
$PM_{2.5}$	particles with an aerodynamic diameter of less than 2.5 microns
PMCAM	Particulate Matter modeling within Comprehensive Air-quality Model with Extensions (CAMx)
POA	primary organic aerosol
PORE	Point Reyes National Seashore
RADM2	the second generation regional acid deposition model chemical mechanism
REDW	Redwood National Park
RH	relative humidity
SAGO	San Gorgonio Wildness
SAPRC99	Statewide Air Pollution Research Center chemical mechanisms
SEARCH	the Southeastern Aerosol Research and Characterization project

SEQU	Sequoia National Park
SHRO	Shining Rock Wildness Area, TN
SIPS	Sipsey Wildness Area, AL
SMOKE	the Sparse Matrix Operator Kernel Emissions modeling system
SOA	secondary organic aerosol
SOC	semivolatile organic compounds
SOS99	1999 Southern Oxidants Study
SQT	sesquiterpenes
TC	total carbon
TOR	thermal-optical reflectance method
TOT	thermal-optical transmittance method
TRP1	biogenic SOA precursors like monoterpenes
TSP	total suspended particulate
UNIFAC	Universal quasichemical Functional group Activity Coefficients
VOC	volatile organic compound
YOSE	Yosemite National Park
YRK	Yorkville, GA
ZSR	Zdanovskii, Stokes and Robinson method

CHAPTER I

INTRODUCTION

1. Perspective

Atmospheric aerosol refers to the solid or liquid particles suspended in the air with a size range from about 0.002 to more than 100 μm (Hinds, 1999). The aerosols directly emitted into the atmosphere from the source are named primary aerosols while those formed through a series of reactions in the atmosphere are called secondary. Secondary aerosols can further be classified as secondary inorganic aerosol and secondary organic aerosol (SOA) based on their chemical composition. Recently secondary organic aerosol (SOA) attracts much attention of the researchers because it comprises approximately 50% of the total aerosol carbonaceous material (Saxena and Hildemann, 1996; Turpin et al, 1991; Lim et al., 2002; Cabada et al., 2002), presents a hazard to people's health (Pope et al, 1995; Donaldson et al., 1998), has profound effect on global climate (Seinfeld and Pandis, 1998; Hinds, 1999 and references therein; Penner et al., 1998; Chung and Seinfeld, 2002) and occasionally damages the local visibility (Seinfeld and Pandis, 1998).

However, accurate simulation of SOA presents a big challenge due to the large number of species presented, the structural complexity of the compounds, gaps in our knowledge about its formation mechanism, and limited experimental data necessary for validating theoretical predictions. Evaluation work carried out on state of the art air quality models, for example, the Community Multi-scale Air Quality system (CMAQ)

developed by EPA (Byun and Ching, 1999), indicates that currently large deviations exist between predicted concentrations of aerosol organic carbon (OC), including primary OC and secondary OC, and field measurements (Morris et al., 2005; Eder and Yu, 2006). Much work, therefore, is underway in many research groups in order to find an appropriate way to represent SOA production in air quality models (Kamens et al., 1999; Kamens and Jaoui, 2001; Pankow et al., 2001; Seinfeld et al., 2001; Griffin et al., 2002a, b, 2003; Pun et al., 2002; Jang et al., 2005).

Generally speaking, empirical parameters from smog chamber experiments are still extensively used to represent the SOA production process in large-scale air quality models, which is a valuable tool to study the formation, transport, and fate of air pollutants at urban or regional scales (Russell and Dennis, 2000 and references therein). However, the empirical parameters obtained under the specific experimental condition may not be sufficient to represent the SOA partitioning characteristics in reality, which is affected by the amount of precursors available, the temperature, the aerosol phase composition, the vapor pressures of individual aerosol components.

Current progress in SOA composition identification makes it feasible to investigate the composition effects on SOA production. Research work by Bowman and Karamalegos (2002) indicates that the aerosol composition may have an effect in magnitude comparable to diurnal temperature variations and semivolatile precursor emission rate fluctuations. However, that work used a single-cell model representing a highly simplified scenario not real atmospheric application, and needs to be extended to get more realistic evaluation on composition effects. Furthermore, the lumping method developed by Bian and Bowman (2002 & 2005) has been shown to approximate the

2

detailed aerosol mixture quite well by using 2 to 3 lumped groups whose parameters are derived from those of the individual components. With the identified SOA components and appropriate method to represent them in large scale air quality models, the composition effects on SOA production can, and should, be studied and quantified and accounted for in SOA simulation, which gives a more realistic description of the SOA production process in real atmosphere. The research described in this dissertation is aiming to meet this need.

2. Research Significance

Accurate simulation of atmospheric organic aerosol presents many challenges. The composition effects on SOA production, as investigated in this study, have long been recognized. However, due to the complexity in representing the aerosol phase composition and the incompleteness of SOA composition information, no systematic study on composition effects has been conducted so far. The composition effects implemented in other studies, for example, the model described in Pun et al (2002), only use one or several specific SOA products as surrogates to demonstrate the composition effects on SOA production. The direct and apparent shortcoming of this approach is that the effects of all other SOA components on the SOA predictions are not accounted for. In other words, the composition effects on SOA production are not completely represented and selection of surrogate compounds presents a significant source of uncertainty. In this study, the lumped groups applied to represent the real aerosol mixture are "averaged" species that can account for all identified SOA components. Although they can not be

identified as any real compounds, it is expected their partitioning behavior can better represent what happens in the real aerosol mixture.

Incorporation of the composition dependent partitioning into air quality models is one step towards more accurate description of SOA formation in real atmosphere. The newly developed aerosol module can reveal the interactions between aerosol components and quantify the composition effects on SOA production. Evaluation of composition effects on SOA production helps identify reasons underlying the discrepancies between simulations and measurements. The target of this research is to set up a framework to represent SOA in air quality models, from which to develop more comprehensive models for SOA prediction with higher accuracy as our understanding of SOA advances, when more experimental data becomes available and model parameters can be determined with less uncertainty.

3. Research Objectives

This research aims to get a better understanding of the SOA production process, particularly the effects of aerosol composition on SOA predictions. Three general research objectives with several sub-objectives were identified as follows,

- Formulation of new SOA representation with the capability to account for the effects of aerosol-phase chemical structures on SOA partitioning.
    - o Product survey for individual SOA precursors.
    - o Formulation of product representation for atmospheric air quality modeling with partitioning parameters reflecting detailed experimental information about the individual SOA products.

o Evaluation and validation of the new SOA representation with both experimental and atmospheric systems.

- Quantification and evaluation of composition effects on SOA production.

    o Development of new organic aerosol module with incorporation of necessary information such as chemical structure of the model species to account for the composition dependent partitioning of SOA.

    o Application of the new organic aerosol module to study and quantify the composition effects on SOA production in Southeastern United States with different POA representation.

    o Identification of the reasons underlying the discrepancy in simulation results.

- Preliminary study of uncertainties in model predictions of SOA.

    o Effects of model parameters with large uncertainties such as vaporization enthalpy of the SOA components.

    o Effects of different lumped groups formulated by different lumped criteria.

    o Effects of organics-related water.

4. Organization of the Dissertation

The dissertation is organized as follows. Chapter II describes in detail the theoretical background and significance of this research. Chapter III includes the detailed product representation and development of the lumped groups, performance comparison of the modified and original SOA products in CMAQ under ideal behavior, interpretation and analysis of the simulation results as well as the reasons underlying the differences. Chapter IV presents the development of the new aerosol module, which incorporates

product structure information as well as its subsequent effects on SOA production, conducts the accuracy evaluation of the new aerosol module, and quantifies the composition effects on SOA production with different POA representation. Chapter V describes simulations to evaluate the uncertainties in simulation results, investigating the effects of different temperature dependence of the lumped groups, organics-related water and its feedback effects on SOA production, and different lumping criteria applied to formulate the lumped groups. Chapter VI summarizes the main results of these studies, presents overall conclusions, and addresses future areas of research.

CHAPTER II

BACKGROUND AND THEORY

1. Secondary Organic Aerosol (SOA)

1.1 Definitions

Atmospheric aerosol refers to the solid or liquid particles suspended in the air with a size range from about 0.002 to more than 100 μm (Hinds, 1999). Based on its origin, the atmospheric aerosol can be classified into primary or secondary. Primary particulate matter (PM) is directly emitted into, and secondary PM is formed through a series of reactions in, the atmosphere. The main sources of primary PM are soil dust, sea salt, botanical debris, volcanic dust and forest fires (Hinds, 1999). Secondary PM comes from gas-to-particle conversion process such as sulfate from SO_2, nitrate from NO_x, and ammonium salt from NH_3, as well as photochemical reactions of anthropogenic or biogenic volatile organic compounds (VOCs) (Seinfeld and Pandis, 1998). The particulate matter formed from photochemical reactions of VOCs with photochemical oxidants such as hydroxyl radicals (OH), ozone (O_3) and nitrate radicals (NO_3) is usually referred to as secondary organic aerosol (SOA).

The majority of primary PM is usually large particles and can not travel long distance; the secondary particles, however, are much smaller and can remain suspended in the air for a long time, even long enough to travel global distance (Hinds, 1999), which implies that the secondary PM has more significant effects on our living environment.

Such fine particles as $PM_{2.5}$ (particles with an aerodynamic diameter of less than 2.5 microns) are easily respirable and have been reported to relate to a number of human health problems such as cardiopulmonary mortality and lung cancer (Pope et al., 1995; Donaldson et al., 1998). Visibility degradation is caused by light scattering or absorption by particles or gases in the air, especially the fine particles (Seinfeld and Pandis, 1998). The tropospheric aerosol can also affect climate by direct and indirect scattering as a result of an increase in cloud reflectivity due to the increase of the concentration of tropospheric condensation nuclei that results in a higher number concentration of cloud droplet (Hinds, 1999).

1.2 Biogenic and anthropogenic sources

The ability of naturally emitted hydrocarbons (HCs) to produce secondary organic aerosol has long been recognized (Went, 1960) but only recently has intensive research been carried out on their potential ability to produce SOA. On a global scale, the contribution from natural sources greatly exceeds that from anthropogenic sources. However, the anthropogenic sources, smaller in amount but concentrated in a smaller area, contribute more than natural sources in the urban area (Hinds, 1999).

The majority of the reactive organic compounds released from the terrestrial vegetation are isoprene (C_5H_8), monoterpenes ($C_{10}H_{16}$), and sesquiterpenes ($C_{15}H_{24}$) (Arey et al., 1991a; König et al., 1995; Puxbaum and König, 1997). The total annual global emission of biogenic hydrocarbons has been estimated between 825 and 1150 Tg-C/yr (Fehsenfeld et al., 1992; Guenther et al. 1995), whereas anthropogenic hydrocarbons have been estimated less than 100 Tg-C/yr (Müller, 1992; Hough and Johnson, 1991).

The natural emission of non-methane volatile organic compounds (NMVOC) in North America was estimated to be 83.9 Tg-C/yr with 29.3 Tg-C/yr of isoprene and 17.9 Tg-C/yr of monoterpenes (Guenther et al., 2000).

Biogenic hydrocarbons larger than isoprene have been proved to be effective sources of aerosol (Pandis et al., 1991; Zhang et al., 1992; Odum et al., 1996; Hoffmann et al., 1997; Griffin et al., 1999; Jaoui and Kamens, 2001; 2003a; 2003b; 2003c; Jaoui et al., 2003; Jaoui et al., 2004; Winterhalter et al., 2003). Isoprene, because of its small size and the high volatility of its oxidation products, has been regarded not to produce SOA at atmospheric levels (Pandis et al., 1991). However, recent laboratory studies have shown that the further heterogeneous particle phase reactions, acid-catalyzed or not, of isoprene and its gas-phase products maybe present a major contribution to SOA formation in natural systems (Jang et al., 2002; Limbeck et al., 2003; Matsunaga et al., 2003; Claeys et al., 2004b; Edney et al., 2005; Kroll et al., 2005). Proposed isoprene oxidation products were also observed in ambient $PM_{2.5}$ particles (Claeys et al., 2004a; Ion et al., 2005; Edney et al., 2005; and Kourtchev et al., 2005). Very recently, Kroll et al (2005) found that isoprene photooxidation under high NO_x concentrations led to 0.9-3.0% SOA yield based on mass basis at ~ 20°C and 40-50% relative humidity. Aerosol formation was also observed in many forests in different countries (Kavouras et al., 1998; Blando et al., 1998; Leaitch et al., 1999; Kavouras et al., 1999; Yu et al., 1999a; Kavouras et al., 1999a; Janson et al., 2001; Spanke et al., 2001; Pio et al., 2001; Kavouras et al., 2002; Alves and Pio, 2005). Estimates of annual global atmospheric organic aerosol from oxidation of biogenic hydrocarbons range among 11.2 Tg (Chung and Seinfeld 2002); 2.5-44.5 Tg

(Tsigaridis and Kanakidou, 2003), 13-24 Tg (Griffin et al., 1999a); 63 Tg (Derwent et al., 2003); 61-79 Tg (Kanakidou et al., 2000) and 30-270 Tg (Andreae and Crutzen, 1997).

The most important anthropogenic source for SOA formation is aromatic hydrocarbons. In the urban atmosphere, aromatic hydrocarbons comprise more than 25% of anthropogenic carbon emissions and are thought to contribute a major fraction to secondary organic aerosol (Odum et al. 1997b). Numerous smog chamber experiments have been carried out to determine their potential ability to produce SOA (e.g., Izumi and Fukuyama, 1990; Odum et al., 1997a; Odum et al., 1997b; Kleindienst et al., 1999, 2000; Hurley et al., 2001; Jang and Kamens, 2001a). Other anthropogenic hydrocarbons capable of producing SOA include long-chain olefins and long-chain alkanes (Strader et al., 1999).

2. SOA Partitioning Modeling

2.1 Technical background

Two steps are involved in the formation of SOA: the condensable vapor production and the subsequent gas/particle partitioning. The whole process is represented in Figure 2.1.

The HCs emitted from both biogenic and anthropogenic sources undergo complicated photochemical reactions in the atmosphere, forming hundreds of different products, which may further react with the oxidants present in the atmosphere. This kind of series reactions finally brings about low volatility products, which can contribute to the SOA mass via self-nucleation or gas/particle (G/P) partitioning on preexisting organic
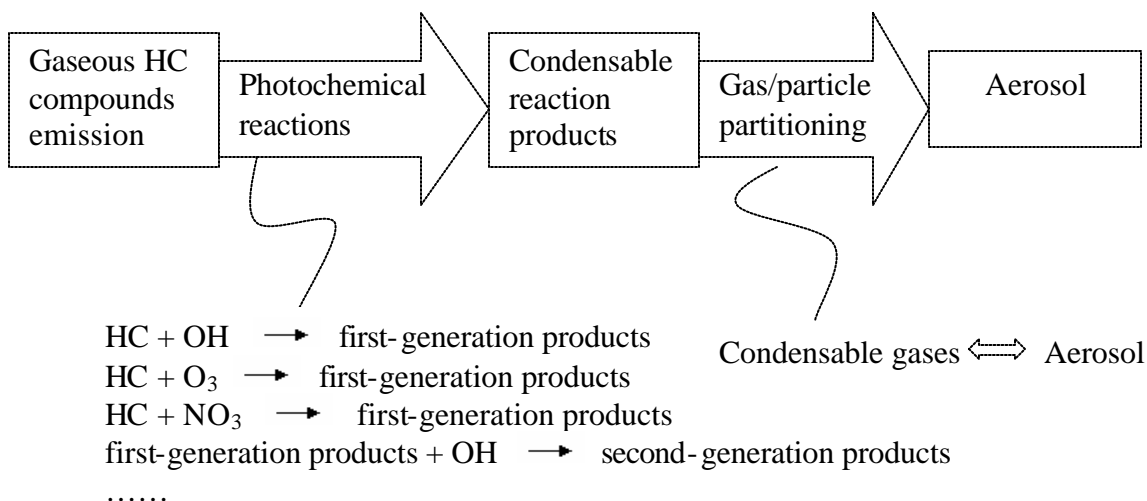
Figure 2.1. SOA production process.

matter.

Although some tentative mechanisms describing the kinetic reaction process are available for certain individual HC such as *a*-pinene, ***b***-pinene and *d*-limonene (Kamens et al, 1999; Jenkin et al., 2000; Kamens and Jaoui, 2001; Leungsakul et al., 2005a, b; Chen and Griffin, 2005), and some of the tentative mechanisms have been coupled into the large-scale application air quality models (Barthelmie and Pryor, 1999; Jenkin et al., 2000; Kamens and Jaoui, 2001; Andersson-Sköd and Simpson, 2001; Griffin et al., 2002a), the detailed gas-phase chemistry mechanism for most of the SOA precursors is still not well known and many uncertainties exist. Thus, generally speaking, empirical parameters from smog chamber experiments are still extensively used to represent the SOA production process.

Different types of gas/particle partitioning are prevalent for different kinds of semivolatile compounds. In 3-D Eulerian air quality models, which are used to describe the formation, transport, and fate of air pollutants at urban or regional scales (Russell and

11

Dennis, 2000 and references therein), four major different approaches are used to simulate the gas/particle partitioning of organic species: vapor saturation, adsorption onto particle surfaces, absorption into a liquid organic phase, and dissolution into an aqueous phase (Seigneur, 2001). Given the wide variety of organic compounds existing in the atmosphere, with different chemical properties, it is reasonable to anticipate that different mechanisms prevail for the transfer of semivolatile organics with different characteristic functional groups and different polarities.

Odum et al. (1996) showed from smog chamber studies that the condensation of the photooxidation products which form secondary organic aerosol (SOA) is very well described by an absorptive partitioning model, which is derived from the gas/particle partitioning theory of Pankow (1994a, b). The absorptive mechanism has also been successfully applied to other smog chamber experiments results (Odum et al. 1997b; Jang et al, 1997; Hoffmann et al. 1997; Griffin et al. 1999; and Cocker III, et al, 2001a, 2001b; Keywood et al., 2004). In absorptive mechanism, the semivolatile condensable vapor can go into the particulate phase even if its partial pressure is lower than its corresponding saturation vapor pressure. Thus vapor saturation approach is not appropriate for compounds that may partition into the particulate phase, though it may hold true for compounds having very low vapor pressures. So the actual process happening in the atmosphere may be a somewhat combination of the other three mechanisms mentioned above, such as was treated in Pun et al (2002) and Griffin et al (2003), where SOA partitioning process was assumed to occur by both absorption and dissolution. However, dissolution is a significant mechanism only for water-soluble semivolatile organic compounds (SOC) when water presents (Pun et al., 2002; Pun et al., 2003). Additionally

the Henry's law coefficients do not exist for the identified SOA products and many uncertainties exist for the hygroscopic properties of the organic aerosol components and the interaction between the aerosol organic and inorganic species.

Although adsorption mechanism would be important when atmospheric particulate material is comprised solely of mineral materials, urban particulate material generally contains a significant amount of amorphous organic carbon. So absorptive mechanism probably plays the dominant role in urban air and also in air affected by urban sources (Liang et al., 1997; Mader and Pankow, 2003).

2.2. Absorption model

For absorptive partitioning, the following theoretical equation is obtained for the partitioning coefficient (Pankow, 1994a, b)

$$K_{ab,i} = \frac{C_{aer,i}/TSP}{C_{gas,i}} = \frac{f_{om}760RT}{MW\mathbf{V}_i P_{L,i}^{0}10^6} \tag{2.1}$$

where $K_{ab,i}$ is the absorptive partitioning coefficient for species i, $C_{aer,i}$ ($\mu g/m^3$) and $C_{gas,i}$ ($\mu g/m^3$) are respectively the concentrations of species i in aerosol phase and gas phase, TSP ($\mu g/m^3$) is the total particulate concentration, f_{om} is the weight fraction of organic absorbing phase, R is the universal gas constant (8.2×10^{-5} m^3atm/mol-K), T (K) is the temperature, MW (g/mol) is the mean molecular weight of the absorbing aerosol phase, $\mathbf{z}_i$ is the activity coefficient of species i in the absorbing aerosol phase, and $P_{L,i}^{0}$ (torr) is the sub-cooled liquid vapor pressure of species i. The mean molecular weight is defined as

$$MW = \sum_i x_i MW_i \tag{2.2}$$

where x_i is the mole fraction of species i in the aerosol phase and MW_i (g/mol) is the molecular weight of the compound i.

The absorptive partitioning coefficient can be defined in a slightly different form (Odum et al., 1996) as

$$K_{om,i} = \frac{C_{aer,i} / M_o}{C_{gas,i}} = \frac{K_{ab,i}}{f_{om}} \qquad (2.3)$$

where M_o is the amount of organic matter present in the aerosol phase.

2.3 Yield

As described in section 1.2, SOA precursors include many HC compounds. The absence of the knowledge about the reaction mechanisms and semivolatile products for most of the SOA precursors makes it difficult at present to accurately simulate and predict SOA production. Under this condition, smog chamber data are used to derive the reaction stoichiometry empirically (i.e., the amount of condensed matter formed per reactant reacted). The aerosol yield, Y ($\mu g/m^3/\mu g/m^3$), resulting from the oxidation of a single parent hydrocarbon is defined as the amount of aerosol produced when a certain amount of HC reacts,

$$Y = \frac{\Delta M_0}{\Delta HC} \qquad (2.4)$$

where ΔHC ($\mu g/m^3$) is the amount of HC that has reacted and ΔM_0 ($\mu g/m^3$) is the amount of organic aerosol created.

It can be described as the sum of the yields of each organic product, Y_i, as follows (Odum et al, 1996),

$$Y = \sum Y_i \qquad (2.5)$$

$$Y_i = M_0 \frac{a_i K_{om,i}}{1 + K_{om,i} M_0}$$
(2.6)

where a_i is the dimensionless mass-based stoichiometric product coefficient, M_0 ($\mu g/m^3$) is the mass concentration of the absorbing mass present and includes both the initial absorbing mass present before the partitioning process begins C_{init} and the sum of compounds that partition into aerosol phase $C_{aer,i}$.

$$M_0 = \sum C_{aer,i} + C_{init}$$
(2.7)

Although numerous products are formed in the oxidation of a single parent hydrocarbon (e.g.Yu et al., 1999; and Forstner et al., 1997), it has been shown that an empirical two-product model accurately represents yield data obtained for more than 30 parent hydrocarbons in smog chamber experiments (Odum et al., 1996; Hoffmann et al., 1997; and Griffin et al., 1999). Essentially, one product represents the more volatile compounds while the other describes the products of lower volatility (Odum et al., 1996). This 2-product fitting approach has been applied in air quality models such as CMAQ (Binkowski, 1999) and PMCAMx (Environ, 2003). Although this approach greatly simplifies the work of integrating SOA into air quality models, it does not provide a fundamental tracking of the chemical structure of the modeled species and can not be used to incorporate composition effects on SOA production.

From equation (2.6), it can be seen that the yield, Y, is not only a function of reaction stoichiometry and the absorptive partitioning coefficient of each condensable component but also of the amount of condensed organic materials, which in turn depends upon the quantities of absorbate and absorbent available and the thermodynamics of absorbate-absorbent interactions (in term of activity coefficients). Environmental factors,

such as temperature and relative humidity, have much effect on the partitioning coefficient, one of the key parameters governing the partitioning process (Seinfeld and Pankow, 2003).

2.4 Temperature effects

The absorption model utilized by Odum et al. (1996, 1997b) in general shows a strong dependence on temperature, which is also supported by some smog chamber experiments (Cocker et al., 2001b; Takekawa et al., 2003). Cocker III et al. (2003) found that the aerosol yield from one parent hydrocarbon compound varies significantly with temperature when the same amount of organic matter presents in the system. Low temperature favors the partitioning of semivolatile compounds into the aerosol phase due to the larger partitioning coefficient at lower temperature. They also observed that under the same temperature the SOA yield increases with the amount of organic matter present in the system. More organic matter provides more absorbent in the system, which allows more semivolatile compounds to partition into the aerosol phase.

Temperature effects are mainly reflected in the equilibrium partitioning coefficient K_{om}. For a given compound sorbing to a given type of atmospheric particulate material, this temperature dependence can be described by the following formula (Yamasaki et al., 1982; Pankow et al., 1994), which has been confirmed in many laboratory studies (Kaupp and McLachlan, 1999; Leach et al., 1999).

$$\log K_p = m_p / T + b_p \tag{2.8}$$

where m_p and b_p are constants for given species.

The relationship expressed in equation (2.8) is implicitly present in equation (2.1) due to the temperature dependence of P_L^0. The temperature dependence of P_L^0 can be represented by Clausius-Clapeyron equation as follows,

$$P_{L,i}{}^0 = B_i \exp(\frac{-H_i}{RT}) \tag{2.9}$$

where B_i (K) is the pre-exponential constant of product i; H_i (kcal/mol) is the enthalpy of vaporization of product i.

Substitute (2.9) into equation (2.1), the following equation is obtained for the temperature dependence of $K_{om,,i}$.

$$K_{om,i} = \frac{RT10^{-6}}{MW V_i B_i} \exp(\frac{H_i}{RT}) \tag{2.10}$$

The above equation is equivalent to equation (2.8) assuming that V_i, MW, B_i are constants for the temperature range interested.

So in theory, the temperature effects can be indicated through the following two aspects: 1) directly through the T and $\exp(\frac{1}{T})$ terms, and 2) indirectly through V_i and MW terms. The activity coefficient of species i varies slightly with temperature when the SOA composition is held constant. Furthermore, experiments carried out by Jang and Kamens (1999) indicate that the composition of SOA is different with different temperature. Different composition of SOA results in different activity coefficients and different mean molecular weight of the aerosol phase, which have effects on the partitioning coefficient and the partitioning process as well.

2.5 Composition effects

Only recently has the aerosol composition effect been included in some of the air quality models (Pun et al, 2002; Griffin et al., 2002a), as a result of more and more SOA components identified. The composition effect works through the activity coefficient of each aerosol product in the aerosol mixture and mean molecular weight of the absorbing phase. Theoretical predictions indicate that while activity coefficients may not vary significantly for mixtures containing similar polarity compounds, they change greatly within dissimilar compounds mixtures (Jang et al., 1997; Pankow et al., 2001; and Seinfeld, et al., 2001). Theoretical predictions made with a single-cell model indicate that aerosol composition has an effect in magnitude comparable to diurnal temperature variations and semivolatile precursors emission rate fluctuations (Bowman and Karamalegos, 2002).

2.5.1 Identified SOA components

Identification of the SOA components has become an extensive research area. Identification of the aerosol molecular composition allows theoretical estimation of aerosol production, including the interaction with liquid water (Jang and Kamens, 1998; and Ansari and Pandis, 2000). The research results are also useful for identifying the species that trigger the nucleation process and elucidating the chemistry mechanism for the SOA production process. Some laboratory-identified components have also been detected in the ambient aerosols (Pio et al., 2001; Edney et al., 2003; Kleindienst et al., 2004; Baltensperger et al., 2005; and Jaoui et al., 2005).

Product identification work is mostly on α-pinene (Glasius et al., 1999; 2000; Yu et al., 1998, 1999; Jang and Kamens, 1999; Larsen et al., 2001; Hoffmann et al., 1998; Koch et al., 2000; Christoffersen et al., 1998; Jaoui and Kamens, 2001, 2003a; Gao et al., 2004b; Sax et al., 2005), β-pinene (Yu et al., 1999; Glasius et al., 2000; Larsen et al., 2001; Koch et al., 2000; Jaoui and Kamens, 2003a, b), Δ^3-Carene (Yu et al., 1998; 1999; Glasius et al., 2000; Larsen et al., 2001; Koch et al., 2000), sabinene (Yu et al., 1999; Glasius et al., 2000; Koch et al., 2000; Larsen et al., 2001), and limonene (Glasius et al., 2000; Koch et al., 2000; Larsen et al., 2001) as representation of natural SOA producing sources. In addition, smog chamber experiments were also conducted on sesquiterpenes due to their expected and then verified high SOA production capabilities (Jaoui and Kamens, 2003c; Jaoui et al., 2003, 2004). Toluene is the most studied anthropogenic SOA-producing source (Forstner et al., 1997; Jang and Kamens, 2001a; Smith et al., 1998; Kleindienst et al., 2004; Hamilton et al., 2005). Several studies have also focused on cycloalkenes (Kalberer et al., 2000; Gao et al., 2004b; Ziemann, 2003; Bahreini et al., 2005) and linear alkenes (Forstner et al., 1997; Tobias and Ziemann, 2000; Tobias et al., 2000; Gong et al., 2005). Other studied anthropogenic gas-phase precursors include xylenes (Forstner et al., 1997; Smith et al., 1999; Bahreini et al., 2005), ethylbenzene (Forstner et al., 1997), ethyltoluene (Forstner et al., 1997), 1,2,4-trimethylbenzene (Forstner et al., 1997; Smith et al., 1999), 1,3,5-trimethylbenzene (Smith et al., 1999; Fisseha et al., 2004; Sax et al., 2005) and n-alkanes (Lim and Ziemann, 2005). The major identified aerosol-phase products as well as their structures corresponding to different precursors are summarized in Appendix A.

Despite the extensive efforts in SOA product identification, the identifiable fraction of the aerosol phase varies a lot from precursor to precursor. For sabinene and cyclohexene, the SOA produced can be ~100% accounted for on a molecular level (Yu et al., 1999; Kalberer et al., 2000). However, currently only 10% of the aerosol mass can be identified corresponding to toluene (Hamilton et al., 2005). The identifiable SOA fraction for different precursors is summarized in Table 2.1.

Table 2.1. Literature data for identifiable SOA fractions for different precursors.

Precursor	Identified fraction of SOA produced
α-pinene	>90% [a]
β-pinene	>83% [a]
Sabine	~100% [a]
Δ^3-Carene	61% [a]
Aromatics [b]	15-30% [c]; ~10% for toluene [d]
1-Decene	37-45% [e]
1-Octene	37-50% [e]
Cyclohexene	100% [e]; 45% [g]
Cyclopentene	89% [g]
1-methyl-cyclopentene	67% [g]
1-methyl-cyclohexene	79% [g]
3-methyl-cyclohenxene	90% [g]
Cycloheptene	53% [g]

[a] Yu et al., 1999.
[b] Includes toluene, *m*-xylene, *p*-xylene, ethylbenzene, *m*-ethyltoluene, *p*-ethyltoluene, ethylbenzene, *m*-ethyltoluene, *p*-ethyltoluene and 1,2,4-trimethylbenzene.
[c] Forstner et al., 1997a.
[d] Hamilton et al., 2005.
[e] Forstner et al., 1997b.
[f] Kalberer et al., 2000.
[g] Gao et al., 2004b. The values indicate the fractions of all identified species including both low-MW compounds and oligomers in the total SOA mass.

2.5.2 UNIFAC model

The UNIFAC group contribution method (Fredenslund et al., 1977) for estimating liquid phase activity coefficients was developed to get around the absence of experimental data for liquid mixtures. Due to the overwhelming variety of organic compounds, it is not likely to get experimental data for every mixture of interest. UNIFAC model, by reducing the hundreds of organic species to about 60 classes of functional groups, provides a state-of-the-art method to predict the activity coefficients in those mixtures where little or no experimental data are available. It has been proved to be a successful group contribution method used for chemical process design.

UNIFAC assumes that the logarithm of the activity coefficient is the sum of two contributions: a combinatorial part and a residual part. The combinatorial part represents the contributions due to differences in size and shape of the molecules in the mixture, which are obtained from group volume and area constants R_k and Q_k; and the residual part represents the contributions due to energy interaction in the mixtures. Essentially it is assumed that physical properties of a fluid are the sum of the contributions made by the molecule's functional groups and one group's contribution is independent of the other's. The constants R_k and Q_k were originally obtained from atomic and molecular structure data, the van der Waals group volumes and surface areas V_k and A_k. But now R_k and Q_k are found from fitting the experimental data.

So in order to use the UNIFAC model, parameters R_k and Q_k and the group interaction parameters a_{nm} between groups must be known. Several studies have been conducted to evaluate UNIFAC performance to predict semivolatile organic compound (SOC) partitioning and water activity associated with SOA components (Saxena and

21

Hildmann, 1997; Jang et al., 1997; Jang and Kamens, 1998; Peng et al., 2001; and Chandramouli et al., 2003). UNIFAC predicts well the properties of small monofunctional compounds in usually highly concentrated solution systems. It must be noted, however, that for the highly polar SOA components with multifunctional groups, UNIFAC does not perform well (Saxena and Hildemann, 1997). Ming and Russell (2002) combined the Pitzer-Simonson-Clegg model and UNIFAC with new additional functional groups interaction parameters to improve the thermodynamic predictions for atmospheric aerosols containing inorganic species, water and organic compounds. Similar efforts by other researchers should lead to improved performance of UNIFAC (Peng et al., 2001)

2.5.3 Relative humidity

The absorption of water into the aerosol phase may alter the activity of the organic constituents in the solution and shift the thermodynamic equilibrium achieved between the gas- and aerosol- phase organics. This perturbation results in different organic mass ended in aerosol phase from that when water is absent because the water absorbed can significantly affect the activity coefficient, V, and the mean molecular weight, *MW*, of the absorbents.

The effects of RH on the partitioning coefficient work through the average molecular weight of the absorbing phase (organic + water) and the compound specific activity coefficient z (Seinfeld et al., 2001) as the relationship derived from equation (2.1) is expressed as follows,

$$\frac{d \ln K_{ab}}{dRH} = -\frac{d \ln MW}{dRH} - \frac{d \ln V}{dRH}$$

(2.11)

22

If only organics and water are present in the system, the first item is always positive when RH increases because of the very low *MW* of water as compared to those of the condensable compounds. But the water effect on **z** is much more complicated with four possible results for the second term when RH goes up: always positive; first positive then negative; always negative; first negative then positive. For a hydrophilic compound, $-\dfrac{d \ln \boldsymbol{V}}{dRH}$ is likely to be positive when more water presents in the absorbing phase; for a hydrophobic compound, $-\dfrac{d \ln \boldsymbol{V}}{dRH}$ is expected to be negative when RH increases.

Contradictory experimental results on humidity effect on the SOA yields (Jang et al., 2002 & 2003a; Cocker et al., 2001a & 2001b; and Edney et al., 2000) make it difficult to draw conclusions on humidity effects. Furthermore, effect of the organic matter on the hygroscopic behavior of inorganic aerosol is a more difficult subject. This interaction between the aerosol-phase organics and inorganics may also have effect on the mass of the inorganic components finally staying in aerosol phase. ZSR (Zdanovskii, Stokes and Robinson) method was employed recently in some models to account for the additional aerosol water associated with the organics (Ansari and Pandis, 2000; Pun, B.K. et al, 2002). This approach, however, may not be appropriate when the organics present affect the hygroscopic behavior of the inorganic components. Many lab experiments have been carried out to test the hygroscopic properties of the organic aerosol as well as the effect of the organic matter on the hygroscopic behavior of the inorganic aerosol (Virkkula, et al., 1999; Cruz and Pandis, 2000; Peng et al., 2001a; Peng et al., 2001b; Peng and Chan, 2001; Choi and Chan, 2002; and Demou et al., 2003). Field studies on the liquid water concentration (LWC) of ambient aerosols from different sites reported

inconsistent results on the effect of organic matter on the hygroscopic property of the inorganic aerosol (Saxena et al., 1995; Dick et al., 2000; and Speer et al., 2003). All these findings indicate that water uptake by organic aerosol needs further research efforts.

2.6 Lumping approach

Because of the large number of products identified corresponding to each precursor, it is impossible to individually track each of them in air quality models. To simplify this process, 2 general approaches are adopted in SOA modeling communities. The first one is to use a 2-product model to fit smog chamber experimental data (Odum et al., 1996; Hoffmann et al., 1997; Griffin et al., 1999; Kalberer et al., 2000). The two imaginary products are used to represent the partitioning characteristics of the real multicomponent aerosol mixture under the specific experimental conditions. Further simplification is possible when aerosol-forming hydrocarbons that form similar products can be treated as a single class of precursor, such as has been shown for the aromatic fraction of gasoline (Odum et al., 1997a & b). The other approach is to choose a few specific aerosol products as surrogate compounds to represent the whole mixture, for example, the SOA simulation treated in the Caltech Atmospheric Chemistry Mechanism (CACM) (Griffin et al, 2002a; Seinfeld et al., 2002).

Although these approaches greatly simplify the work of integrating SOA into air quality models, they do not provide a fundamental tracking of the chemical structure of the modeled species (2-product model) or do not reflect the effect of other individual products (surrogate approach) on the SOA mass produced. The lumped method described in Bian and Bowman (2002 & 2005) has been shown to approximate the detailed SOA

mixture quite well and overcome the inadequacy of the two aforementioned simplified approaches. When more SOA products and experimental data become available, it is easy to incorporate the up-to-date information into the model to improve the simulation results.

In the lumped method approach, for each precursor 2 or more lumped groups are used to represent the partitioning characteristics of the whole product mixture. Given the parameters (p_i^o, MW_i, B_i, a_i, and chemical structure information) for the individual components, the parameters for lumped groups can then be determined.

3. CMAQ

The Community Multi-scale Air Quality (CMAQ) (Byun and Ching, 1999) modeling system is an air quality model developed by the U.S. EPA incorporating the most recent scientific research results from different areas of air quality studies such as tropospheric ozone, aerosol, acid deposition, etc. It adopts a module structure which makes it easy to incorporate the newest research results in one area while keep other modules untouched. It is called multi-scale air quality model due to its application to the air quality issues nation-wide, region-wide or in a small area specifically interested.

3.1 Framework of CMAQ

The framework of CMAQ is represented in Figure 2.2. Detailed information can be found in Byun and Ching (1999).
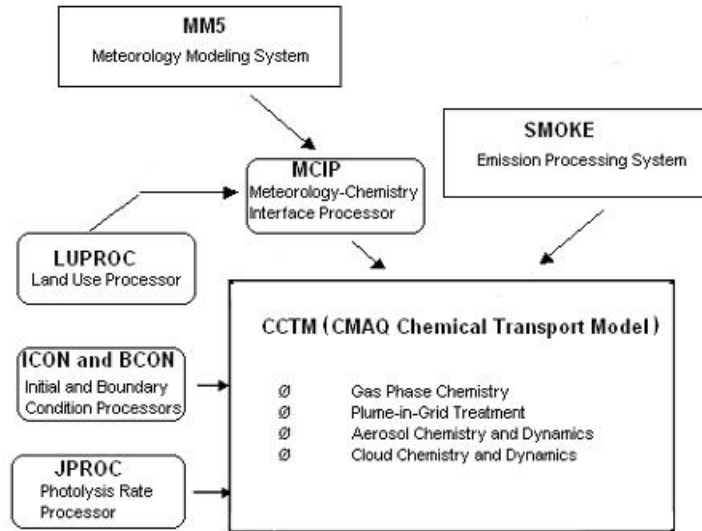
Figure 2.2. Framework of emissions and meteorological modeling systems and the CMAQ chemical transport model and interface processors (adapted from Byun and Ching, 1999).

In order to run CMAQ, the following input files are necessary: meteorological files, emission files, initial condition (IC) and boundary condition (BC). The data from these files are put into CMAQ through the interface processors after conversion and interpretation: meteorology-chemistry interface processor (MCIP) for meteorological data, initial conditions processor (ICON) and boundary conditions processor (BCON) for IC and BC data files, respectively. Emission files are currently processed by the Sparse Matrix Operator Kernel Emissions (SMOKE) modeling system and are in the ready-to-use data form. The core part of CMAQ is the chemical-transport model processor (CTM) which deals with the major atmospheric chemistry, transport and deposition processes. CMAQ CTM (CCTM) includes the following process modules: Horizontal advection; Vertical advection; Mass conservation adjustments for advection processes; Horizontal

diffusion; Vertical diffusion; Gas-phase chemical reaction solver; Aqueous-phase reactions and cloud mixing; Aerosol dynamics and size distributions; Plume chemistry effects; Aerosol deposition velocity estimation; Photolytic rate computation; and Process analysis.

SOA processes are defined by gas-phase chemistry and aerosol dynamics. Below is a brief review of the gas-phase chemistry module and aerosol module in CMAQ.

3.2 Gas-phase chemistry mechanisms

In the real atmosphere, hundreds of species participate in thousands of reactions. In large sophisticated grid-based air quality models like CMAQ, it is impossible to explicitly represent all the gas-phase chemistry due to the too great demand on processor time and memory. So condensed chemistry mechanisms were developed to represent what is really happening in the atmosphere. Because the inorganic chemistry has well been studied and been relatively well understood, all the currently available mechanisms treat inorganics explicitly. However, the uncertainties associated with the chemistry of VOCs render different approaches used to parameterize and simplify the chemistry for these species. Usually speaking, the individual compounds in the atmosphere are lumped together based on structure or molecular similarity. In the lumped structure approach, organics are regarded to be composed of smaller reaction elements while the lumped molecule approach uses a particular compound or a generalized species to represent similar organics.

The CMAQ system possesses the capability to use more than just one chemical mechanism. In the version 4.4 used for this study, 3 gas-phase chemistry modules are

available: RADM2 (Stockwell et al., 1990, Gross and Stockwell, 2003), CB4 (Gery et al., 1989) and SAPRC99 (Carter 1990; Carter 2000a; 2000b). The CB4 mechanism is a lumped structure type while RADM2 and SAPRC99 are lumped species type (Dodge, 2000; Gipson and Young, 1999; Gross and Stockwell, 2003). Each of them has been modified and linked to aqueous chemistry and to aerosol formation process. All 3 mechanisms are frequently updated to correct errors and/or to incorporate new available information from kinetic and mechanistic studies. Detailed information can be found in Byun and Ching (1999) and Carter (2000b).

Before running CMAQ, the gas-phase chemistry mechanism used for the simulation must be first selected. Once the gas-phase chemistry is chosen, the processor JPROC produces mechanism specific photolysis rates. ICON and BCON provide appropriate initial condition and boundary condition, respectively. In this study, SAPRC99 was used to do all the simulations.

3.3 Current aerosol module

The evolution of the aerosol module in CMAQ is documented in Binkowski et al., 1995; Binkowski 1999; and Binkowski and Roselle, 2003 as well as the release notes on the EPA website (EPA, 2006). The particle size distribution is represented by three log normal modes: aitken mode (particles < 0.1 µm), accumulation mode (particles falling between 0.1 µm and 2.5 µm) and coarse mode (those between 2.5 µm and 10 µm). The aerosol processes taken into account include nucleation, condensation, coagulation (both intermodal and intramodal), and wet and dry deposition. Aitken and accumulation modes are merged when they grow to similiar sizes. Model ISORROPIA (Nenes et al., 1998 &

28

1999) is used to simulate the inorganic gas/aerosol equilibrium and water uptake by inorganic species. An absorption approach is adopted to describe the SOA partitioning (Schell, 2001). The secondary components considered include sulfate, nitrate, ammonium, water, biogenically derived secondary organic carbon, and anthropogenically derived secondary organic carbon. Primary species included in the module are primary organic carbon, elemental carbon, primary material not specified and wind-blown dust.

Many evaluation studies have been conducted on CMAQ (Zhang et al., 2004; Morris et al., 2005; Tesche et al., 2006; Zhang et al., 2006a; 2006b; 2006c). It was found in most of the studies that CMAQ under-predicts the concentration of OC all the time especially in summer. The reason accounting for this under-prediction may include uncertainties in primary OC emission and some missing precursors and processes associated with SOA production (Morris et al., 2005). Improving CMAQ OC performance involves many aspects including taking into account the composition effect on SOA production to provide a more accurate and realistic description of what happens in the atmosphere. CMAQv4.4 was used for the basis of this study.

3.3.1 Current SOA partitioning parameters

The aerosol module in CMAQ v4.4, aero3, represents the whole SOA formation process indicated in Figure 2.1. Six important classes of hydrocarbons capable of producing SOA while photo-oxidized are included: "long" alkanes (ALK5 in SAPRC99), internal alkenes (OLE2 in SAPRC99), three categories of aromatics (ARO1, ARO2 and CRES in SAPRC99), and one general biogenic source representing monoterpenes (TRP1 in SAPRC99). These six SOA precursors form a total of 10 condensable products. The

respective partitioning parameters of the 10 condensable products are based on smog chamber experiments. Experimental K_{om} values are converted to K_{om}^* values corresponding to 298K using a modified form of equation (2.10) as described by Sheehan and Bowman (2001). A similar module, only with different gas-phase precursors and different partitioning parameters for the semivolatile condensable products, has been tested by Schell et al. (2001) both in a box model and coupled to the comprehensive European Air Pollution and Dispersion/Modal Aerosol Dynamics Model for Europe (EURAD/MADE) air quality model system. Although limited by many uncertainties, their simulation results provide preliminary insights about the SOA formation process, for example, the mutual effects between the anthropogenic and biogenic sources, i.e., they cannot be treated separately.

The primary assumptions in aero3 about SOA include:

1) The gas/particle partitioning of SOA compounds is an absorption process.

2) $V_i = 1$ is assumed for all compounds and no composition effects are considered.

3) No water is taken up by organics.

4) Organics and inorganics have no interaction.

5) Thermodynamic equilibrium is assumed.

Assumptions 1) and 2) imply a quasi-ideal solution of the products. In such a quasi-ideal solution, Raoult's law can be applied and the effective saturation concentration of species i, $C_{sat,i}$, can be expressed as

$$C_{sat,i} = X_i C_{sat,i}^* \tag{2.12}$$

where X_i is the mole fraction of species i in the aerosol phase and $C_{sat,i}^*$ is the saturation concentration of the pure compound i, which is the mass concentration equivalent of the

saturation vapor pressure. The inverse of $C^*_{sat,i}$ is equal to the partitioning coefficient

defined by Pankow (1994a, 1994b) and Odum et al (1996) when $z_i = 1$ and $MW_i = MW$,

$$C^*_{sat,i} = \frac{P^0_i MW_i 10^6}{RT} = \frac{1}{K_{om,i}}$$

(2.13)

The SOA gas phase precursors and partitioning parameters used in aero3 are

summarized in Table 2.2.

Table 2.2. SOA precursors and parameters used in aero3.

Compounds (reactive organic gas precursors)	$MW_{rog,j}$ (g/mol)	MW_i (g/mol)	a_i ($\mu g/m^3/\mu g/m^3$)	$C^*_{sat,i}$ ($\mu g/m^3$)
"long" alkanes (ALK5 in SAPRC99)	114.0	150	0.0718	0.3103
Internal alkenes (cyclohexene, OLE2 in SAPRC99)	82.0	150	0.36 0.32	10.103 90.925
Aromatics like xylene (ARO2 in SAPRC99)	106.0	150	0.038 0.167	2.165 64.946
Aromatics like cresol (CRES in SAPRC99)	108.01	150	0.05	0.2611
Aromatics like toluene (ARO1 in SAPRC99)	92.0	150	0.071 0.138	1.716 47.855
Monoterpenes (TRP1 in SAPRC99)	136.0	177	0.0864 0.3857	0.865 11.804

3.3.2 Current partitioning calculation method

Figure 2.3 presents the calculation procedure of the SOA module in aero3.

For each time step, input variables are $DHC_{j,t}$ (ppm), $SOC_{i,t-1}$ (ppm), POA_t ($\mu g/m^3$), T (K)

and P (Pa). $DHC_{j,t}$ is the amount of VOC reacted during the target time step. $SOC_{i,t-1}$

$$totrog_{j,t} = \frac{P \times MW_{rog,j}}{RT} \times \Delta HC_{j,t}$$

$$Ctot_{i,t-1} = \frac{P \times MW_i}{RT} \times SOC_{i,t-1}$$

$$Ctot_{i,t} = \alpha_i totrog_{j,t} + Ctot_{i,t-1}$$

$$C^{\bullet}_{sat,i} = C^{\bullet}_{sat,i(298k)} \times \frac{T}{298} \times \exp[B_i(\frac{1}{T} - \frac{1}{298})]$$

Compute $C_{aer,i,t}$ $(i = 1,10)$

$$C_{aer,i,t} = Ctot_{i,t} - C^{\bullet}_{sat,i} \frac{C_{aer,i,t}/MW_i}{\sum_{k=1}^{10}(C_{aer,k,t}/MW_k) + POA_t/MW_{POA}}$$

$C_{aer,i,t}$ $(i = 1,10)$

$$SOA\_B_t = \sum_{i=9}^{10} C_{aer,i,t}$$

$$SOA\_A_t = \sum_{i=1}^{8} C_{aer,i,t}$$
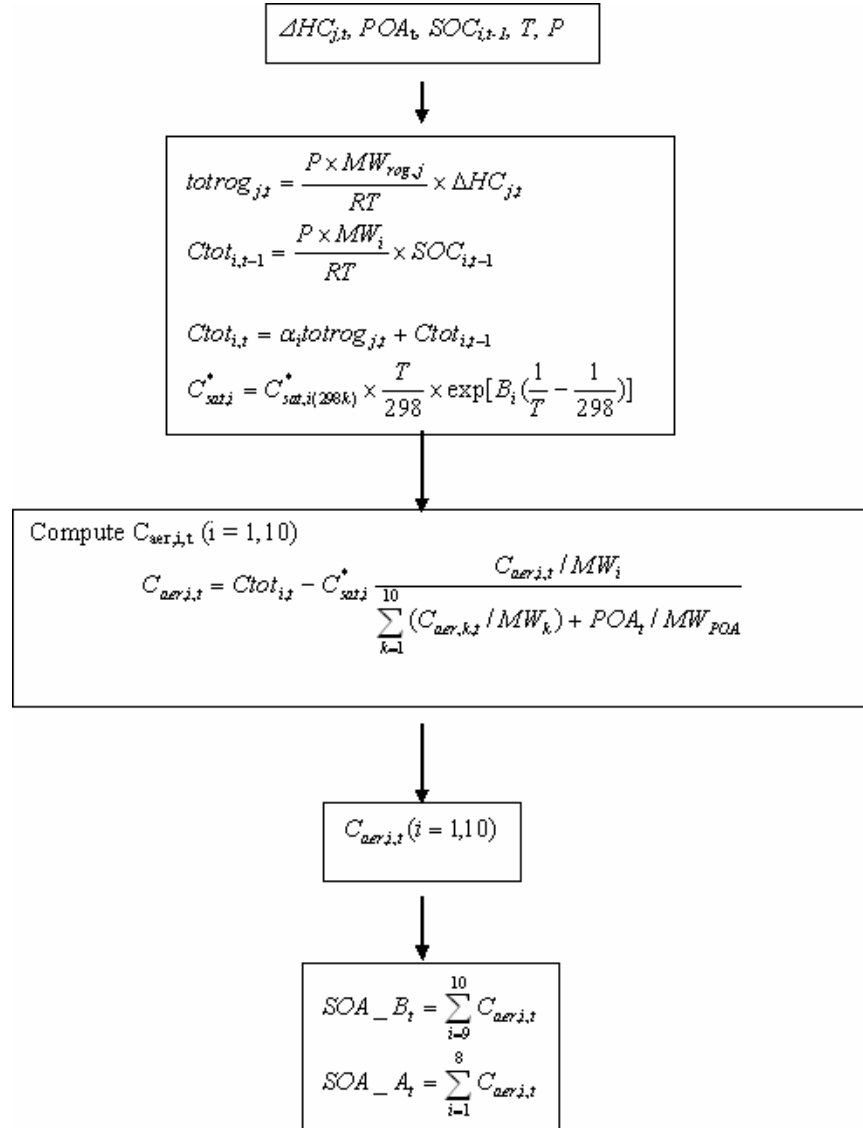
Figure 2.3. The scheme of computation process of aero3.

is the amount of semivolatiles, including that in both gas-phase and aerosol-phase, transferred from the previous time step. POA_t is the amount of primary organic aerosol present. T and P are the corresponding ambient temperature and pressure, respectively.

For partitioning process calculation, unit conversion from ppm to $\mu g/m^3$ is first performed on $\mathbf{\Delta HC}_{j,t}$ and $SOC_{i,t-1}$ to get $totrog_{j,t}$ and $Ctot_{i,t-1}$ using the ideal gas law,

$$totrog_{j,t} = \frac{P \times MW_{rog,j}}{RT} \times \Delta HC_{j,t} \tag{2.14}$$

$$Ctot_{i,t-1} = \frac{P \times MW_i}{RT} \times SOC_{i,t-1} \tag{2.15}$$

where $MW_{rog,j}$ is the molecular weight of the reactive gas-phase organic compound; MW_i is the molecular weight of condensable products; R is the ideal gas constant (8.314510 $m^3Pa/mol \bullet K$).

At the beginning of the partitioning process, the total amount of individual condensable compound partitioning between aerosol phase and gas phase, $Ctot_{i,t}$, is calculated as the sum of the amount produced from the VOC reacted during this time step, and its pre-existing concentration

$$Ctot_{i,t} = \mathbf{a}_i totrog_{j,t} + Ctot_{i,t-1} \tag{2.16}$$

During the partitioning process, the sum of gas and aerosol concentrations is assumed constant

$$Ctot_{i,t} = C_{gas,i,t} + C_{aer,i,t} \tag{2.17}$$

At the end of each time step, thermodynamic equilibrium is assumed to be obtained, which means

$$C_{gas,i,t} = C_{sat,i} = X_i C^*_{sat,i} \tag{2.18}$$

where the mole fraction is calculated as

$$X_i = \frac{C_{aer,i,t}/MW_i}{\sum_{k=1}^{10}(C_{aer,k,t}/MW_k) + POA_t/MW_{POA}}$$

(2.19)

and the saturation concentration is adjusted for temperature

$$C_{sat,i}^* = C_{sat,i(298k)}^* \times \frac{T}{298} \times \exp[B_i(\frac{1}{T} - \frac{1}{298})]$$

(2.20)

Then the amount of the condensable vapor ended up in the particulate phase during each time step can be got by solving the equation set created by combining equations (2.18)-(2.20)

$$C_{aer,i,t} = Ctot_{i,t} - C_{sat,i}^* \frac{C_{aer,i,t}/MW_i}{\sum_{k=1}^{10}(C_{aer,k,t}/MW_k) + POA_t/MW_{POA}}$$

(2.21)

The aero3 routine transforms these equations into a set of ten vectors that are minimized using a globally convergent Newton's method to efficiently compute the values $C_{aer,i,t}$ (i = 1, 10). *SOA_A* and *SOA_B*, the respective amount of anthropogenic and biogenic SOA produced in time step *t* are then calculated for application in subsequent aerosol processes, for example, updating the mass concentration. Tracking SOA only as *SOA_A* and *SOA_B* favors model efficiency.

If absorptive partitioning is not able to occur, ie, both of the following conditions are not met,

$$\sum_{i=1}^{10}(Ctot_{i,t}/C_{sat,i}^*) > 1$$

(2.22)

$$\frac{POA_t}{MW_{POA}} > 10^{-19}$$

(2.23)

then no organic aerosol is formed in this time step. These two equations imply that when no POA pre-exists, no condensable organics partition into aerosol phase until the concentration of the semivolatiles reaching a threshold (Bowman et al., 1997).

This currently used approach with empirically derived partitioning parameters does not account for the composition effect on the partitioning process. Adding composition effects to the treatment of SOA formation process is definitely necessary to provide a more realistic description of the SOA production process in the atmosphere (Turpin et al., 2000). The composition effects on the semivolatile partitioning process, as described in section 2.5, need to be incorporated into air quality model to provide further insight about SOA production process. The advancement in SOA component identification makes it the right time to launch such an effort.

COMPOSITION EFFECTS ON SECONDARY ORGANIC AEROSOL (SOA) PARTITIONING: CMAQ MODULE PARTITIOING PARAMETER DEVELOPMENT AND EVALUATION

1. Introduction

Secondary organic aerosol (SOA) attracts much attention of the researchers because it comprises approximately ~50% of the total aerosol carbonaceous material (Saxena and Hildemann, 1996; Turpin et al, 1991; Lim et al., 2002; Cabada et al., 2002), presents a hazard to people's health (Pope et al, 1995; Donaldson et al., 1998), has profound effect on global climate (Seinfeld and Pandis, 1998; Hinds, 1999 and references therein; Penner et al., 1998; Chung and Seinfeld, 2002) and can damage the local visibility (Seinfeld and Pandis, 1998). These well recognized adverse environmental effects of SOA are despite the fact that its formation mechanisms are not well established and some, but maybe important, SOA products are still not identified although the initial interest on SOA can trace back to 1960s (Went, 1960). Although some tentative mechanisms describing the kinetic reaction process are available for certain individual HC, for example, a-pinene (Kamens et al, 1999; Jenkin et al., 2000; Kamens and Jaoui, 2001), and some of the tentative mechanisms have been coupled into large-scale air quality models (Barthelmie and Pryor, 1999; Jenkin et al., 2000; Kamens and Jaoui, 2001; Andersson-Sköd and Simpson, 2001; Griffin et al., 2002a), the detailed chemistry mechanism for most of the SOA precursors is still not well known and many uncertainties exist. Thus, the accurate simulation of atmospheric SOA presents a big

challenge because of the complexity of potential reaction pathways of the precursors, the large number of species presented, the structural complexity of the compounds, and, most important, the absence of the critical experimental data necessary for theoretical predictions. So generally speaking, empirical parameters from smog chamber experiments are still extensively used to represent the SOA production process in air quality models, which are used to study the formation, transport, and fate of air pollutants at urban or regional scales (Russell and Dennis, 2000 and references therein).

Odum et al. (1996) showed from smog chamber studies that the condensation of photooxidation products which form secondary organic aerosol (SOA) is very well described by an absorptive gas/particle partitioning model with 2 imaginary semi-volatile products, which is derived from the gas/particle partitioning theory of Pankow (1994a, b). The 2-product absorptive mechanism has also been successfully applied to other smog chamber experiments results (Odum et al. 1997b; Jang et al, 1997; Hoffmann et al. 1997; Griffin et al. 1999; Cocker III, et al, 2001a, 2001b; Keywood et al., 2004). Thus, this SOA production mechanism has been frequently used to represent SOA formation in regional as well as global air quality models (Tsigaridis and Kanakidou, 2003; Schell et al., 2001; Binkowski and Roselle, 2003).

The community multi-scale air quality modeling system (CMAQ) developed by EPA (Byun and Ching, 1999) currently simulates SOA production as an absorption process. Smog chamber data are used to describe the SOA production potential of six categories of hydrocarbons: "long" alkanes (ALK5 in SAPRC99, a lumped species gas-phase chemistry mechanism developed by Carter (1990, 2000a, 2000b)), internal alkenes (OLE2 in SAPRC99), three categories of aromatics (ARO1, ARO2 and CRES in

SAPRC99), and one general biogenic source representing monoterpenes (TRP1 in SAPRC99). While effect of temperature on SOA production is included, an ideal mixture is assumed (ζ_i =1 for all compounds) and no composition effects on the partitioning process are considered. The current partitioning parameters used to simulate SOA can be found in section 3.3.1 in Chapter II. The details and evolution of the aerosol module in CMAQ is documented in Binkowski et al., 1995; Binkowski 1999; and Binkowski and Roselle, 2003 as well as the release notes on the EPA website (http://www.epa.gov/asmdnerl/CMAQ/CMAQscienceDoc.html). Briefly, the secondary aerosol components considered include sulfate, nitrate, ammonium, inorganics-related water, biogenically derived secondary organic carbon, and anthropogenically derived secondary organic carbon. Primary aerosol species included in the module are primary organic carbon, elemental carbon, primary material not specified and wind-blown dust. The particle size distribution is represented by three log normal modes: aitken mode, accumulation mode and coarse mode.

Evaluation work carried out on CMAQ indicates that large deviations exist between predicted concentrations of organic aerosol (OA), including primary organic aerosol (POA) and secondary organic aerosol (SOA), and field measurements (Zhang et al, 2004; Morries et al., 2005). Many factors, including the composition effects on the partitioning of the semi-volatiles, contribute to this discrepancy. The composition effect works through the activity coefficient of each aerosol product in the aerosol mixture and mean molecular weight of the absorbing phase. Theoretical predictions indicate that while activity coefficients may not vary significantly for mixtures containing similar polarity compounds, they change greatly within dissimilar compounds mixtures (Jang et

al., 1997; Pankow et al., 2001; Seinfeld, et al., 2001). Bowman and Karamalegos (2002) estimated with a single-cell model that the aerosol composition has an effect in magnitude comparable to diurnal temperature variations and semivolatile precursor emission rate fluctuations.

So interest arises on quantification of composition effects on SOA production in 3-D air quality models. The simple 2-product model currently used in CMAQ, with the assumption of ideal behavior, provides no chemical structure information about the aerosol phase formed through the oxidation of the gas-phase precursors. In this study, therefore, the SOA production process in CMAQ was modified to incorporate product structure information as well as its succeeding effects on SOA production. As the first part of this study, the development of product representation and partitioning parameters are detailed in this chapter. The performance of the new SOA production representation is then evaluated in both experimental and atmospheric systems. To allow a direct comparison with the original aerosol module in CMAQ, an ideal system, i.e., with activity coefficients set to 1 for all the model species and no composition effects accounted for on organic aerosol concentration predictions, is assumed for this initial evaluation. In this way, the effects of the general SOA product representation can be considered separately from the composition effects. An evaluation of the new aerosol module including composition effects is presented in Chapters IV and V. For experimental system evaluation, the aerosol yields predicted by the new SOA production representation and the current partitioning parameters in CMAQ were compared to smog chamber experimental data while for evaluation in atmospheric system, the model values, from CMAQ framework incorporated with either the modified and original CMAQ

organic aerosol module, were compared against ambient organic carbon (OC) measurements from SEARCH, IMPROVE and SOS99-Nashville monitoring sites obtained during the period from July 3 to July 17, 1999.

The contents of this chapter are organized as follows: Section 2 details the product representation and development of the lumped groups; The evaluation results of the new SOA representation against current parameters in CMAQ in experimental and atmospheric system are presented in section 3 and section 4, respectively. The factors accounting for the disparity in the results are also analyzed and indicated. Section 5 concludes the findings in this study

2. New SOA Representations

In order to ultimately incorporate composition effects into the module, the molecular composition of the aerosol phase must be taken into consideration. The lumped method described in Bian and Bowman (2002 & 2005) has been shown to approximate the detailed SOA mixture quite well and was applied in this study, therefore, to formulate the lumped groups for modeling purpose. It is easy to incorporate the up-to-date information into the Bian and Bowman model (2002 & 2005) to improve the simulation results as more SOA products and experimental data become available.

In the new module, 5, instead of 6, classes of gas-phase precursors are used because of the merge of cresol into high-yield aromatics ARO1. Smog chamber experiments on cresol are spare and the partitioning parameters in the original CMAQ comes from theoretical estimate from Strader et al (1999). Due to the absence of the experimentally derived aerosol composition from cresol and because cresol is not a

significant SOA producer, it is assumed that SOA from cresol has the same composition as those from ARO1.

In order to get the structure information of the lumped groups for modeling purpose, a survey of the experimentally identified SOA products was first conducted and products corresponding to each gas-phase precursor class were selected for the lumping procedure. The properties of each selected individual SOA component were determined from published experimental/model data or by theoretical estimation. It should be pointed out that the absence of interaction parameters between some functional groups in UNIFAC excludes the selection of some representative products, such as nitrate organics and quinine-like compounds, identified in smog chamber experiments.

In this section, the detailed SOA components for each precursor are presented followed by the calculated properties of the lumped model species. a_i, the dimensionless mass-based stoichiometric product coefficients, for the individual products were obtained from experimental data where available, and adjusted by emissions-based weighting factors for the precursors. p_i^{o*}, the vapor pressure of the individual components at the same temperature as that adopted for the corresponding chamber experiments, were obtained from published predictions or calculated based on the thermodynamic and chemical structural properties of the compound (Joback and Reid, 1987; Stein and Brown, 1994; Myrdal and Yalkowsky, 1997). All compounds were assumed to have a temperature dependence of $B_i = H_i / R = 18,762$ K to be consistent with CMAQ.

2.1 Biogenics-TRP1

The major biogenic hydrocarbons considered to produce SOA are α-pinene, β-pinene, Δ^3-carene, sabinene and limonene. Besides isoprene, they are the most abundant hydrocarbons emitted by vegetation and have been proved to be effective sources of aerosol (Pandis et al., 1991; Zhang et al., 1992; Odum et al., 1996; Hoffmann et al., 1997; Griffin et al., 1999; Andersson-Sköld and Simpson, 2001; Jaoui and Kamens, 2001; 2003a; 2003b; Winterhalter et al., 2003). The extensive chamber studies on these compounds provide a long list of aerosol products (Christoffersen, et al., 1998; Hoffmann et al., 1997; 1998; Jang and Kamens, 1999; Koch et al, 2000; Glasius et al., 1999; Jaoui and Kamens, 2001; 2003a; 2003b; Glasius et al., 2000; Yu et al., 1999; Griffin et al., 1999; Iinuma et al., 2005). Pankow et al. (2001), based on Yu et al. (1999), provide a complete summary of the properties for the individual products from α-pinene, β-pinene, Δ^3-carene, and sabinene. These properties include the mass-based stoichiometry coefficients α based on the chamber experiments and the vapor pressures at 308 K estimated by a UNIFAC-based group contribution method. In this study, the properties of the lumped groups are calculated based on the properties of those individual products presented in Pankow et al. (2001). Limonene was assumed to have the same products as a-pinene due to the absence of corresponding detailed product information.

Stoichiometric coefficient values from single hydrocarbon experiments for β-pinene, sabinene , Δ^3-carene, and limonene were adjusted by factors of 1.6, 2.5, 2 and 1.5, respectively, to better fit the single hydrocarbon photooxidation experimental data. This adjustment intends to account for - 1) the experimental condition difference in Yu et al. (1999) and Griffin et al. (1999); 2) particle phase reactions that favor the partitioning of

semi-volatiles into aerosol phase as well as other differences that may arise from other sources - to make better match between the predicted and measured aerosol yield in each individual experiment. Yu et al. (1999) provides the stoichiometric coefficients for this

Table 3.1. SOA products and individual partitioning properties for monoterpenes (TRP1).

Precursor	SOA Components[a]	a_i[a]	p_i^{o*}[b] (torr)	MW_i
	caronaldehyde	0.0315	2.97×10^{1}	168
	hydroxy caronaldehyde	0.0130	5.38×10^{-2}	184
	pinonaldehyde	0.0802	4.63×10^{-2}	168
	hydroxy sabina ketones	0.1182	2.93×10^{-2}	154
	sabina ketone	0.0198	9.49×10^{-3}	138
	nor-3-caronic acid	0.0086	5.55×10^{-3}	170
	3-caronic acid	0.0170	1.46×10^{-3}	184
	hydroxy pinonaldehyde	0.0419	2.29×10^{-4}	184
	norpinonic acid	0.1181[c]	8.17×10^{-8}	170
TRP1	norsabinonic acid	0.0147	8.17×10^{-6}	170
	norpinic acid	0.0022	7.50×10^{-6}	172
	norsabinic acid	0.0321	7.50×10^{-6}	172
	hydroxy nopinonic acid	0.0398	6.93×10^{-6}	186
	pinonic acid	0.0346	2.22×10^{-6}	184
	3-caric acid	0.0078	2.10×10^{-6}	186
	pinic acid	0.0633	2.10×10^{-6}	186
	sabinic acid	0.0041	2.10×10^{-6}	186
	hydroxy 3-caronic acid	0.0049	2.03×10^{-6}	200
	hydroxy pinonic acid	0.0245	2.03×10^{-6}	200
	X[d]	0.0132	1.0×10^{-12}	184

[a] values from Pankow et al., 2001 adjusted first to better fit individual smog chamber experiment data for β-pinene, sabinene , Δ^3-carene, and limonene by factors of 1.6, 2.5, 2 and 1.5, respectively, and further weighted by parent monterpene emission significance of 0.4, 0.25, 0.1, 0.15, and 0.1 for α-pinene, β-pinene, sabinene , Δ^3-carene, and limonene, respectively.

[b] values from Pankow et al., 2001, which were estimated by UNIFAC vapor pressure method at 308 K.

[c] This value includes the unidenfied aerosol mass from Δ^3-carene. The α value from Pankow et al., 2001 of the unidenfied aerosol mass from Δ^3-carene was first adjusted by a factor of 2 to better fit the smog chamber experiment data for Δ^3-carene and then weighted by 0.15 to account for the emission significance of Δ^3-carene. The final α value was grouped together with that of norpinonic acid

with the assumption that the unidentified aerosol mixture from Δ^3-carene has the same vapor pressure and molecular structure as norpinonic acid.

[d] X represents the total unidentified aerosol mass from α-pinene, β-pinene, sabinene, and limonene. Its a value was determined by first adjusting the individual a values in the experiments corresponding to β-pinene, sabinene , and limonene by factors of 1.6, 2.5, and 1.5, respectively, then further weighting its individual a values in each experiment by relative emission factors 0.4, 0.25, 0.1, and 0.1 for α-pinene, β-pinene, sabinene, and limonene, respectively. Its arbitrarily assigned low vapor pressure means that it remains in aerosol phase all the time. X was assumed to have the same structure as pinonic acid.

study but the experiments were all carried out in a dark system only with presence of O_3. However, the partitioning parameters used in current CMAQ stems from the two-product model fit data –the mass-based stoichiometric coefficients (a_1 and a_2) and the partitioning coefficient ($K_{om,1}$ and $K_{om,2}$)– in Griffin et al (1999), which were obtained from hydrocarbon/photooxidation experiments. Unlike other modeling studies such as Jenkin (2004) and Johnson et al. (2004 & 2005) which increased the partitioning coefficients of SOA components by 5 to 30 times to get a match between the predicted aerosol mass concentrations and the measured ones, the α values of the individual components were adjusted in this study to get a better fit between the predicted and measured aerosol yield.

In order to get the final individual product information, the adjusted stoichiometric coefficient values from single hydrocarbon experiments are further weighted by the relative emission factors 0.4, 0.25, 0.1, 0.15, and 0.1 for α-pinene, β-pinene, sabinene , Δ^3-carene, and limonene, respectively, determined by their emission significance and consistent with CMAQ. Table 3.1 presents the detailed property information for the individual products.

2.2 High-yield Aromatics (ARO1) and Low-yield Aromatics (ARO2)

The most important anthropogenic source for SOA formation is aromatic hydrocarbons, which are mainly from transport road emissions and solvent use (Photochemical oxidants review group, 1997). In the urban atmosphere, aromatic hydrocarbons comprise more than 25% of anthropogenic carbon emissions and are thought to contribute a major fraction to secondary organic aerosol (Odum et al. 1997b).

Table 3.2. SOA products and individual partitioning properties for high-yield aromatics (ARO1) and low-yield aromatics (ARO2).

Precursor	SOA Components	a_i	$p_i^{o* \text{ g}}$ (torr)	MW_i
ARO1	p-toluic acid [a]	0.085	9.91×10^{-3}	136
	2-hydroxybenzoic acid [b]	0.085	1.94×10^{-3}	138
	2,3-dihydroxy-4-oxobutanoic acid [c]	0.085	1.74×10^{-4}	134
	2,3-dihydroxy-4-oxopentanoic acid [c]	0.085	8.70×10^{-5}	148
	X [d]	0.085	2.00×10^{-6}	148
ARO2	3,4-dimethylbenzoic acid [a]	0.048	9.36×10^{-3}	150
	fluoranthene [e]	0.048	2.33×10^{-4}	202
	Phthalic acid [f]	0.048	1.78×10^{-4}	166
	4-methylphthalic acid [a]	0.048	1.06×10^{-4}	180
	pyrene [e]	0.048	5.17×10^{-5}	202
	chrysene [e]	0.048	5.08×10^{-6}	228

[a] Forstner et al., 1997.
[b] Jang and Kamens, 2001a.
[c] Kleindienst e al., 2004.
[d] Compound X added to better fit experimental data and assumed to have same structure as 2,3-dihydroxy-4-oxopentanoic acid.
[e] Harner and Bidleman, 1998.
[f] Ray and McDow, 2005; Zheng et al., 2002.
[g] Predicted at 308 K by Myrdal and Yalkowsky, 1997 using estimated T_b by Joback and Reid, 1987 with adjustment by Stein and Brown, 1994.

Numerous smog chamber experiments have been carried out to determine their potential ability to produce SOA (e.g., Izumi and Fukuyama, 1990; Odum et al., 1997a; Odum et al., 1997b; Kleindienst et al., 1999, 2000; Hurley et al., 2001; Jang and Kamens, 2001a). Odum et al. (1997b) classified the aromatic compounds into high-yield and low-yield aromatics based on their SOA production capability. High-yield aromatics, as defined by Odum et al (1997b), refers to the aromatic compounds with at most one methyl substituent and at most one ethyl substituent such as toluene, ethylbenzene and ethyltoulene. Low-yield aromatics are those containing more than one methyl substituents such as xylene and dimethylethylbenzenes. Although several chamber experiments on aromatic precursors provide some information on the molecular composition in the SOA phase (Forstner et al., 1997a; Jang and Kamens, 2001a; Kleindienst et al., 2004; Fisseha et al., 2004; Halmilton et al., 2005), complete aerosol product composition and experiment-derived quantitative stoichiometric coefficients are unavailable for aromatic precursors. Thus, in this study, the aromatic products used were selected with the intent to represent the wide range of chemical structures of the identified products for which the estimated saturation vapor pressures are lower than 10^{-2} torr at 308 K. Their identified presence in atmospheric aerosol was also a factor taken into consideration. The aromatic product information used for this study is shown in Table 3.2. Due to the lack of full product information, the same stoichiometric coefficients are assigned to each product, with the value determined by fitting the experimental data.

2.3 Internal Alkenes (OLE2)

Cyclohexene is a representative precursor for SOA produced from internal alkenes. Kalberer et al. (2000) and Pankow et al. (2001) provide detailed molecular information and chemical properties for the cyclohexene products that partition between the gas and aerosol phase. Those individual products, therefore, with minor adjustment for the vapor pressure of the unresolved product X (included to fit the experimental data) were used to obtain the information for the lumped products. The detailed individual product information is shown in Table 3.3.

Table 3.3. SOA products and individual partitioning properties for internal alkenes (OLE2).

Precursor	SOA Components[a]	a_i[a]	$p_i^{o*a, b}$ (torr)	MW_i
OLE2	2-hydroxy-pentanoic acid	0.0158	1.52×10^{-3}	118
	4-hydroxy-butanaldehyde	0.0303	1.24×10^{-3}	88
	oxalic acid	0.0703	2.03×10^{-4}	90
	malonic acid	0.0969	1.59×10^{-4}	104
	1,4-butanedial	0.0061	1.54×10^{-4}	86
	4-oxo-butanoic acid	0.0963	1.45×10^{-4}	102
	succinic acid	0.0096	9.64×10^{-5}	118
	glutaraldehyde	0.006	7.82×10^{-5}	100
	5-oxo-pentanoic acid	0.0688	7.49×10^{-5}	116
	glutaric acid	0.1064	5.09×10^{-5}	132
	adipaldehyde	0.0262	3.62×10^{-5}	114
	6-oxo-hexanoic acid	0.0714	3.53×10^{-5}	130
	adipic acid	0.0406	2.47×10^{-5}	146
	2-hydroxy glutaric acid	0.0331	1.40×10^{-7}	148
	2-hydroxy adipic acid	0.0187	7.76×10^{-8}	162
	X[c]	0.0505	1.00×10^{-5}	118

[a] values from Pankow et al., 2001.
[b] values from Pankow et al., 2001, which were estimated by UNIFAC vapor pressure method at 298k.
[c] Compound X represents all the unidentified mass. Its vapor pressure was determined by fitting experimental data. Product X was assumed to contain 2CH2 and 2COOH UNIFAC function groups, just the same structure as used in Pankow et al., 2001.

At default, in the framework of CMAQ v4.4, SOA from OLE2 is excluded because of low yield and high vapor pressure products. Preliminary simulations for this study indicated that olefin SOA had almost no effect on the simulation results because emissions of olefins in the selected simulation domain (Southeastern US focused on TN) are very small. Therefore, for application in this study, SOA production by olefins was turned off as it is in CMAQ v4.4. However, for applications focused on other domains, for example, northern California, where the emissions of olefins are pretty high and cannot be ignored as indicated by the emission files, the case would be quite different, and olefin production should be included.

2.4 Long Alkanes (ALK5)

Few data exists about secondary organic aerosol formation from long chain alkanes (Lim and Ziemann, 2005), which contains more than 7 carbons. Accordingly no detailed product information exists either. The low pressures of speculated products, however, render them expected SOA precursors. In this study, the products are assumed to be long-chain acids and diacids containing 7~30 carbons, which are presented in Table 3.4. The vapor pressures of the individual products fall into range 10^{-3} to 10^{-10} torr at 308 K. The organic compounds with such saturation vapor pressures are usually considered to be semi-volatile or non-volatile and will substantially partition into aerosol phase (Turpin et al., 2000; Stroud et al., 2004). Due to the absence of detailed experimental data, the same stoichiometric coefficients were assumed for each individual product in this study with the value determined by matching the original CMAQ results.

Table 3.4. SOA products and individual partitioning properties for long alkanes (ALK5).

Precursor	SOA Components	a_i	p_i^{o*a} (torr)	MW_i
	capric acid	0.011	8.61×10^{-3}	172
	undecanoic acid	0.011	4.45×10^{-3}	186
	dodecanoic acid	0.011	1.54×10^{-3}	200
	tridecanoic acid	0.011	5.41×10^{-4}	214
	pimelic acid	0.011	3.97×10^{-4}	160
	myristic acid	0.011	2.40×10^{-4}	228
	suberic acid	0.011	1.93×10^{-4}	174
	pentadecanoic acid	0.011	1.11×10^{-4}	242
	palmitic acid	0.011	1.01×10^{-4}	188
ALK5	azelaic acid	0.011	9.58×10^{-5}	256
	sebacic acid	0.011	4.77×10^{-5}	202
	heptadecanoic acid	0.011	1.99×10^{-5}	270
	stearic acid	0.011	5.40×10^{-6}	284
	eicosanoic acid	0.011	2.05×10^{-6}	312
	heneicosanoic acid	0.011	8.80×10^{-7}	326
	docosanoic acid	0.011	3.70×10^{-7}	340
	n-tricosanoic acid	0.011	1.53×10^{-7}	354
	tetracosanoic acid	0.011	6.21×10^{-8}	368
	hexacosanoic acid	0.011	9.69×10^{-9}	396
	nonxacosanoic acid	0.011	1.87×10^{-10}	452

[a] Predicted at 308 K by Myrdal and Yalkowsky, 1997 using estimated T_b by Joback and Reid, 1987 with adjustment by Stein and Brown, 1994.

2.5 Lumped Groups

The detailed products corresponding to each of the 5 SOA precursors were lumped together using the method of Bian and Bowman (Bian and Bowman, 2005). Given the parameters (p_i^o, MW_i, B_i, etc.) for the individual components, the parameters for lumped groups can then be determined. This lumped approach has been shown to approximate the detailed SOA mixture quite well (Bian and Bowman, 2002 & 2005). When more SOA products and experimental data become available, it is easy to

incorporate the up-to-date information into the model to improve the simulation results. Furthermore, the method allows exploring the composition effect on SOA production.

For application in this study, the individual products were divided into groups based on their vapor pressures at 308 K, using 10^{-5} torr and 10^{-9} torr as dividing lines. A total of 12 lumped products were obtained corresponding to 5 precursors, ALK5 and TRP1 each with 3 products, and ARO1, ARO2, and OLE2 each with 2 products. The lumping method was the same as that presented in Bian and Bowman (2002 & 2005) except that mole-based, instead of mass-based, coefficients were used to determine the molecular weight and the structure of the lumped products. Table 3.5 and Table 3.6 present the partitioning properties and the chemical structures, respectively, of the lumped groups.

Table 3.5. Partitioning properties of lumped groups.

Lumped Group	Model Name	α	p^{o*} (torr)[a]	MW	B (K)
TRP1					
a	SOA9	0.330	2.41×10^{-4}	163.7	17492
b	SOA10	0.346	5.76×10^{-7}	179.0	18084
c	SOA12	0.013	1.29×10^{-13}	184.0	18762
ARO1					
a	SOA7	0.255	8.49×10^{-5}	136.0	15999
b	SOA8	0.170	1.06×10^{-6}	148.0	14537
ARO2					
a	SOA5	0.144	3.78×10^{-5}	170.1	15949
b	SOA5	0.144	1.79×10^{-6}	201.5	16320
OLE2					
a	SOA3	0.645	7.02×10^{-5}	111.1	17812
b	SOA4	0.102	1.16×10^{-6}	133.4	13304
ALK5					
a	SOA1	0.099	3.86×10^{-5}	198.7	17826
b	SOA2	0.099	4.49×10^{-7}	279.1	11961
c	SOA11	0.022	6.83×10^{-10}	422.2	18131

[a] p^{o*} is corresponding to 298K, which is the reference temperature in CMAQ.

It is important to note that the properties and the structures of the lumped groups were determined directly on the basis of the partitioning and structural information of each individual product. Although the lumped groups cannot be identified as any real compounds, their partitioning characteristics are expected to represent the mixtures of corresponding real individual products. Performance evaluation of the lumped groups was conducted in both experimental and atmospheric systems as detailed in sections 3 and 4, respectively.

3. Performance Evaluation with Experimental System

Before the lumped groups were used in 3-D air quality model to represent the detailed SOA products, their partitioning properties were compared against smog chamber data, where available, and with those currently used in CMAQ, which are either the results of 2-product fit model or from theoretical prediction. The evaluation was performed based on aerosol yield Y with two M_0 ranges. The smaller M_0 range 0~ 10 ug/m^3 represents the typical ambient OA concentration; and the larger M_0 range 0~200 ug/m^3 is the aerosol concentration observed in smog chamber experiments. Figure 3.1 to 3.5 represents the partitioning performance of the lumped groups for TRP1, ARO1, ARO2, OLE2 and ALK5, respectively. In each figure, the lump-308 (or lump-310) and lump-298 curves represent the partitioning performance of the lumped groups at 308 K (or 310 K) and 298 K. CMAQ-308 (or CMAQ-310) and CMAQ-298 curves show the yields predicted with the partitioning parameters currently used in CMAQ at 308 K (or 310 K) and 298 K. Y-exp data points indicate the experimental data observed in smog

Table 3.6. UNIFAC structural properties of lumped groups.

Precursor	Lumped group	UNIFAC functional groups ID#												
		CH3	CH2	CH	C	ACH	AC	ACCH3	OH	ACOH	CH3CO	CH2CO	CHO	COOH
TRP1	a	2	1.83	1.77	1.38				0.53		0.55	0.45	0.48	0.07
	b	2	1.38	2.11	1				0.19		0.50	0.08	0.11	1.31
	c	2	2	2	1						1			1
ARO1	a			0.68		2.65	0.66	0.33	0.68	0.33			0.34	1
	b			2					2		1			1
ARO2	a					5.31	2.75	0.76						1.06
	b					7.98	4.51	0.37						0.75
OLE2	a	1	2.25	0.02					0.08				0.54	1.37
	b		2.15	0.44					0.44					2
ALK5	a	0.65	8.74											1.35
	b	0.85	16.1											1.15
	c	1	25.9											1

chamber experiments, which were measured at 310 K for ARO1 and ARO2 and 298 K for OLE2.

Overall, compared against experimental aerosol yields, where available, the lumped groups approximate the partitioning properties of the real aerosol mixture quite well. When no experimental data are available for the gas-phase precursor, i.e., ALK5 and TRP1, performance of the lumped groups was compared with those currently used in CMAQ. The general agreement between the simulation performance of the lumped groups and the current partitioning parameters in use suggests the lumped groups and the current parameters will predict very close SOA concentrations when ideal behavior is assumed, which is verified by the similar model values from CMAQ_L (simulation from the revised aerosol module but with no composition effects accounted for) and CMAQ in section 4.

3.1 Biogenics-TRP1

Figure 3.1 presents the predicted organic aerosol yield for TRP1 by using the 3 new lumped groups and the 2 original products in CMAQ. As a general biogenic precursor that represents a mixture of monoterpenes, no experimental data are available to directly evaluate the model performance of the final formulated parameters. Compared with the performance of current parameters in CMAQ, the new formulated ones give excellent agreement in the M_0 range from 0~10 µg/m^3 at 308 K, which is assumed to be the experimental temperature for all individual monoterpene experiments (actual experimental temperatures ranged from 308 to 320 K, with most near 308 K). Even for the large M_0 range from 0~200 µg/m^3, the difference in the predicted aerosol

yields is pretty small. Although the difference becomes pretty large at 298K at higher M_0, this will have no much effects on the SOA concentration prediction when applied in atmospheric aerosol modeling considering the typical ambient OA concentration is in the range of 0-10 $\mu g/m^3$. Figure 3.1 also indicates that the partitioning of the lumped groups have smaller temperature dependence than current model species in CMAQ. This smaller temperature dependence is not determined only by the B values of the lumped groups, which are less than 18762 K, the value for all products in the original CMAQ, but also related to differences in the combination of stoichiometric coefficients and vapor pressures used for the individual products.
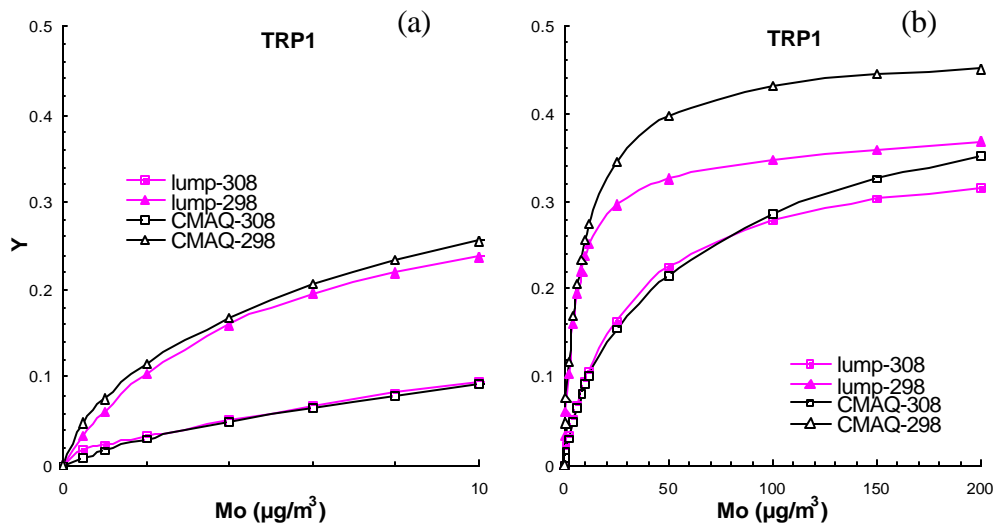

Figure 3.1. Comparison of organic aerosol yield predicted by the 3 lumped groups in this study and the 2 products in CMAQ as a function of organic aerosol mass for biogenic monoterpenes.

3.2 High-yield Aromatics (ARO1)

The comparison of the predicted organic aerosol yield for high-yield aromatics is shown in Figure 3.2. Compared against the smog chamber data, which are from Odum et al. (1997b), overall the lumped groups predict a higher aerosol yield at higher M_0 both at 308 K and at 298 K. However, when look at yield prediction in the M_0 range of 0-10 $\mu g/m^3$, which is of much more importance, the lumped groups predict a slightly lower yield for 298 K and Mo<5 than the current parameters in CMAQ; For M_0<10, almost same aerosol yields are predicted by the lumped groups and the parameters currently in use. This agreement indicates that in the M_0 range relevant to atmospheric application the lumped groups present a very good fit of the experimental data. The performance of the lumped groups is certainly not perfect but based on current available product information, still an excellent approximation.
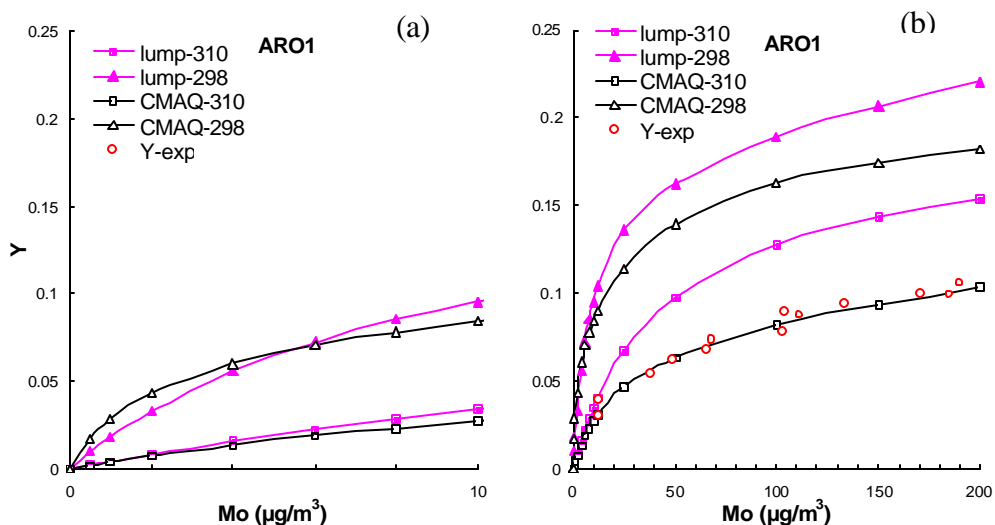

Figure 3.2. Comparison of predicted and measured organic aerosol yields as a function of organic aerosol mass for high-yield aromatics.

3.3 Low-Yield Aromatics (ARO2)

Compared with the lumped groups for ARO1, those for ARO2 approximate the partitioning of the detailed product mixture much better over the whole M_0 range. The
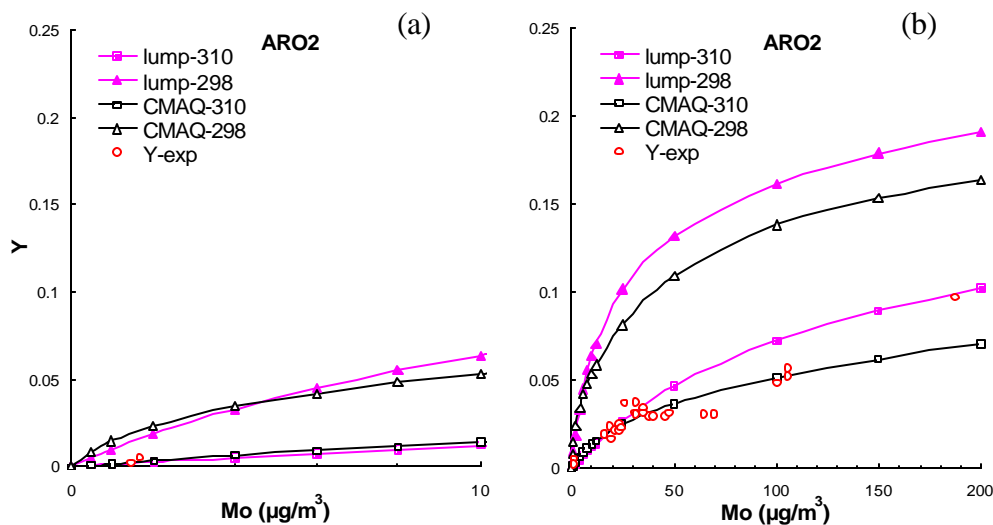

Figure 3.3. Comparison of predicted and measured organic aerosol yields as a function of organic aerosol mass for low-yield aromatics.

measured aerosol yield data come from Odum et al (1996 & 1997b). As shown in Figure 3.3, at the experimental temperature 310K, both the lumped groups in this study and the model species from 2-product fit model used in CMAQ give excellent prediction of the experimental aerosol yield over the organic mass range 0~10 $\mu g/m^3$. When the organic aerosol concentration is high, the simulation with lumped groups tends to give higher prediction than CMAQ. Just as ARO1, no complete list of SOA products corresponding to ARO2 is available to formulate the lumped groups. Product selection is somewhat arbitrary with the intention to represent the chemical structure characteristics and

partitioning properties of the whole mixtures. The lumped groups can be easily updated to incorporate new product information when becomes available.

3.4 Internal Alkenes (OLE2)

Figure 3.4 compares the predicted and measured aerosol yield for internal alkenes. The full list of identified products corresponding to cyclohexene (Kalberer et al. 2000 and Pankow et al. 2001) was used to formulate the lumped groups. The complete product
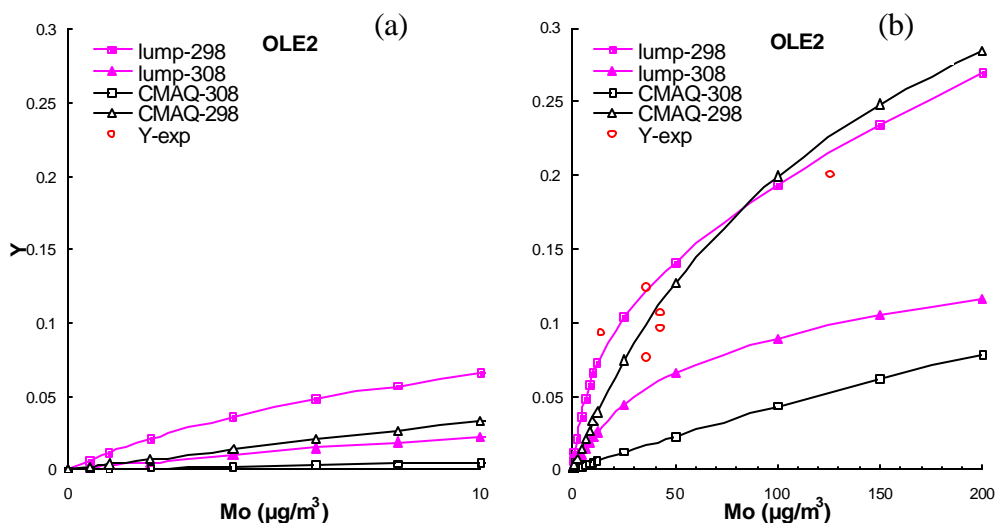
Figure 3.4. Comparison of predicted and measured organic aerosol yields as a function of organic aerosol mass for internal alkenes.

information precludes much uncertainty in product selection. Over the whole M_0 range, the simulation with lumped groups gives excellent prediction of the measured aerosol yield at the experimental temperature 298K. Compared with the performance of model species in CMAQ, the lumped groups predicts higher aerosol yield at low M_0 value while lower aerosol yield at high M_0 value. However, both the lumped groups and the current partitioning parameters in CMAQ provide a good fit of the experimental data over the M_0

range of 0-140µg/m^3, which suggests that the difference may be caused by the uncertainties in empirical fit and the vapor pressure estimates, which influence the partitioning coefficients of the lumped groups.

3.5 Long Alkanes (ALK5)

The aerosol yields as a function of organic aerosol mass for ALK5 predicted by using either the lumped groups or the model species in CMAQ are presented in Figure 3.5. Compared with the model species in CMAQ, whose partitioning properties is
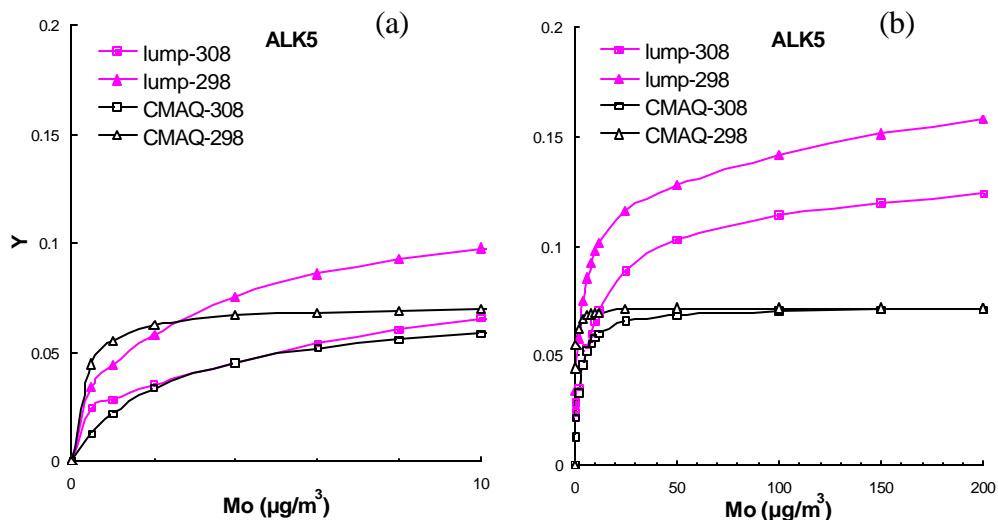
Figure 3.5. Comparison of organic aerosol yield predicted by the lumped groups and current parameters in CMAQ as a function of organic aerosol mass for long chain alkanes.

estimated based on theoretical prediction from Strader et al. (1999), the lumped groups predicts higher aerosol yield most of the time. Lim and Ziemann (2005) reported that for the reactions of C_8-C_{15} n-alkanes with OH in the presence of NO_x, their SOA yields at ~ 25ºC can be from about 0.5% to about 50%. The author also mentioned that although the

SOA yields for C_8 to C_{10} increase gradually from about 0.5% to about 4%, the yields for C_{11} to C_{15} go up quickly from 8% for C_{11}, 25% for C_{12}, 49% for C_{13}, to greater than 50% for C_{14} and C_{15}. Due to the limited information on SOA production from long-chain alkanes, the lumped groups for ALK5 give a reasonable performance.

4. Performance Evaluation with Atmospheric System

In atmospheric application, the organic aerosol module in CMAQ was revised to use the 12 lumped groups, instead of the original 10 model species, to simulate the SOA production but with the assumption of ideal behavior, i.e., activity coefficients for all the 12 lumped groups were set to 1 with no consideration of composition effects. Simulation results from CMAQ framework incorporated with the revised aerosol module but with no composition effects on SOA production accounted for (referred as CMAQ_L hereafter) are compared with those from the original CMAQ (referred as CMAQ hereafter). Simulation results can be used to compare the partitioning performance of the lumped groups in atmospheric application against that of the model species currently used in CMAQ with assumption of ideal behavior.

Table 3.7 summarizes the major process configuration commonly for both sets of simulations. The difference in organic aerosol module is presented in Table 3.8. Briefly stated, for SOA production, CMAQ_L uses the 12 lumped groups formulated based on the vapor pressures of identified individual SOA components, instead of the 10 empirical model species in CMAQ, to represent the SOA products corresponding to 5 categories of gas-phase precursors. The lumped groups, which include chemical structure information,

Table 3.7. Configuration for the major processes commonly used in simulations CMAQ_L and CMAQ.

Process	Configuration
CMAQ framework version	4.4
Gas-phase chemistry	Saprc99
Gas-phase chemistry solver	Euler backward iterative (EBI) solver
Aqueous-phase chemistry	RADM (bulk)
Horizontal advection	Piecewise parabolic method
Vertical advection	Piecewise parabolic method
Horizontal diffusion	K theory
Vertical diffusion	K theory
Dry deposition	Resistance transfer approach
Wet deposition	Henry's law equilibrium for gases; complete scavenging for accumulation and coarse mode particles; transit scavenging for aiken mode particles
Aerosol processes	
Size distribution	3 modes
Inorganic species	Thermodynamic equilibrium with ISOPROPIA
Organic species	Refer to table 3.8
Coagulation	Modal approach of Binkowski and Shankar (1995)
Nucleation	Parameterization of Youngblood and Kreidenweis (1994)
Condensational growth/shrinkage by voltalization	Modal approach of Binkowski and Shankar (1995) for inorganic species; for organic species, mass distributed immediately after condensation in proportion to the ratio of organic aerosols in Aiken and accumulation modes at the end of the previous step
Gas/particle mass transfer	Full equilibrium approach

make it feasible to explore the composition effects on SOA production, as will be discussed in Chapter IV. However, for the simulations presented in this chapter, when all the activity coefficients are fixed to 1, i.e., when no composition effects are considered, it is expected that CMAQ_L and CMAQ would give similar organic aerosol concentration predictions. This is due to the fact that the partitioning parameters for lumped groups in CMAQ_L and for model species in CMAQ are developed based on the same sets of smog chamber data.

Table 3.8. Overview of the organic aerosol module in CMAQ_L and CMAQ.

Model version		CMAQ	CMAQ_L
SOA precursors		6 categories	5 categories[a]
SOA	# of products	10	12
	$C_{sat(T)}$	experimentally derived empirical parameters with temperature adjustment	formulated based on the partitioning parameters of identified individual products with temperature adjustment
POA		NA[b]	NA[b]

[a] In the modified module, cresol is treated as high yield aromatics.
[b] Not applicable. No POA composition is needed without consideration of composition effects.

4.1 Modeling Domain and Episodes

Figure 3.6 presents the target simulation domains. The coarse grid domain with horizontal resolution of 32km covers the entire continental U.S. and surrounding areas and is divided into 178×124 grid cells. The 8km sub-domain has 122×122 cells, which covers the whole Tennessee and Kentucky states and large part of Georgia, Alabama, Mississippi, Arkansas, Illinois, Indiana as well as part of Ohio, West Virginia, Virginia, North Carolina, South Carolina, Missouri, and a little bit of Louisiana, Iowa and Pennsylvania. The modeling domain extends from the surface to a height of about 15,000 m, determined by the vertical extent of the meteorological-modeling domain, and is divided into 18 vertical layers with finer resolution near the surface consistent with those in the emission files. The specific sigma levels of the layers, i.e. the height of layer defined using the difference between the layer pressure (P) and the pressure value assigned for the model top (P_{top}) normalized by the difference between the bottom surface pressure (P_{srf}) and P_{top} (sigma = $(P-P_{top})/(P_{srf}-P_{top})$), are as follows: 1.000 0.995 0.990 0.985 0.980 0.970 0.960 0.945 0.930 0.910 0.890 0.865 0.840 0.780 0.700 0.600 0.450

0.300 0.000. July 03 – July 17, 1999 was selected for the simulations because this was the period during which extensive monitoring was carried out in the Southern Oxidants Study in Nashville/Middle Tennessee in 1999 (SOS99-Nashville) and O_3 and particulate matter (PM) built up throughout the region.
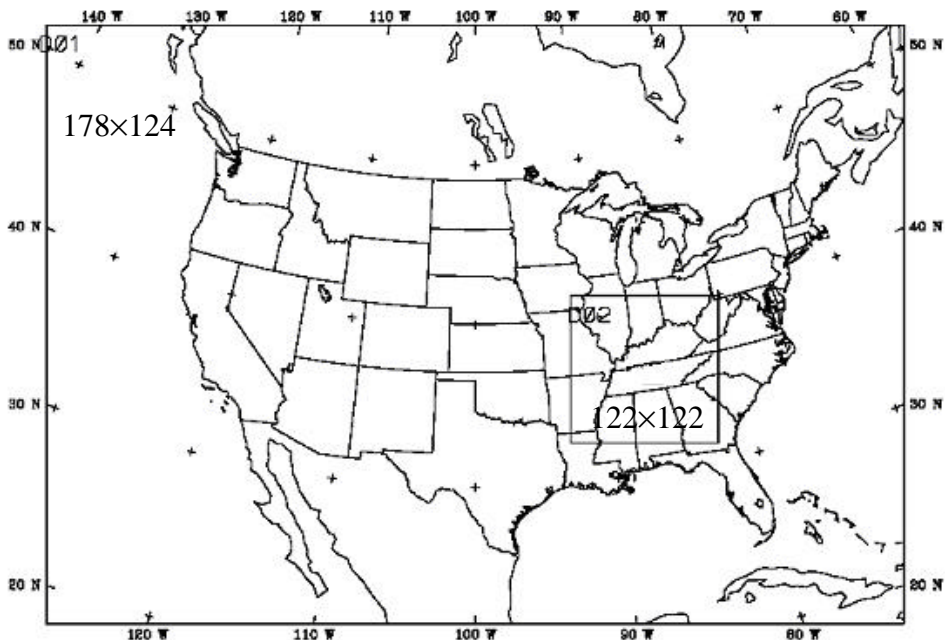

Figure 3.6. 32-km continental U.S. and 8-km Southeast U.S. modeling domains.

For model evaluation, organic carbon ($OC_{2.5}$, sum of primary organic carbon and secondary organic carbon) field measurements corresponding to $PM_{2.5}$ (particulates with aerodynamic diameter less than 2.5 μm) were used from 2 routine monitoring networks (the Interagency Monitoring of Protected Visual Environments -IMPROVE and the Southeastern Aerosol Research and Characterization project -SEARCH) and 1 field measurement campaign (the Southern Oxidants Study (SOS) Nashville study in 1999). In

the IMPROVE network, two 24-h samples, on Wednesdays and Saturdays, are collected each week beginning at midnight local time (Malm et al., 1994). Four IMPROVE sites with ambient data available are located in the target finer grid simulation domain and were used for model evaluation: Mammoth Cave National Park [MACA], KY; Great Smoky Mountains National Park [GRSM], TN; Shining Rock Wildness Area [SHRO], TN; and Sipsey Wildness Area [SIPS], AL. In the SEARCH network, daily $OC_{2.5}$ concentrations of the 4 sites located in the target sub-domain were used: 2 rural sites (Yorkville [YRK], GA and Centreville [CTR], AL) and 2 urban sites (Jefferson Street [JST], Atlanta; North Birmingham [BHM], AL (Hansen et al., 2003). In addition, hourly $OC_{2.5}$ data only available at JST are also used for model evaluation. Daily and hourly $EC_{2.5}$ concentrations (the elemental carbon concentrations corresponding to $PM_{2.5}$) were used to derive the SOA concentrations at JST to evaluate the model performance. Data used for model evaluation also include the daily average $OC_{2.5}$ data collected every other day at Dickson (DI) and Hendersonville (HEN) and hourly $OC_{2.5}$ data collected at Cornelia Fort (CF) during SOS99-Nashville.

4.2 Model Inputs

In order to run CMAQ, emission data specific to particular gas phase chemistry and meteorological data are needed. In this study, the Meteorology-Chemistry Interface Processor (MCIP) version 2.3 was used to prepare meteorological input data for CMAQ from MM5 outputs, which were provided by EPA from the separate meteorology model MM5 (Pennsylvania State University (PSU)/NCAR Mesoscale Modeling System Generation 5) with four-dimensional data assimilation. The ready-for-use emission input

data for CMAQ were also obtained from EPA and were prepared by EPA for the SAPRC 99 lumped species gas-phase chemistry mechanism using Continuous Emission Monitoring data for electric utilities, weekly temporal adjustments for ammonia emissions, and BEIS3.1 biogenic emission model. For simulation on the larger 32-km resolution domain, the CMAQ default initial values typical of a clean background atmosphere (Byun and Ching, 1999) were used as initial conditions (ICs) and a typical spin-up of two days was used to minimize the influence of ICs; also, boundary conditions (BCs) used the CMAQ default boundary values (Byun and Ching, 1999). The ICs and BCs for 8-km resolution domain were prepared from the simulation results corresponding to coarse grid domain, thus minimizing boundary effects.

4.3 Simulation Results and Analysis

The simulation results from CMAQ_L and CMAQ are presented in two groups: 1) comparison of the simulated SOA concentrations for CMAQ_L and CMAQ as detailed in section 4.3.2; 2) comparison of the simulated SOA and OA (SOA+POA) concentrations against ambient data, which are presented and analyzed in from section 4.3.3 to section 4.3.6. Before the comparison can be made, the procedures used to manipulate the simulation results are first described in section 4.3.1.

4.3.1 Data Reduction

In CMAQ, the size distribution of aerosol is represented by 3 log-normal modes: aitken mode, accumulation mode and coarse mode (Binkowski and Roselle, 2003). CMAQ v4.4 does not directly provide the mass of components within $PM_{2.5}$, but it does

provide the diagnostic parameters of each mode, i.e., the standard deviation σ_g and the

mean diameter D_g. Usually speaking, the aerosol mass in aitken mode will completely

fall into $PM_{2.5}$; coarse mode will contribute less than 1% of its mass to $PM_{2.5}$. However,

the fraction of the mass in accumulation mode fitting into $PM_{2.5}$ can vary from 0.6 to 1.

In order to directly compare the simulated results against the field data, first the mass

concentration of the components corresponding to $PM_{2.5}$ were calculated using the same

procedure as in the recently released CMAQ v4.5, which is adapted from Jiang et al

(2006).

Briefly, the 2.5 um size cut was first transformed to its equivalent Stokes

diameter, $D_{st,k}$, for each mode using the following equation,

$$D_{st,k} = 0.5 \times \left(\sqrt{\frac{4 \times 2.5 \times (2.5 + B) \times 1000}{r_k}} + B \times (B - 1.0) \right) \qquad (3.1)$$

where r_k (kg/m^3) is the average density of the particles in each mode obtained by

dividing the total mass by the total volume of the particles in each mode; B (μm) is the

Cunningham slip-correction approximation parameter and is given the value of 0.21470.

Then the fraction of mass in PM2.5, f_k, of each log-normal mode was calculated by

$$f_k = 1 - \frac{1}{2} erfc \left(\frac{\ln D_{st,k} - \ln D_{g,k}}{\sqrt{2} \ln s_{g,k}} - \frac{3}{\sqrt{2}} \ln s_{g,k} \right) \qquad (3.2)$$

where k refers to aitken, accumulation and course mode. $erfc$ is the complimentary error

function. Finally the mass concentration, M, of a given component in PM2.5 is the sum of

the mass concentration of the component in each mode, T_k, multiplied by the

corresponding fraction f_k,

$$M = \sum_k T_k \times f_k \qquad (3.3)$$

Thus, the difference between CMAQ_L and CMAQ comes from two aspects: firstly, the absolute amount of SOA in aitken and accumulation modes may differ due to the difference in partitioning parameters applied; secondly, the fraction of SOA mass in each mode classified as $PM_{2.5}$ can also change due to different standard deviation and mean diameter of each mode caused by the first effect. This second effect, though not significant, not only affects the organic aerosol concentration in $PM_{2.5}$ but also affects the total $PM_{2.5}$ mass concentration due to the assumption of aerosol as internally mixed mixture.

4.3.2 Comparison of Predicted SOA concentrations

In this section, comparison of the simulated SOA concentrations from CMAQ_L and CMAQ is presented. In each figure, CMAQ represents the simulation results from the original modeling system; CMAQ_L represents the output from the revised aerosol module with activity coefficients for all the lumped groups set to 1.

Figure 3.7 and Figure 3.8 present the temporal distribution of predicted SOA in $PM_{2.5}$ for JST (an urban site) and YRK (a rural site), respectively. In each figure, part (a) shows the sum of predicted SOA concentrations from both biogenic and anthropogenic sources corresponding to the target grid with horizontal resolution of both 32km and 8km; part (b) and part (c) present the biogenic (AORGB) and anthropogenic (AORGA) SOA concentrations in the target grid with grid size of 32km and 8km, respectively. The total SOA as well as AORGB and AORGA concentrations are plotted for the whole simulation period from 07/03 0:00 to 07/17 0:00. Same temporal variation, as indicated by the figures, was predicted at both sites by simulations CMAQ and CMAQ_L.
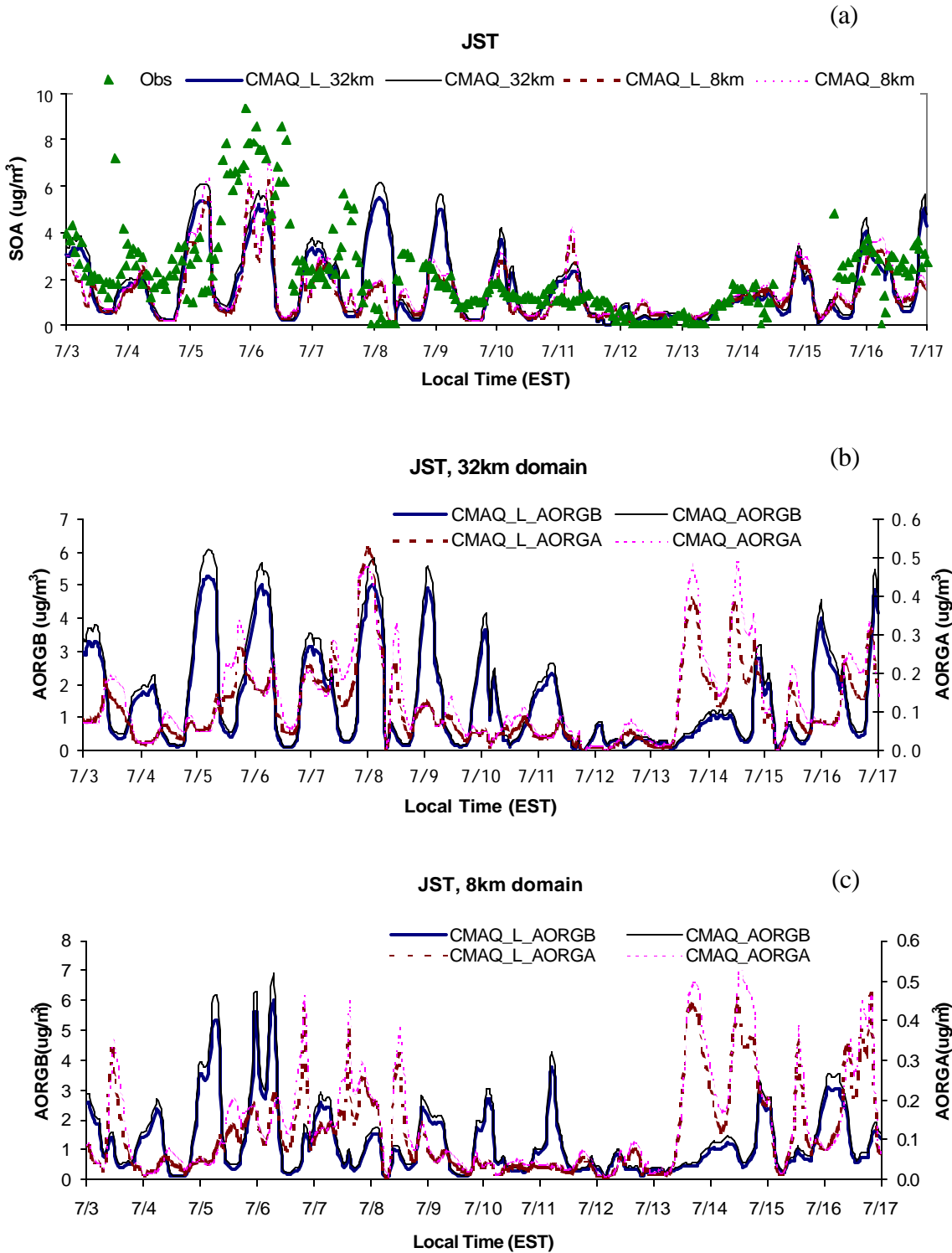
Figure 3.7. Temporal distribution at JST of simulated SOA concentration with horizontal resolution of 32km and 8km against hourly observations (a); simulated biogenic and anthropogenic SOA concentration with horizontal resolution of 32km (b) and 8km (c).

However, CMAQ predicts higher SOA concentration than CMAQ_L all the time, especially at the points with daily maximum. Further check on the respective biogenic and anthropogenic SOA concentrations presented in part (b) and part(c) indicates that for the simulation on the 32-km grid size domain, CMAQ_L predicts less AORGB than CMAQ during the whole simulation period; however, occasionally predicts higher AORGA concentrations. Simulation results also indicate that AORGB dominates the total concentration of SOA, which is supported in other studies as well on quantifying the SOA contribution to $PM_{2.5}$ ambient aerosol (Lewis et al., 2004; Tanner et al., 2004).

The difference between the simulated SOA concentrations is caused by the different partitioning parameters applied in CMAQ_L and CMAQ with consideration of all the same input data and the same treatment of other aerosol processes. The output concentration of SOA reflects the combined effects of partitioning parameters on the related aerosol processes. The lower SOA concentration predicted by CMAQ_L can be expected by examining the partitioning performance of the lumped groups in experimental system in the smaller M_0 range. The simulated POA concentrations at JST are less than 8 ug/m^3 most of the time while at YRK are less than 4 ug/m^3 during the whole simulation period. For the M_0 range 0-8 ug/m^3, the lumped groups for TRP1 tend to predict lower aerosol yield than the parameters in CMAQ, which agrees with the simulation results considering the overwhelming contribution of AORGB to the total SOA concentration.

The different temporal distribution of predicted SOA concentrations corresponding to the coarse and fine grid domains reflect the effect of grid resolution on the simulation results. Both the emission data and the meteorological data corresponding
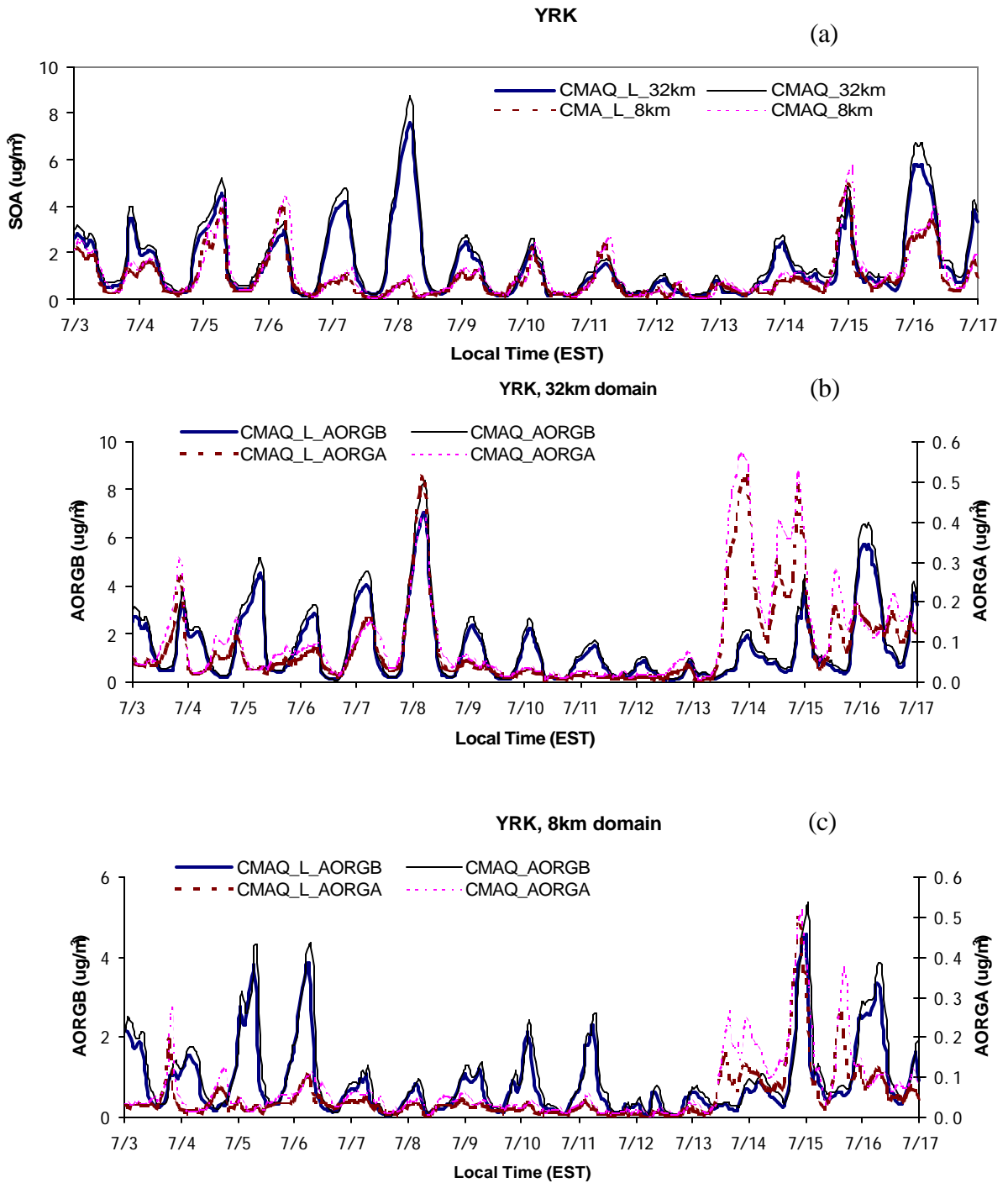
Figure 3.8. Temporal distribution at YRK of simulated SOA concentration with horizontal resolution of 32km and 8km (a); simulated biogenic and anthropogenic SOA concentration with horizontal resolution of 32km (b) and 8km (c).

to the grids where the monitoring sites are located are affected by the selected simulation resolution. The non-linearity of the chemical reactions also contributes to the simulation results difference between different grid resolutions, i.e., the change in emissions may not result in the same kind of changes in all the compounds related.

4.3.3 Comparison of Predicted SOA Concentrations against Ambient Data at JST.

Due to the current absence of direct chemical analysis methods to distinguish SOA from POA, indirect methodologies have to be used to evaluate SOA formation in ambient aerosols, for example EC tracer method. This method has been used in many applications to estimate the ambient SOA concentration (Turpin and Huntzicker. 1995; Strader et al., 1999; Castro et al., 1999; Lim and Turpin, 2002; Cabada et al., 2004). In this method, EC, which is mainly emitted from combustion processes, is used as a tracer of the primary OC. The application of EC tracer method is based on the fact that primary OC and EC mostly come from the same emission sources. However, much difference exists in the OC/EC emission ratios for different emission sources. Therefore, in order to get meaningful value of OC_{pri}/EC for an application, the meteorological condition and characteristics of local emissions must be taken into consideration when the ambient measurements are analyzed. In addition to use the ambient measurements, the OC_{pri}/EC ratio for an area of interest can also be determined by developing an emission inventory of the main primary sources using emission factors (Cabada et al., 2002).

Lim and Turpin (2002) estimated the secondary organic carbon concentration in Atlanta, GA using EC tracer method during the Atlanta Supersite Experiment from August 3 to September 1, 1999 (Solomon et al., 2003). Although the exact time period is

different from the simulation time selected for this study (from July 3 to July 17, 1999), it is reasonable to use their (OC/EC) $_{pri}$ ratio to get the concentration of the secondary organic carbon (OC$_{sec}$) because they are both in the summer season of the same year and the aerosol samples were collected from the same sampling site.

To apply the Lim and Turpin results to the SEARCH data used in this study, a correction is made to account for different OC/EC measurement methods. The concentrations of OC and EC were determined using thermal-optical transmittance (TOT) method in Lim and Turpin (2002) while thermal-optical reflectance method (TOR) was used to determine the concentration of OC and EC in SEARCH. The TOR method was also used to define the split between OC and EC for most of the emission sources for NEI99 (Yu et al., 2004), which is the basis to get the emission files for this study. Chow et al (2001) have investigated the effect of these two methods on the determined OC and EC concentrations. It has been found that the OC concentration determined by TOR is 10-15% lower and EC concentration by TOR is typically two times higher than those by TOT. Thus, in this study the EC concentration obtained for JST in SEARCH is divided by 2 to account for this difference in the thermal evolution protocols. Lim and Turpin (2002) suggested a value of 2.1 as an upper limit for the OC$_{pri}$/EC ratio and the noncombustion primary OC to be zero considering the small intercept for data in the lowest 10% by OC$_{tot}$/EC ratio. OC$_{tot}$ represents the total observed concentration of primary and secondary organic carbon. For application in this study, therefore, OC$_{pri}$/EC = 1.05, primary organic carbon (OC$_{pri}$) = 1.05×EC and secondary organic carbon (OC$_{sec}$) = OC$_{tot}$ − OC$_{pri}$ are used to get the concentration of secondary organic carbon. SOA concentration was calculated by multiplying the obtained OC$_{sec}$ by a factor of 1.4, the

typical organic molecular weight per carbon weight commonly used to convert the mass concentration of organic carbon to organic aerosol (Turpin and Lim, 2001).

Before the comparison is presented, it should be pointed out first that the hourly measurement and the daily average data are not from the same data source. For the hourly data, TC is measured with the R&P 5400 Particulate Carbon Monitor and EC measured with the Radiance Research PSAP. OC was calculated as the difference between the concentration of total carbon (TC) and elementary carbon (EC), when both are available. The problem is that the measured hourly concentrations of TC and EC are neither the same as measured by TOR nor as by TOT, but tend to be a bit closer to those by TOT (Eric S. Edgerton 2006, personal communication). For data analysis here, hourly TC concentration was assumed to be comparable to that determined by TOR. During the periods from 7/7/99 16:00 ~ 7/7/99 7:00 and 7/8/99 19:00 ~ 7/11/99 23:00, when TC is available but EC is not, the original OC concentration was calculated as $0.71 \times TC$, with 0.71 is the average OC/TC from 7/3 to 7/17 at JST. The original hourly OC concentration was scaled by multiplying 3.09/3.68, the average OC concentration during the selected simulation period calculated from the hourly OC concentration data over that computed from the daily average OC data available on SEARCH data website. Then the average OC concentrations during the whole period from 7/3 to 7/17 is the same no matter what data are used. However, the daily average OC concentration on specific day computed from the hourly data is not the same as that directly from SEARCH. The data from SEARCH are used in the comparison on daily average basis in order to minimize uncertainties. This data manipulation intends to make the OC hourly data comparable to those determined by TOR. Finally EC was calculated by extracting the scaled OC

concentration from the original TC concentration. Note although the same average OC concentration computed from both hourly and daily data for the simulation period from 7/3 to 7/17, the average concentration of derived SOA concentration over the whole simulation period is not the same. The average SOA concentration calculated using the hourly data is 2.18 μg/m^3 while using the daily data is 2.50 μg/m^3.

Figure 3.7 (a) compares the hourly predictions from CMAQ and CMAQ_L against hourly measurements of the SOA concentration at JST. The SOA concentration was calculated based on the procedure described above. When the calculated SOA is negative, no SOA is supposed to form at that moment. The simulations on both grids reproduce the temporal distribution of SOA concentrations reasonably well except the apparent failure from the noon on 7/7 to 7/8. Significant underprediction occurs in the afternoons when the SOA concentration is low. However, during early morning period overprediction is a problem such as on 7/5, 7/8, 7/9, 7/10 and 7/11 for the coarse grid prediction and on 7/5 and 7/11 for fine grid prediction. Even so, throughout the whole simulation period, simulations on both grids tend to slightly underpredict the ambient SOA concentrations. The percent underpredictions in the mean predictions for the coarse grid simulation and fine grid simulation are 24% and 37% for CMAQ_L and 12% and 28% for CMAQ, respectively.

Figure 3.9 (a) and (b) presents 24-hr average simulated SOA concentration in PM$_{2.5}$ along with the observations at JST from 32km-grid resolution domain and 8km-grid resolution domain, respectively. No observations are available on 7/7, 7/8, 7/9 and 7/10. It can be seen that CMAQ_L and CMAQ both underpredict the concentration of SOA at JST during the whole simulation period except on 7/5. The percent

underpredictions for CMAQ_L in the mean predictions are 41% for coarse grid simulation and 44% for fine grid simulation while for CMAQ the corresponding values are 31% and 35%, respectively. For other monitoring sites selected for this study, no continuous/semi-continuous OC and EC sample data are available to do the EC tracer analysis.

The values used to obtain the concentration of secondary OC (1.05) and the factor to convert the concentrations between secondary OC and SOA (1.4) both present somewhat uncertainties. 1.6 and 2.1 were suggested to be more accurate than 1.4 to represent the average organic molecular weight per carbon weight for urban and nonurban aerosol, respectively (Turpin and Lim, 2001). In addition, interpretation of the measurement data presents a big challenge due to the different sampling protocols and operation procedures to split OC and EC. During this data interpretation process, some uncertainties was involved. However, it is very important to account for the data inconsistency caused by different OC/EC measurement methods.

Another important source of uncertainty comes from the way to make data comparison (the incommensurability uncertainty, Seinfeld and Pandis, 1998; Eder and Yu, 2006). The ambient data is measured at a specific point but the predicted value is a volumetric averaged value over the whole grid. Scatter plots of the coarse-grid hourly SOA predictions against observations depicts a large scatter with correlation coefficients around 0.26 (Figure 3.11 (a) and (b)). However, the Scatter plots of the $OM_{2.5}$ predictions (SOA plus POA) versus observations (Figure 3.11 (c) and (d)) show that vast majority of the predictions fall within a factor of two of the observations and the correlation coefficients (~0.49) are all increased dramatically compared with those between SOA
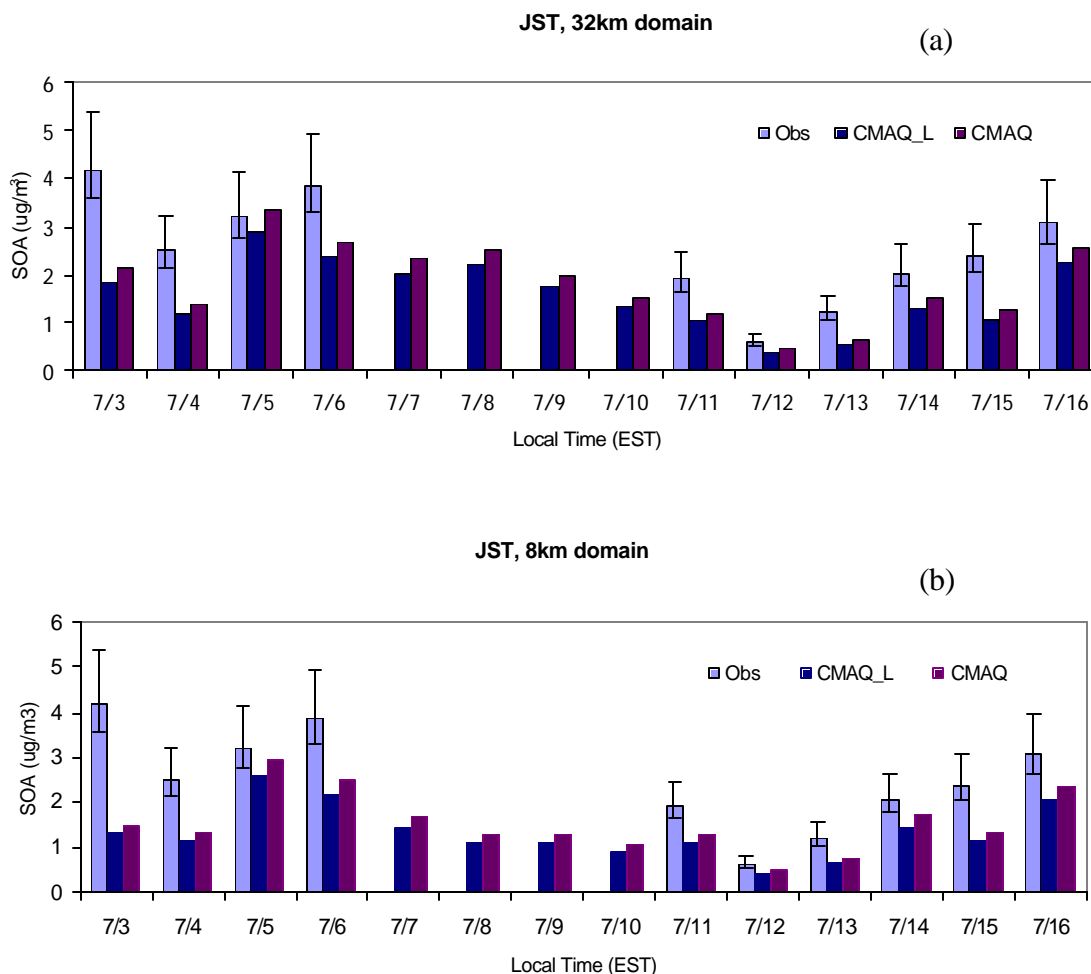
74

(a)

(b)

Figure 3.9. 24-hr average simulated SOA concentrations compared with observations for JST, with horizontal resolution of (a) 32km; (b) 8km. The observations were calculated using a value of 1.05 for the primary OC/EC ratio and a factor of 1.4 for conversion between the concentrations of calculated secondary carbon and secondary organic aerosol. The error bars represent a range of 1.2 to 1.8 to convert the concentration of secondary OC to that of secondary organic aerosol.

predictions and ambient SOA concentrations (~0.26). The difference in data distribution suggests that the uncertainties involved in deriving SOA concentrations are notable. The $(OC/EC)_{pri}$ ratio may be not a constant throughout the simulation period. Some of the "observed" SOA probably should be classified as POA or the modeled POA is

overpredicted. The underprediction of SOA by the models may be not that much as indicted in this study.

4.3.4 Comparison of hourly organic aerosol predictions against measurements at Jefferson Street (JST), Atlanta, GA

Figure 3.10 presents the temporal distribution of predicted and measured organic aerosol concentration in $PM_{2.5}$ ($OM_{2.5}$) at JST. Note that the ambient $OM_{2.5}$ data was adjusted from the original values to account for the difference in measurement methods.
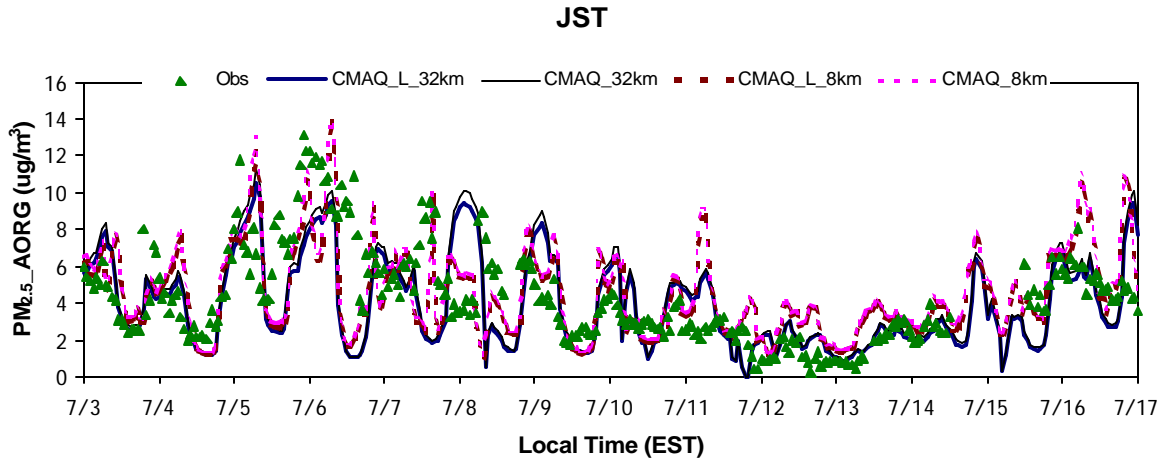
JST

Figure 3.10. Comparison of predicted hourly $OM_{2.5}$ concentrations against measurements at Jefferson Street (JST), Atlanta, GA. The factor of 1.4 was used to obtain the concentration of organic aerosols from the concentration of observed organic carbon.

Generally speaking, CMAQ_L and CMAQ predict very close $OM_{2.5}$ concentrations on the same grid resolution throughout the whole simulation period except at certain points, for example, during the period from 7/7 22:00 to 7/8 6:00 for the coarse grid simulation. The coarse grid prediction reproduces well the $OM_{2.5}$ temporal variation on 7/3, 7/12 and 7/13 while the fine grid simulation makes better agreement with the ambient data on7/7, 7/8 and 7/9. The mean $OM_{2.5}$ predictions, calculated by excluding the data points without
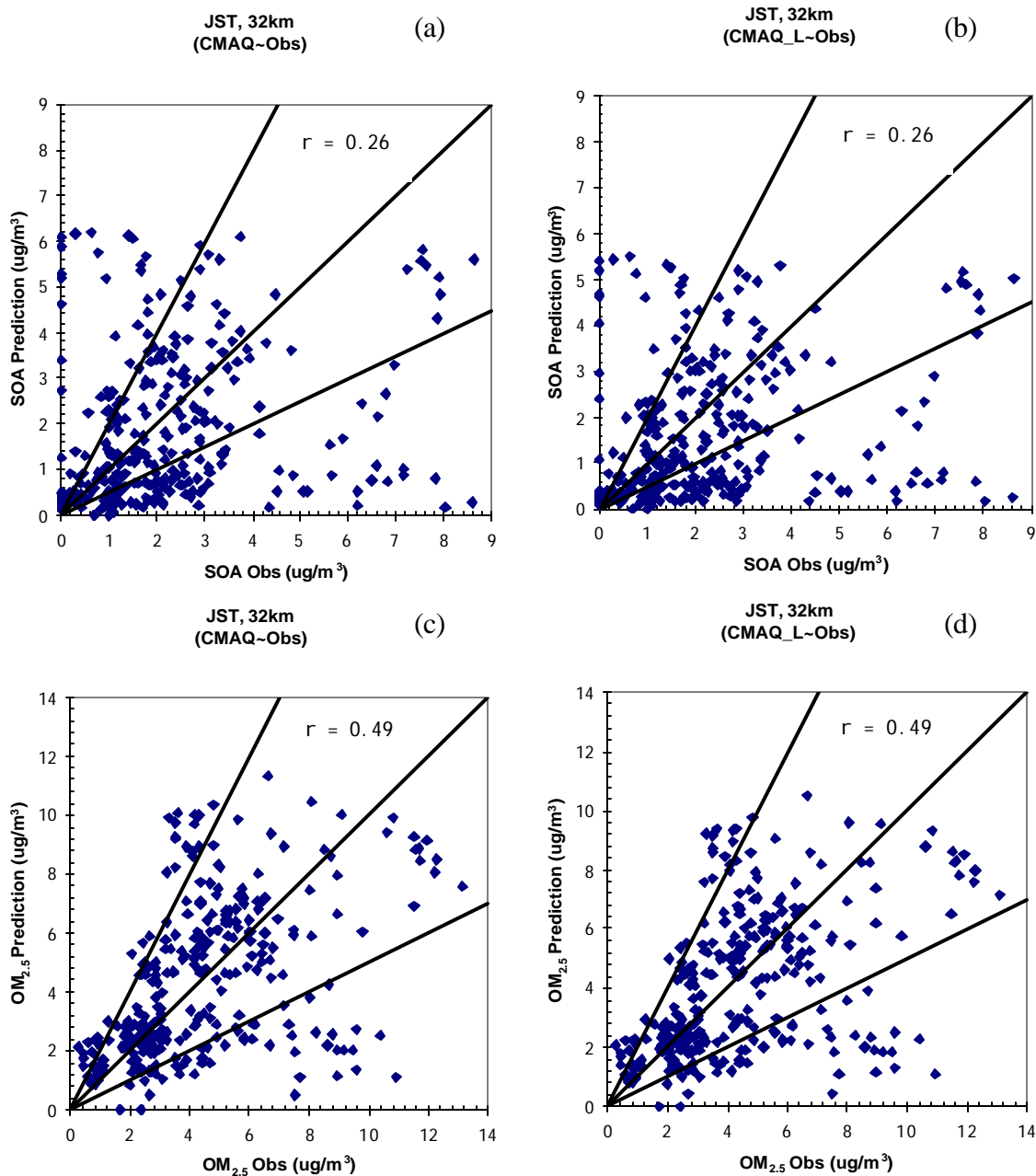
Figure 3.11. Scatter plots of hourly SOA and OM$_{2.5}$ coarse-grid predictions from CMAQ and CMAQ_L (abscissa) versus observations (ordinate). 1:1, 1:2 and 2:1 lines are provided for reference.

corresponding ambient data, on the coarse grid domain are 4.02 and 4.27 $\mu g/m^3$ for CMAQ_L and CMAQ, respectively, while for the fine grid simulation, the corresponding mean predictions are 4.52 and 4.73 $\mu g/m^3$. The mean predictions from simulations on both grids agree very well with the mean $OM_{2.5}$ measurement (4.33 $\mu g/m^3$) throughout the simulation period. Scatter plots of the $OM_{2.5}$ coarse-grid predictions versus observations (Fig. 3.11 (c) and (d)) show that vast majority of the coarse-grid predictions from either CMAQ_L or CMAQ fall within a factor of two of the observations. Similar plots are obtained for fine-grid simulations with a little bit higher correlation coefficients. Figures 3.10 and 3.11 both suggest that both CMAQ_L and CMAQ present a very good $OM_{2.5}$ prediction at JST.

Compared with the simulation results (Fig. 6) in Zhang et al (2006), which also applied CMAQ version 4.4 to study the same episode from 7/1 to 7/10, the simulations in this study gave a much better agreement with the ambient $OM_{2.5}$ data. The discrepancy may be mainly attributed to the different emission inventories used to develop the corresponding emission files (NEI99 in this study and NET96 in Zhang et al. (2006)) and the different gas-phase mechanisms applied in these two studies (SAPRC99 in this study and CB4 in Zhang et al. (2006)). Although the same model species for SOA production are used in CB4 and SAPRC99, the applied emission adjustment factors of the SOA precursors -ALK5 and ARO1- in SAPRC99 is not a region specific value but an average value across the States (EPA, 2003).

4.3.5 Comparison of hourly organic aerosol predictions against measurements at Cornelia Fort (CF), Nashville, TN

Figure 3.12 compares the hourly model simulations with the hourly measurements of organic aerosol concentrations available at Cornelia Fort (CF), Nashville, TN, which were obtained in the 1999 Southern Oxidants Study carried out in Nashville/Middle Tennessee. For the coarse grid domain simulation, the difference in the simulation results from CMAQ_L and CMAQ are more visible than those from the fine grid domain simulation. However, simulations with the same horizontal resolution from CMAQ_L and CMAQ give pretty close simulation results. Due to the limitation of the hourly ambient data, it is hard to quantify the model performance on $OM_{2.5}$. Overall the simulations with both grids do not reproduce the temporal variations of $OM_{2.5}$ well at CF except the coarse grid simulation from the evening, July 5, to the morning, July 6.
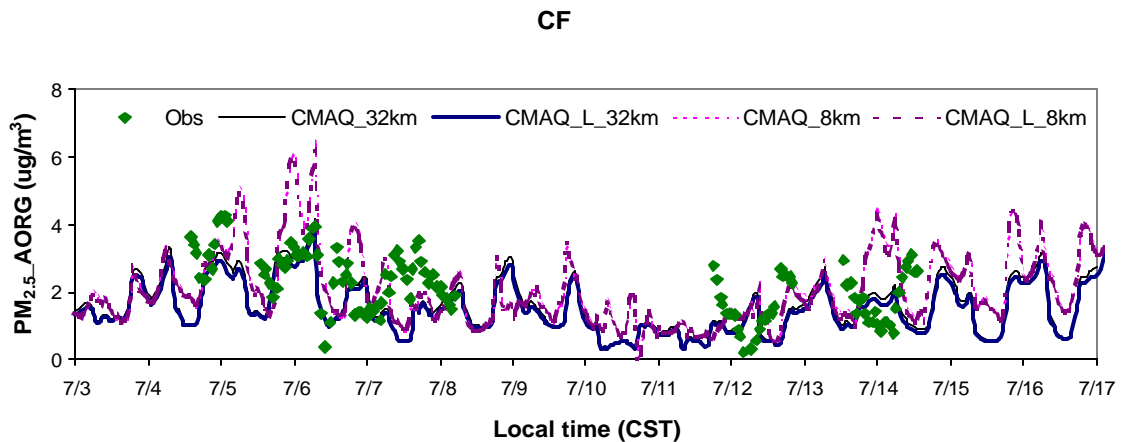

Figure 3.12. Comparison of predicted hourly aerosol concentration against measurements at Cornelia Fort (CF), Nashville, TN. The factor of 1.4 was used to obtain the concentration of organic aerosols from the concentration of observed organic carbon.

4.3.6 Comparison of daily average OM$_{2.5}$ predictions against ambient data at JST and YRK

Comparison of daily average OM$_{2.5}$ predictions against ambient data (from SEARCH website) for JST and YRK are shown in Figure 3.13 and 3.14, respectively. At
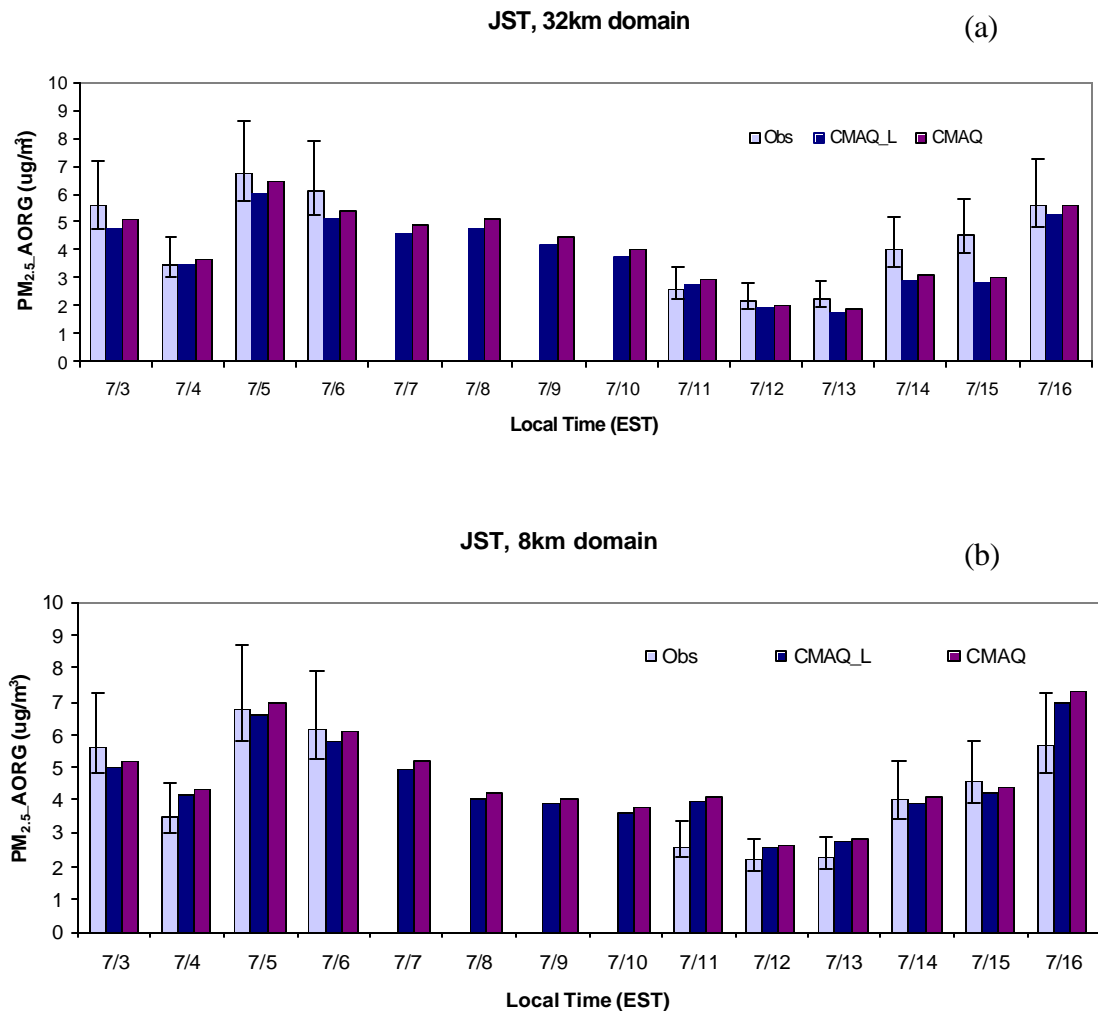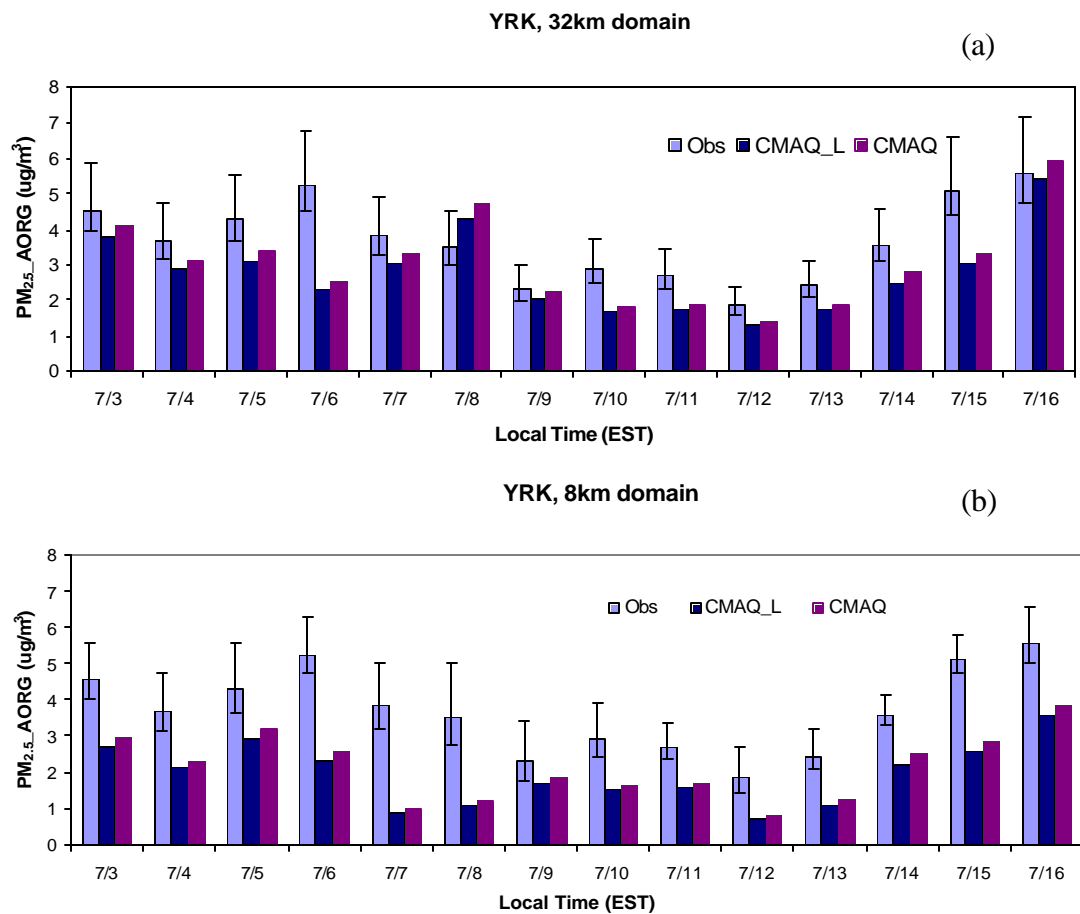

Figure 3.13. 24-hr average simulated organic aerosol concentrations compared with observations for JST, with horizontal resolution of (a) 32km; (b) 8km. The factor of 1.4 was used to obtain the concentration of organic aerosols from the concentration of observed organic carbon. The error bars represent a range of 1.2 to 1.8 to convert the concentration of measured OC to that of organic aerosol.

both sites, during the selected simulation period, CMAQ always give a little higher prediction than CMAQ_L. At JST, for most of the days the simulated daily average organic aerosol concentrations are within the variations of the observations caused by the conversion between the observed OC concentration and the calculated OA concentration except the underpredictions on 07/14 and 07/15 for coarse grid simulation and the overprediction on 07/11 for fine grid domain simulation. However, at YRK both

YRK, 32km domain

(a)

YRK, 8km domain

(b)

Figure 3.14. 24-hr average simulated organic aerosol concentrations compared with observations for YRK, with horizontal resolution of (a) 32km; (b) 8km. The factor of 1.4 was used to obtain the concentration of organic aerosols from the concentration of observed organic carbon. The error bars represent a range of 1.2 to 1.8 to convert the concentration of measured OC to that of organic aerosol.

CMAQ_L and CMAQ tend to underpredict the daily average aerosol concentrations. For the coarse grid domain simulation, significant underpredictions occur on 7/6, 7/10, and 7/15 while the fine grid domain simulation significantly underpredicts the daily average aerosol concentration all the time but on 7/9. Throughout the simulation period, the simulation over the subdomain at YRK underpredicts the daily average aerosol concentration by from 21% on July 9 to 74% on July 7 for CMAQ and from 26% on July 9 to 77% on July 7 for CMAQ_L. Overall the simulations on coarse grids give better results than those on fine grids.

4.4 Statistical Performance Evaluation

Traditionally mean error (ME), mean bias (MB), mean normalized error (MNE), mean normalized bias (MNB), normalized mean error (NME), normalized mean bias (NMB), mean fractional error (MFE) and mean fractional bias (MFB) have been used to evaluate the performance of air quality models (EPA, 2001; Seigneur et al., 2000). The advantage and disadvantage of each model performance evaluation metrics can be found in Boylan et al. (2006) and Boylan and Russell (2006). Briefly stated, the metrics with normalization are more meaningful and easier to interpret than ME and MB while NME and NMB (normalized by the sum of observations), MFE and MFB (normalized by the sum of observations and corresponding predictions) are more robust than MNE and MNB when small measurement data are involved in the data analysis. ME and MB provide actual measurement of the model performance but are not easy to interpret if no observations are provided along for evaluation. In addition to the traditional metrics, Yu et al. (2006) proposed a set of new statistical metrics to evaluate the air quality model

performance, which overcome the non-symmetric problem associated with the traditional metrics such as MNB/MNE and NMB/NME. This study aims to quantify the composition effects on SOA production within the same modeling framework. The afore mentioned traditional metrics can serve this purpose well and they were used to evaluate the performance of CMAQ and CMAQ_L on daily average $OM_{2.5}$.

Table 3.9 presents the statistical analysis results for daily average $OM_{2.5}$ concentration at the 11 monitoring sites across the sub-grid domain over the simulation period from July 3 to 17, 1999. CMAQ and CMAQ_L present the typical PM modeling performance of current air quality models. Both CMAQ_L and CMAQ underpredict the mean organic aerosol concentrations for both grid simulations. The percent underpredictions in the mean predictions for CMAQ_L in the mean predictions are 46% for coarse grid simulation and 44% for fine grid simulation while for CMAQ the corresponding values are 42% and 40%. The values of MNB (~ -35), NMB (~ -43) and MFB (~ -55) for CMAQ_L and CMAQ on both grids indicate an overall significant underprediction of organic aerosol concentrations from both CMAQ_L and CMAQ. Overall, predictions on both grids have no distinct difference.

Based on the performance goals recommended by EPA (EPA, 2001) in terms of MNB ($\leq$ 15%) and MNE ($\leq$ 30%) for a good performance of PM, both CMAQ_L and CMAQ present a relatively poor prediction of $OM_{2.5}$. Considering that the simulation of particulate matter, which is a mixture of hundreds of compounds, is much more complicated than modeling single pollutant like O_3, Boylan and Russell (2006) have proposed that for major components of $PM_{2.5}$, for example, $OM_{2.5}$, in terms of MFE and MFB the model performance goal are less than or equal to approximately ±50% and

Table 3.9. Performance statistics for daily average concentration of OM$_{2.5}$.

Mean Observation (ug/m³)	Data Pair	Simulations	Simulations	Mean predictions (ug/m³)	ME[2]	MB[3]	MNE[4] (%)	MNB[5] (%)	NME[6] (%)	NMB[7] (%)	MFE[8] (%)	MFB[9] (%)
4.53	78[1]	32km	CMAQ_L	2.46	2.26	-2.07	45.8	-37.6	49.9	-45.7	65.7	-59.2
			CMAQ	2.64	2.15	-1.89	43.6	-33.1	47.4	-41.8	61.2	-53.0
		8km	CMAQ_L	2.54	2.18	-1.99	46.3	-37.0	48.2	-43.9	65.7	-59.0
			CMAQ	2.71	2.08	-1.82	44.2	-32.8	46.0	-40.2	61.1	-52.8

Table 3.10. Performance statistics for SEARCH daily average OM$_{2.5}$ concentration.

Mean Observation (ug/m³)	Data Pair	Simulations	Simulations	Mean predictions (ug/m³)	ME[2]	MB[3]	MNE[4] (%)	MNB[5] (%)	NME[6] (%)	NMB[7] (%)	MFE[8] (%)	MFB[9] (%)
4.36	52[1]	32km	CMAQ_L	3.12	1.52	-1.23	32.8	-20.3	34.8	-28.3	39.9	-30.1
			CMAQ	3.34	1.40	-1.02	30.7	-14.9	32.1	-23.3	36.0	-23.7
		8km	CMAQ_L	3.17	1.48	-1.18	35.6	-21.7	33.9	-27.1	44.2	-34.1
			CMAQ	3.36	1.39	-1.00	34.2	-17.1	31.8	-22.8	40.7	-28.3

Table 3.11. Performance statistics for IMPROVE daily average OM$_{2.5}$ concentration.

Mean Observation (ug/m³)	Data Pair	Simulations	Simulations	Mean predictions (ug/m³)	ME[2]	MB[3]	MNE[4] (%)	MNB[5] (%)	NME[6] (%)	NMB[7] (%)	MFE[8] (%)	MFB[9] (%)
2.84	13[1]	32km	CMAQ_L	0.87	1.97	-1.97	67.6	-67.6	69.5	-69.5	107	-107
			CMAQ	0.96	1.87	-1.87	64.1	-64.1	66.1	-66.1	99.3	-99.3
		8km	CMAQ_L	1.00	1.83	-1.83	62.8	-62.8	64.7	-64.7	96.9	-96.9
			CMAQ	1.13	1.70	-1.70	57.8	-57.8	60.1	-60.1	87.0	-87.0

Table 3.12. Performance statistics for SOS99-Nashville daily average $OM_{2.5}$ concentration.

Mean Observation (ug/m³)	Data Pair	Simulations	Simulations	Mean predictions (ug/m³)	ME[2]	MB[3]	MNE[4] (%)	MNB[5] (%)	NME[6] (%)	NMB[7] (%)	MFE[8] (%)	MFB[9] (%)
6.93	13[1]	32km	CMAQ_L	1.40	5.53	-5.53	76.4	-76.4	79.8	-79.8	128	-128
			CMAQ	1.50	5.43	-5.43	74.8	-74.8	78.3	-78.3	124	-124
		8km	CMAQ_L	1.57	5.36	-5.36	72.2	-72.2	77.4	-77.4	121	-121
			CMAQ	1.67	5.26	-5.26	70.5	-70.5	75.9	-75.9	117	-117

[1]The statistics are calculated by using the simulation~observation data pairs with the observed organic aerosol concentration $> 0.5\ \mu g/m^3$.

[2]Mean Error: $ME = \dfrac{1}{N}\sum_{1}^{N}\left|Model - Obs\right|$

[3]Mean Normalized Gross Error:

$$MNE = \dfrac{1}{N}\sum_{1}^{N}\left(\dfrac{\left|Model - Obs\right|}{Obs}\right)\bullet 100\%$$

[4]Mean Bias: $MB = \dfrac{1}{N}\sum_{1}^{N}(Model - Obs)$

[5]Mean Normalized Bias: $MNB = \dfrac{1}{N}\sum_{1}^{N}\left(\dfrac{Model - Obs}{Obs}\right)\bullet 100\%$

[6]Normalized Mean Error: $NME = \dfrac{\sum_{1}^{N}|Model - Obs|}{\sum_{1}^{N}Obs}\bullet 100\%$

[7]Normalized Mean Bias: $NMB = \dfrac{\sum_{1}^{N}(Model - Obs)}{\sum_{1}^{N}Obs}$

[8]Mean Fractional Error: $MFE = \dfrac{2}{N}\sum_{1}^{N}\left|\dfrac{Model - Obs}{Model + Obs}\right|$

[9]Mean Fractional Bias: $MFB = \dfrac{2}{N}\sum_{1}^{N}\left(\dfrac{Model - Obs}{Model + Obs}\right)$

±30%, respectively; the model performance criteria are less than or equal to approximately ±75% and ±60%, respectively. The performance goal and criteria, as defined by the author, refers to the best and acceptable level of accuracy, respectively, that the model is expected to achieve in modeling applications. According to these model performance evaluation criteria, for the simulation of $OM_{2.5}$, the performance of both CMAQ_L and CMAQ is acceptable.

However, further examination of the model performance on each of the individual data sets indicates that the model performance varies with different data sources. Table 3.10, 3.11 and 3.12 presents the statistical model performance for SEARCH, IMPROVE and SOS99-Nashville daily average $OM_{2.5}$ data sets, respectively. The models perform best on SEARCH data, with the percent underpredictions for CMAQ_L on both grids in the mean predictions are ~28% while for CMAQ the corresponding values are 23%. Large underpredictions exist for $OM_{2.5}$ at IMPROVE and SOS99-Nashville monitoring sites. The worst case is with SOS99 data set. The percent underpredictions in the mean predictions for simulations on both grids are ~ 78% for CMAQ_L and ~ 77% for CMAQ. The values of MNB and MFB are ~75 and ~125 for both CMAQ and CMAQ_L on both grids. These values indicate an overall significant underprediction of organic aerosol concentrations from both CMAQ_L and CMAQ and an unacceptable models performance on $OM_{2.5}$ at SOS99 monitoring sites.

For IMPROVE data set, the percent underpredictions for CMAQ_L on both grids in the mean predictions are ~ 65% while for CMAQ the corresponding values are ~ 63%. However, it should be pointed out that CMAQ and CMAQ_L do not perform always so poor on IMPROVE data sets. For the coarse-grid simulation, 7 randomly selected

IMPROVE monitoring sites located in California (REDW, PORE, YOSE, PINN, SAGO, LAVO and SEQU) are used to check the model performance. Scatter plot of the predicted (by CMAQ_L) and measured $OM_{2.5}$ concentrations is presented in Figure 3.15. The plot shows that CMAQ_L predicts reasonably well on the CA IMPROVE monitoring sites. So model performance study on all appropriate IMPROVE sites is recommended to get a complete evaluation of the model.
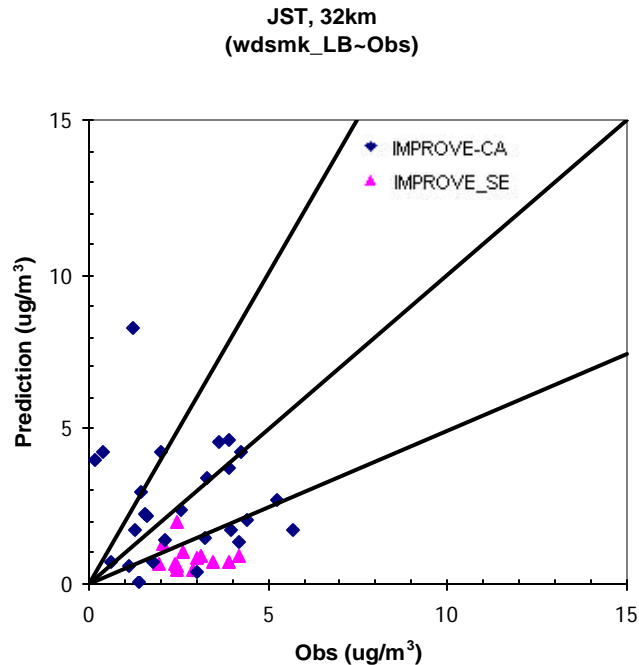
JST, 32km
(wdsmk_LB~Obs)

Figure 3.15. Scatter plots of daily $OM_{2.5}$ coarse-grid predictions (abscissa) from CMAQ_L versus observations (ordinate) on IMPROVE sites in Southeastern US and California (CA), 1:1, 1:2 and 2:1 lines are provided for reference.

4.5 Potential Sources of Error and Uncertainty

To identify the factors contributing to the underpredictions of $OM_{2.5}$, a systematic evaluation study, as has been done in Zhang et al. (2006a, 2006b, 2006c), would need to be carried out on input data such as meteorological data and emission data as well as the

representation of the major aerosol processes in the model. However, such kind of evaluation is beyond the scope of this study. It is well known that the OC emission inventory has larger uncertainties than other aerosol components. The accurate measurements of OC also present a great challenge (Turpin et al., 2000). Besides the uncertainties related with POA emissions and OC measurements, the underprediction of $OM_{2.5}$ by CMAQ modeling framework may be attributable to the following reasons related to SOA production:

1) No simulation of some potential SOA gas-phase precursors such as sesquiterpenes, isoprene and benzene. On a reacted mass basis, chamber experiments on SQT (e.g. b-caryophyllene, a-humulene and a-cedrene) show that SQT have much higher aerosol potentials than monoterpenes (Hoffmann et al, 1997; Griffin et al., 1999; Jaoui and Kamens, 2003a,b; Jaoui et al., 2004). Model studies by Andersson-Skold (2001) and Vizuete et al (2004) suggest that SQT may contribute significantly to ambient SOA depending on their actual emissions. Recent research indicates that the further heterogeneous acid-catalyzed particle phase reactions of isoprene and its gas-phase products present a major contribution to SOA formation in natural systems (Jang et al. 2002; Jang et al., 2003b; Claeys et al., 2004a, b; Limbeck et al., 2003; Matsunaga et al., 2003). Very recently, Kroll et al (2005) found that isoprene photooxidation under high NO_x concentrations led to 0.9-3.0% SOA yield on mass basis. Although the aerosol yield value is small compared to other larger-size biogenic volatile organic compounds, the large emission amount of isoprene makes it a promising primary contribution to atmospheric biogenic SOA. Compared to sesquiterpenes and isoprene, benzene probably is not a significant potential SOA precursor but some studies have shown that SOA

indeed can be formed from benzene oxidation (Martín-reviejo and Wirtz, 2005; Johnson et al., 2005).

2) Incomplete account for the heterogeneous aerosol-phase reactions due to the reversible absorption assumption. The formation of large molecules in aerosol phase due to heterogeneous aerosol-phase reactions may result in a non-reversible uptake of organics into the particle phase.   The assumption of non-reversible uptake of organics into aerosol phase has significant effects on the amount of SOA produced (Tsigaridis and Kanakidou, 2003).

3) Uncertainties related to the smog chamber experimental data. The experimental data obtained under the specific experimental condition may not be sufficient to represent the SOA partitioning characteristics in reality, which is affected by the amount of precursors available, the aerosol phase composition, the temperature, the vapor pressures of individual aerosol components. Recent studies also show that the particular experimental conditions such as the presence of UV radiation (Presto et al. 2005a), the NO_x concentration (Presto et al. 2005b), the presence of OH scavengers (Docherty and Ziemann 2003; Keywood et al., 2004; Iinuma et al., 2005) and the presence of neutral or acidic particles (Czoschke et al., 2003; Jang et al., 2002; 2003a, b; Gao et al. 2004a; Iinuma et al., 2004; 2005) can have significant effects on the SOA yield and the relative abundance of the individual components in aerosol phase. So the chamber data currently used in this study may include significant uncertainties when estimating the SOA production capability of the gas-phase precursors under atmospheric conditions.

Despite of the insufficiency mentioned above, the models reproduce really well the JST hourly $OM_{2.5}$ data and daily $OM_{2.5}$ data from the four SEARCH sites located in

the fine grid domain. Generally speaking, CMAQ and CMAQ_L represent the PM modeling accuracy level that can be expected from current air quality models.

5. Conclusions

In this study, the lumped groups with the capacity to explore the composition effects on SOA production were formulated and applied in CMAQ. The partitioning parameters and structure information for the lumped groups are calculated directly from the corresponding properties of the individual SOA products. The partitioning performance of the lumped groups was evaluated in both experimental and atmospheric systems. Under ideal behavior situation, the lumped groups predict very close SOA concentrations as the model species in CMAQ.

Compared against ambient daily average data for organic aerosol, underprediction is the common trend. The MFE and MFB for the predictions with the lumped groups over the southeastern U.S. domain with horizontal resolution of 32 km are, respectively, 66 and –59 compared with 61 and –53 for CMAQ. Similar results are obtained for the 8km grid domain. However, the model performance differs a lot on different ambient data sources, which indicates that the accurate simulation of organic matter presents a great challenge, involving the OC emission inventory development, accurate OC measurements and SOA production treatment. The aspects related to SOA production which may contribute to the underprediction may include uncertainties in precursor emissions, limited theoretical and experimental data upon which partitioning parameters are based, potential SOA production capability of isoprene and other uncertainties in

aerosol-producing gas-phase chemistry, as well as incomplete understanding of aerosol-phase reaction processes.

Our understanding on SOA production process is still in its infancy. Many uncertainties exist and at the same time many efforts are going on trying to elucidate all the affecting factors in the SOA production process. The lumped groups formulated in this study present the atmospheric SOA production quite well and can be used to study the composition effects on SOA production and bring one step towards more accurate descriptions of SOA production in the real atmosphere.

CHAPTER IV

COMPOSITION EFFECTS ON SECONDARY ORGANIC AEROSOL (SOA) PARTITIONING: INITIAL EVALUATION IN THE SOUTHEASTERN US

1. Introduction

In this chapter, a modified SOA production process, incorporating product structure information as well as its subsequent effects on SOA production, was developed and coupled into CMAQ v4.4. The new SOA production parameters formulated in Chapter III were used to represent the partitioning parameters as well as product structure information corresponding to 5 categories of SOA precursors. For quantifying composition effects on SOA production, 3 sets simulations were performed with each consisting of simulations on both a coarse 32-km grid domain and a nested 8-km sub domain. The coarse grid domain covers the contiguous US and the fine grid domain covers an area of southeastern US. The detailed description of the modeling domains, the basic configuration of the model and the databases used can be found in Chapter III. Evaluation work, which is focused on the sub domain with horizontal resolution of 8km, was then carried out using the ambient data from SEARCH, IMPROVE and SOS99-Nashville measurements in the southeastern United States obtained during July 3-16, 1999. Incorporation of partitioning composition effects into air quality models is one step towards more accurate descriptions of atmospheric SOA production. The capability of this modified module to quantify the composition effects on SOA production provide us a basis to gain further insights of the atmospheric aerosol phase composed of POA and

SOA. The module can be updated along with the advancement of the molecular identification technology and development in thermodynamics.

The contents of this chapter are organized as follows: section 2 describes the calculation procedure in the new module related to SOA production; section 3 presents the simulation results from CMAQ incorporated with the revised aerosol module as well as data analysis against available ambient data; statistical evaluation of module performance is summarized and shown at the end of this section. Some critical findings in this study are summarized in the section 4.

2. Calculation Procedure in the New Aerosol Module

Figure 4.1 presents the revised calculation scheme incorporating the composition effects on the SOA partitioning process. The key modifications to the procedure are the inclusion of aerosol-phase activity coefficients, on-line calculation of the saturation concentration of pure compound i, $C^*_{sat,i}$, and the representations of the SOA products.

During each time step t, same calculation procedures as those detailed in Chapter II are applied to get $Ctot_{i,t}$, the total amount of individual condensable compound partitioning between aerosol phase and gas phase. $Ctot_{i,t}$ ($\mu g/m^3$), POA_t ($\mu g/m^3$) - the concentration of primary organic aerosol at time step t, and $C^*_{sat,i}$ ($\mu g/m^3$) - the effective saturation concentration of pure species i under ambient temperature T are needed to calculate the aerosol phase concentration of each component. Below describes the on-line calculation of $C^*_{sat,i}$, which incorporates the composition and temperature effects.

As indicated in Figure 4.1, the activity coefficient of each organic species is first calculated by UNIFAC, which is a state-of-the-art method to predict the activity

coefficients in liquid mixtures where little or no experimental data are available. Essentially it is assumed that physical properties of a fluid are the sum of the contributions made by the molecule's functional groups and one group's contribution is independent of the other's. Activity coefficient of each component is calculated as a function of x_i, the aerosol-phase mole fraction of product i, s_{ji}, the number of groups j in product i, and temperature T.

$$V_i = f(x_i, \, s_{ji}, T) \tag{4.1}$$

x_i is determined as the molar concentration of species i over the sum of the molar concentrations of all aerosol-phase components, including SOA, POA and water if involved,

$$x_i = \frac{C_{aer,i} / MW_i}{\sum_k (C_{aer,k} / MW_k)} \tag{4.2}$$

where $C_{aer,i}$ ($\mu g/m^3$) and MW_i (g/mol) are the aerosol-phase concentration and molecular weight of species i, respectively.

Temperature effects on $C^*_{sat,i}$ mainly reflect through the relationship between saturation vapor pressure and temperature as indicated by Clausius-Clapeyron equation. With a known saturation vapor pressure at temperature T_{ref}, the vapor pressure at any other temperature T, $P^0_{i,T}$ can be calculated if the enthalpy of product i can be assumed to be constant within the temperature range of interest,

$$P^0_{i,T} = P^0_{i,T_{ref}} \times \exp\left(B_i \left(\frac{1}{T_{ref}} - \frac{1}{T} \right) \right) \tag{4.3}$$

The activity coefficient, z_i, and the saturation vapor pressure of species i under temperature T, $P_{i,T}^0$ (p_a), are used to calculate the effective saturation concentration of pure species i under ambient temperature T (Strader et al., 1999; Schell et al., 2001),.

$$C_{sat,i}^* = \frac{V_i P_{i,T}^0 MW_i 10^6}{RT} \tag{4.4}$$

where MW_i (g/mol) is the molecular weight of product i and R is the universal gas constant (8.314510 $m^3 P_a$/mol-K).

The obtained $C_{sat,i}^*$, together with $Ctot_{i,t}$ ($\mu g/m^3$), POA_t ($\mu g/m^3$), is then used to compute the aerosol-phase concentration of product i (Schell et al., 2001).

$$C_{aer,i,t} = C_{tot,i,t} - C_{sat,i}^* \frac{C_{aer,i,t}/MW_i}{\sum_{k=1}^{12}(C_{aer,k,t}/MW_k) + POA_t/MW_{POA}} \tag{4.5}$$

However, $C_{aer,i,t}$ can not be determined directly. An iterative solution is necessary because activity coefficients are themselves a function of composition. For the first time step, the iteration starts by assuming $z_i = 1$ for all the model species. For the following time steps, the iteration starts with

$$C_{aer,i} = \frac{C_{tot,i,t} \times POA_t}{POA_t + C_{sat,i,t-1}} \tag{4.6}$$

where $C_{sat,i,t-1}$ is the saturation concentration of product i at time step t-1 when the iteration stops. Equation (4.6) is derived from equation (4.5) with assumption of 1) the total amount of absorbing aerosol is equal to POA_t and 2) $MW_{POA} = MW_i$. After the iteration starts, the aerosol-phase concentrations calculated by equation (4.5) then feed back to UNIFAC to repeat the procedure, just as indicated by Figure 4.1. During each time step, the iteration stops when the maximum absolute difference of the individual

$\Delta HC_{j,t}, POA_t, SOC_{i,t-1}, T, P$

x_i, s_{ji}, T

UNIFAC

ς_i

$$totrog_{j,t} = \frac{P \times MW_{rog,j}}{RT} \times \Delta HC_{j,t}$$

$$Ctot_{i,t-1} = \frac{P \times MW_i}{RT} \times SOC_{i,t-1}$$

$$Ctot_{i,t} = \alpha_i totrog_{j,t} + Ctot_{i,t-1}$$

$$P^0_{i,T} = P^0_{i,T_{ref}} \times \exp\left(B_i \left(\frac{1}{T_{ref}} - \frac{1}{T} \right) \right)$$

$$C^*_{sat,i} = \frac{\varsigma_i P^0_{i,T} MW_i 10^6}{RT}$$

Compute $C_{aer,i,k}$ (i=1,12) for iteration n

$$C_{aer,i,n} = C_{tot,i,t} - C^*_{sat,i} \frac{C_{aer,i,n} / MW_i}{\sum_{k=1}^{12} (C_{aer,k,n} / MW_k) + POA_t / MW_{POA}}$$

$C_{aer,i,n}$ (i=1,12)

$Max(C_{aer,n} - C_{aer,n-1}) < 10^{-3}$ or max $((C_{aer,n} - C_{aer,n-1})/C_{aer,n}) < 1\%$

No

Yes

$$SOA\_B_t = C_{aer,9,t} + C_{aer,10,t} + C_{aer,12,t}$$

$$SOA\_A_t = \sum_{i=1}^{12} C_{aer,i,t} - SOA\_B_t$$

Figure 4.1. Revised framework for updating the SOA production in new CMAQ aerosol module. Modifications from original CMAQ 4.4 procedure are highlighted.

aerosol concentrations at iteration n and those at n-1 is $= 10^{-3}$ ($\mu g/m^3$) or the maximum relative difference is $= 1\%$.

Use of UNIFAC requires the composition and chemical structure information of the aerosol phase. Structure and partitioning parameters formulated by the lumping method developed by Bian and Bowman (2002, 2005) was used to provide necessary calculation parameters, such as the number and type of functional groups in each SOA product, the vapor pressures for the lumped products, etc. The revised aerosol module includes 3 biogenic SOA products and 9 anthropogenic SOA products, as described in Chapter III.

Table 4.1. Modeled POA compositions for UNIFAC application.

Component	Model name	x_i	MW_i
wood smoke[a]			
hexadecanoic acid	POA1	0.19	256
pentanedioic acdi	POA2	0.07	132
homovanillic acid	POA3	0.18	182
4-propylbenzenediol	POA4	0.28	152
1-guaiacylpropane	POA5	0.17	166
veratraldehyde	POA6	0.11	166
diesel soot[a]			
heneicosane	POA1	0.45	297
tetracosane	POA2	0.14	339
hexanoic acid	POA3	0.11	116
undecanoic acid	POA4	0.17	186
hexadecanoic acid	POA5	0.06	256
benzoic acid	POA6	0.07	122

[a] Composition data from Jang et al. (1997).

Different approach to represent primary organic aerosol (POA) may have significant effects on the simulation results. For initial evaluation, polar wood smoke and relatively nonpolar diesel soot were used to represent POA because they have been identified as the largest two contributors to fine particulate matter in Southeastern US in summer (Zheng et al., 2002). To simplify the model procedure with the consideration of calculation efficiency, the model species for wood smoke and diesel soot, as listed in table 4.1, use the representative set of compounds suggested by Jang et al. (1997). Compared with diesel soot, wood smoke particles contain higher fraction of polar functional groups, such as carboxyl, aldehyde and alcohol functional groups; Long-chain alkanes and alkanoic acids make up most part of diesel soot particles.

3. Composition Effects on SOA Production in the Southeastern US

3 sets of simulations were performed to evaluate the composition effects on SOA production: CMAQ_L, wdsmk_12 and diesel_12. CMAQ_L refers to the simulation conducted with CMAQ modeling framework but using the newly formulated lumped groups, instead of the models species in CMAQv4.4, to represent the SOA production process. However, as CMAQv4.4, no composition effects on SOA production are considered and ideal behavior is assumed. wdsmk_12 and diesel_12 target on evaluating composition effects on secondary organic aerosol (SOA) production. The modified aerosol module was incorporated into the CMAQ framework with the corresponding POA representation. In wdsmk_12, the pre-existing primary organic aerosol (POA) was represented as wood smoke particles while in diesel_12, POA represented as diesel soot. Differences between simulation CMAQ_L and simulation wdsmk_12 or diesel_12 will

98

indicate the composition effects on the amount of SOA produced; differences between wdsmk_12 and diesel_12 will highlight the effect of POA representation on quantifying the composition effects and on revealing the aerosol composition. Table 4.2 indicates the differences as well as the common features in the three organic aerosol modules.

Table 4.2. Overview of the organic aerosol module in the 3 sets of simulations.

Model version		CMAQ_L	wdsmk_12	diesel_12
SOA precursors		5 categories	5 categories	5 categories
SOA	# of products	12	12	12
	Activity coefficient	1	online calculated by UNIFAC as a function of x_i, s_{ji}, and T	online calculated by UNIFAC as a function of x_i, s_{ji}, and T
POA		NA[a]	wood smoke[b]	diesel soot[b]

[a] Not applicable. No POA composition is needed without consideration of composition effects.

[b] the model composition of wood smoke and diesel soot comes from Jang et al., 1997.

3.1 Simulation Results and Analysis

The detailed description of the modeling domain, model inputs, configuration of the model processes, post-processing procedure of the simulation results as well as the ambient data used for analysis can be found in Chapter III. Here presents the final predictions as well as data interpretation and analysis. As in Chapter III, the simulation results from the 3 sets of simulations are evaluated by 1) comparing the simulated SOA concentrations against each other as detailed in section 3.1.1, and 2) comparing the simulated SOA and OA concentrations against hourly or daily ambient data, which are presented and analyzed in sections 3.1.2 to 3.1.5.

3.1.1 Comparison of hourly SOA predictions for JST and YRK from different versions of aerosol module

In this section, comparison of the SOA concentrations from different simulations is presented. In each figure, CMAQ_L represents the output from the revised aerosol module but with no composition effects accounted for, i.e., activity coefficients for all the lumped groups are set to 1; wdsmk_12 and diesel_12 show the predicted concentrations by the revised aerosol module, including composition effects, with POA represented as wood smoke and diesel soot particles, respectively.

Figure 4.2 and Figure 4.3 present the temporal distribution of predicted SOA in $PM_{2.5}$ for JST (a urban site) and YRK (a rural site), respectively. Predicted SOA concentrations are plotted for the whole simulation period from 07/03 0:00 to 07/17 0:00. Same temporal variation was predicted by the three sets of simulations but with different predicted SOA concentrations, especially at the points with daily maximum. CMAQ_L and wdsmk_12 predict very close SOA concentrations, most of the time with a little bit higher predictions from wdsmk_12. However, diesel_12 predicts much lower SOA concentrations than CMAQ_L and wdsmk_12.

The activity coefficients of the individual SOA components in particulate phase can reveal the underlying reasons for this easily observable composition effect when POA represented as diesel soot and the almost non-visible effect when POA simulated as wood smoke particles. Figure 4.4 presents the predicted activity coefficients for the SOA components at JST from coarse-grid simulation with POA represented respectively as (a) diesel soot and (b) wood smoke. Activity coefficient predictions for fine-grid JST, and fine- and coarse-grid YRK simulations show similar trends as discussed below.

For POA represented as wood smoke particles, predicted activity coefficients of SOA9 and SOA11 present the two extremes over the whole simulation period at both sites no mater what grids applied. SOA9, lumped from the SOA products corresponding to TRP1, is most compatible with wood smoke and its predicted activity coefficients for the coarse-grid simulation range from 0.25 to 0.62 at JST and from 0.30-0.68 at YRK; for the fine-grid simulation from 0.24 to 0.55 at JST and from 0.30 to 0.67 at YRK. SOA11, the most incompatible compounds with wood smoke and representing the 3rd lumped group formulated from ALK5, has predicted activity coefficients from 15 to 32 at JST and 16 to 38 at YRK for the coarse-grid simulation; from 16 to 29 at JST and from 16 to 39 at YRK for fine-grid prediction. The activity coefficients for other SOA components are in a pretty narrow range from 0.84 to 5.7 at JST and from 0.86 to 6.1 at YRK for coarse-grid simulation; from 0.82 to 5.6 at JST; 0.87 to 6.2 at YRK for fine-grid simulation.

It should be noted that the activity coefficients of SOA10 and SOA12, the two largest contributors to the SOA mass production, are around 1, which means that they will produce similar SOA mass concentrations as in CMAQ_L when POA is represented as wood smoke particles. In CMAQ_L, throughout the whole simulation period, the average mass fractions of SOA10 and SOA12 in the total SOA mass at JST for the coarse-grid simulation are 74.5% and 13.3%, respectively; for the fine-grid prediction the values are 75.8% and 11.7%; At YRK the corresponding values are 75.3% and 13.7% for coarse-grid simulation and 72.3% and 20.1% for fine-grid simulation. All other SOA species only make up ~12% of the SOA mass at JST and ~10% of the SOA mass at YRK. Due to the fact that SOA10 and SOA12 dominate the total SOA mass production and

their activity coefficients vary in such a narrow range, the aerosol mixture made up of SOA products and POA represented as wood smoke actually form a quasi-ideal solution. In such a quasi-ideal solution, $\zeta_i=1$ is an acceptable assumption to favor the simulation efficiency.

When POA is simulated as diesel soot, the lumped groups modeling the SOA products from ARO1, SOA8 and SOA7, have the highest predicted activity coefficients all the time and vary in a very large range. For example, for the coarse-grid simulation, the activity coefficients for SOA8 and SOA7 vary from 32 to 8600 and 4.7 to 115, respectively, at JST; and from 13 to 5763 and 3.1 to 89, respectively, at YRK. Similar variation ranges are predicted for fine-grid simulation. The lumped groups corresponding to ALK5, SOA1, SOA2 and SOA11, are the bottom three with lowest activity coefficients, with 0.95~2.3 for SOA1, 0.96~1.4 for SOA2 and 0.84~3.0 for SOA11 at JST; 0.96~2.1 for SOA1, 0.96~2.3 for SOA2 and 0.84~7.0 for SOA11 at YRK for coarse-grid simulation. Similar predictions also occur for fine-grid simulations. Compared with when POA represented as wood smoke particles, the activity coefficients for SOA10 and SOA12, respectively, increase to 1.5~15 and 1.2~8.2 at JST; 1.2~13 and 1.1~7.0 at YRK. This increase in predicted activity coefficients for SOA10 and SOA12 reduces the amount of SOA produced significantly.

The temporal variations of the predicted activity coefficients for all the lumped groups except SOA11 follow the change of POA mole fraction with time, i.e., when the mole fraction of POA in the ambient aerosol is high, so are the predicted activity coefficients for all the lumped groups except SOA11. Actually the predicted activity coefficients of SOA11 only vary slightly with the change of POA mole fraction. This

pattern indicates that all the lumped groups but SOA11 are chemically dissimilar from diesel soot particles. For illustration purpose, the temporal distribution of the mole fraction of POA and the activity coefficients of SOA10 and SOA11 at JST predicted by the fine-grid domain simulation are presented in Figure 4.5. Compared with wood smoke particulates, diesel soot contains a smaller fraction of polar functional groups such as carboxyl, aldehyde and alcohol functional groups. The identified SOA products, however, are generally very polar, containing carboxylic acid and other polar groups, as seen from table 3.7 in Chapter III. The polarity difference between diesel soot and the lumped groups are shown by the elevated activity coefficients predicted by UNIFAC for most of the lumped groups but those corresponding to ALK5 which represents the long chain alkanes containing more than 7 carbons. Their speculated oxidation products are assumed to be long-chain acids and diacids containing 7~30 carbons. So the lumped groups corresponding to ALK5, SOA1, SOA2 and SOA11, are all alkanoic acids with similar structure as diesel soot, with more than 90% of which are composed of long-chain alkanes and alkanoic acids. However, ALK5 is not a main contributor to SOA production at least in southeast US. So when POA is simulated as diesel soot, the overall effect is to decrease the SOA production, especially the daily maximum. The apparent difference in simulated SOA concentrations between CMAQ_L and diesel_12 makes the unit activity coefficient assumption unjustified.

When POA is represented as diesel soot, the composition effects have stronger effect on SOA production at JST than at YRK. The predicted activity coefficients for SOA10, the major contributor to SOA mass at both sites, are always lower at YRK than at JST due to the fact that POA concentrations are higher at JST than at YRK.
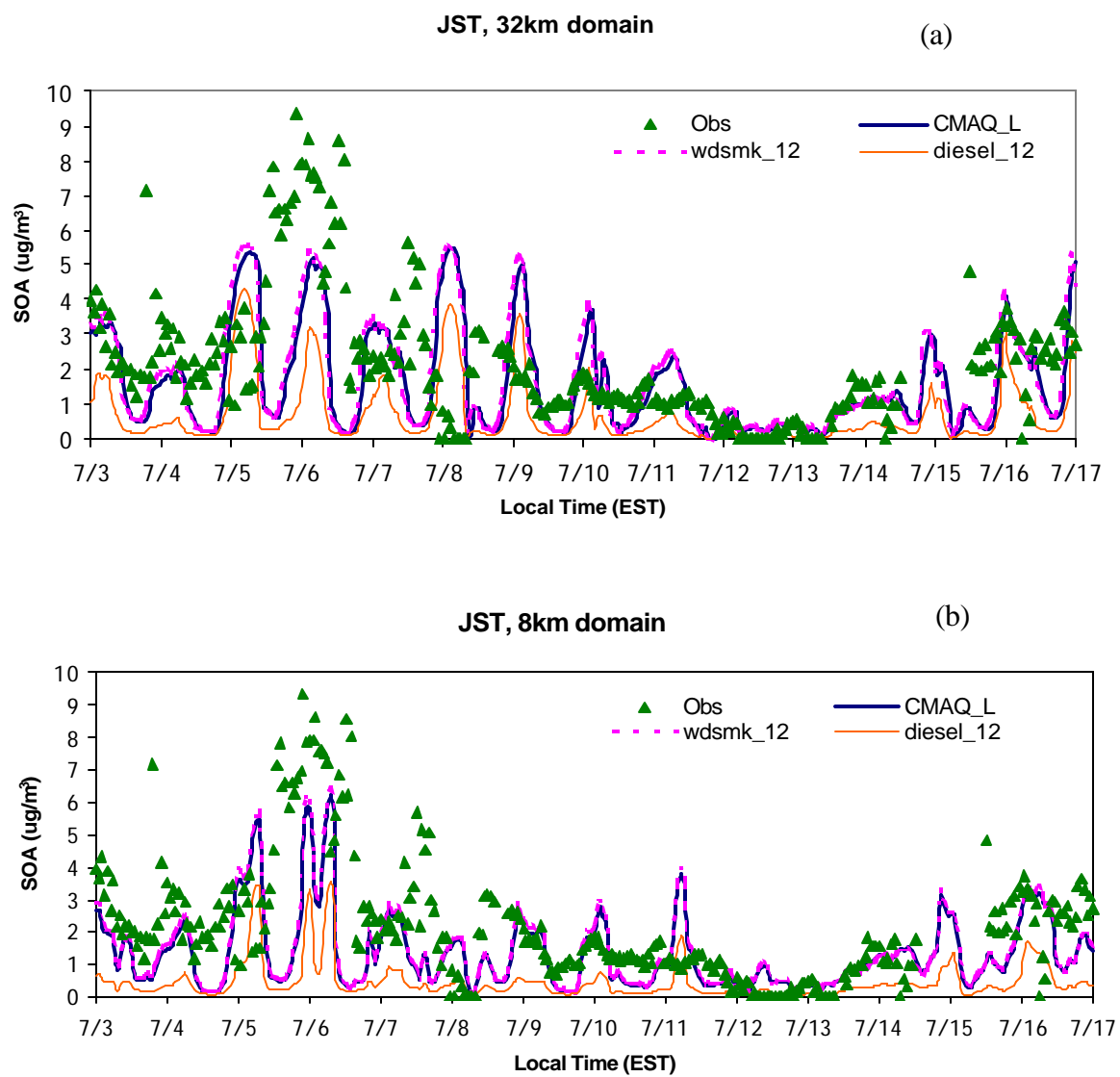
Figure 4.2. Temporal distribution of simulated SOA concentration against hourly observations at JST, with horizontal resolution of (a) 32km domain; (b) 8km.

104

YRK, 32km domain

(a)

YRK, 8km domain

(b)
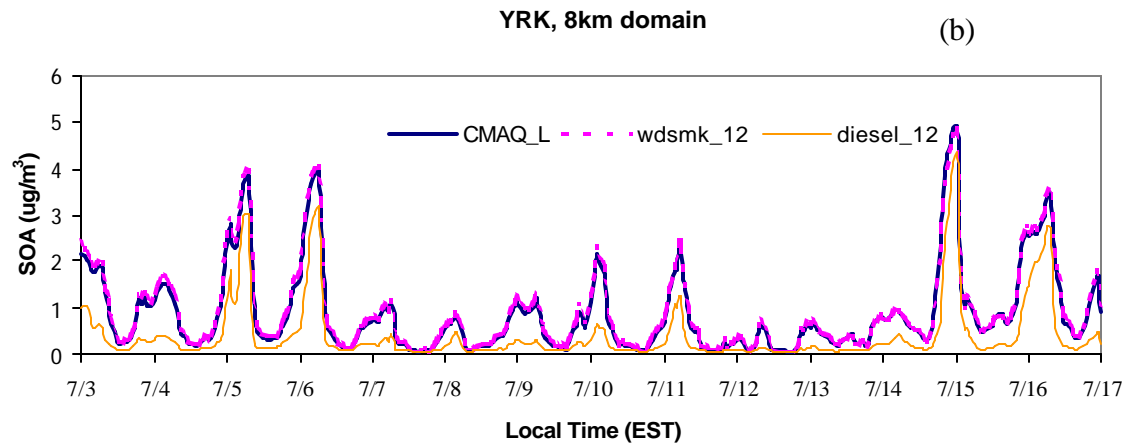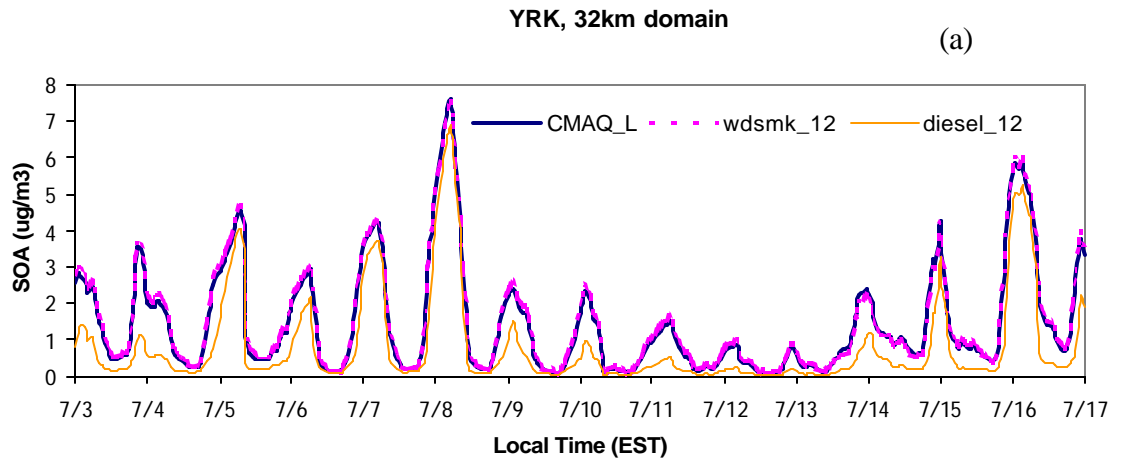
Figure 4.3. Temporal distribution of simulated SOA concentration at YRK, with horizontal resolution of (a) 32km; (B) 8km.

105
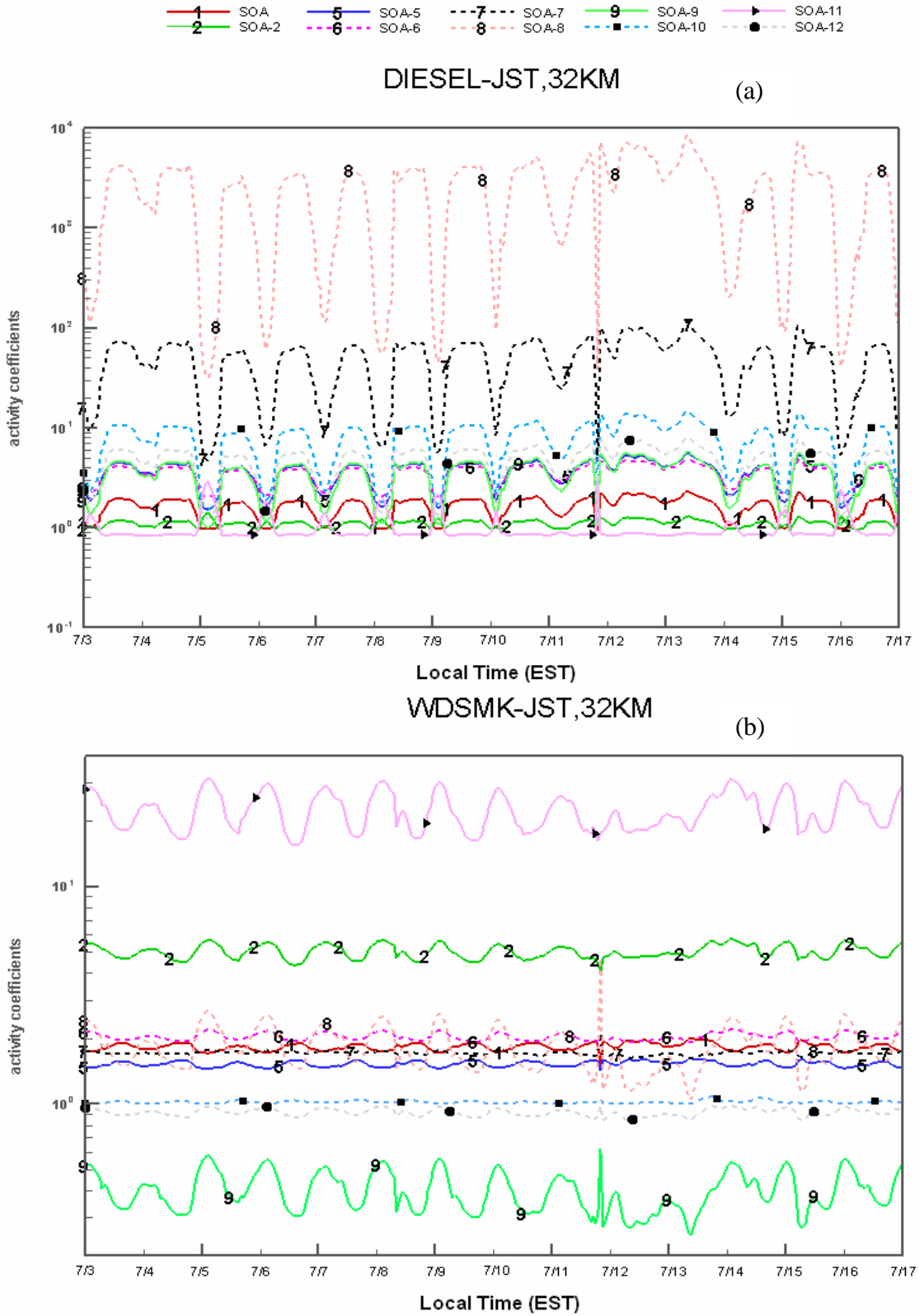
Figure 4.4. Predicted activity coefficients of the SOA compone nts at JST with horizontal resolution of 32km as POA represented as (a) diesel soot; (b) wood smoke.

JST, 8km
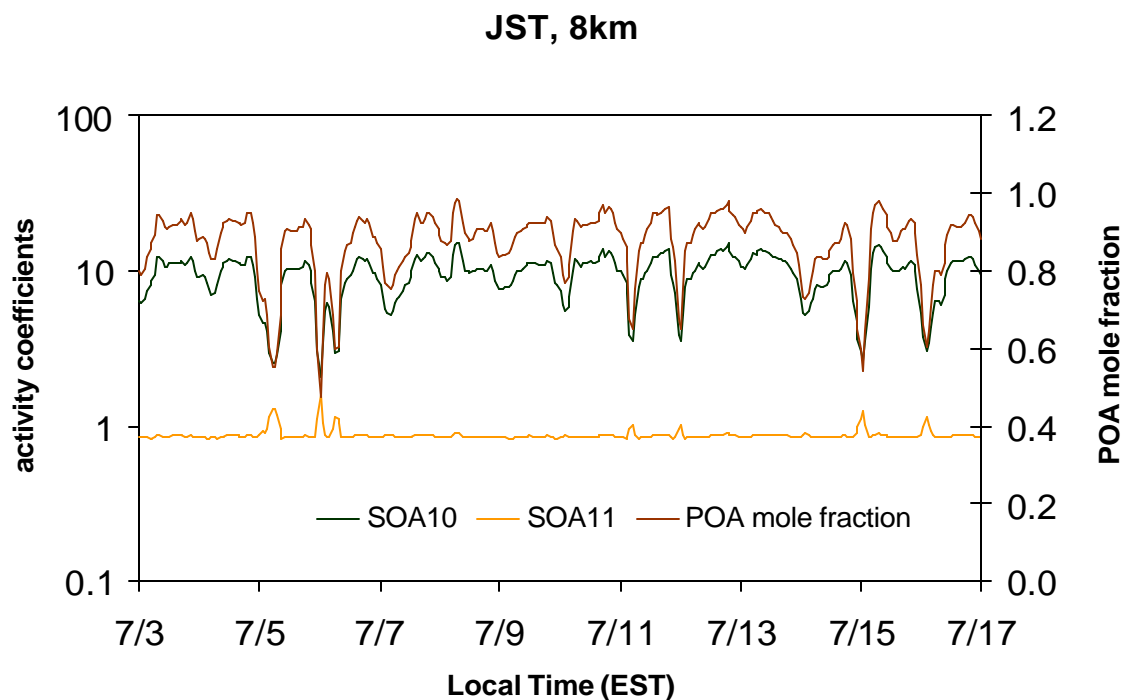
Figure 4.5. Temporal distribution of the mole fraction of POA and activity coefficients of SOA 10 and SOA11 at JST with horizontal resolution of 8km.

3.1.2 Comparison of hourly and daily average SOA predictions against measurements at Jefferson Street (JST), Atlanta, GA.

As in Chapter III, the $(OC/EC)_{pri}$ ratio of 2.1 from Lim and Turpin (2002) are used to estimate the secondary organic carbon concentration in Atlanta, GA, with a correction to account for the different OC/EC measurement methods. Briefly stated, the EC concentration obtained for JST in SEARCH is divided by 2 to account for the difference in the thermal evolution protocols of TOT and TOR. Thus, $OC_{pri}/EC = 1.05$, primary organic carbon $(OC_{pri}) = 1.05 \times EC$ and secondary organic carbon $(OC_{sec}) = OC_{tot} - OC_{pri}$ are used to get the concentration of secondary organic carbon. SOA concentration was calculated by multiplying the obtained OC_{sec} by a factor of 1.4.

Table 4.3. Mean OM$_{2.5}$ observation and predictions from different model versions at JST during the period from 7/3/99 to 7/16/99.

Data Source	Mean Observation (μg/m^3)	Mean Prediction (μg/m^3)					
		CMAQ_L		wdsmk_12		diesel_12	
		32km	8km	32km	8km	32km	8km
Hourly data							
SOA	2.18	1.65	1.38	1.74	1.48	0.71	0.45
OA	4.33	4.02	4.52	4.11	4.61	3.08	3.60
SEARCH daily average data							
SOA	2.50	1.48	1.40	1.57	1.49	0.61	0.47
OA	4.33	3.70	4.59	3.78	4.68	2.84	3.66

Figure 4.2 compares the hourly predictions from CMAQ_L, wdsmk_12 and diesel_12 against hourly measurements of the SOA concentration at JST. The SOA concentration was calculated based on the procedure described above. Generally speaking, the simulations on both grids reproduce the temporal variations of SOA concentrations at JST pretty well except on 7/8 for coarse-grid simulations. However, for most of the time throughout the whole simulation period, diesel_12 on both grids significantly underpredicts the SOA concentrations at JST except during the early morning period on 7/5 and for the period when little SOA is considered to form based on the calculation, for example, on 7/12. For CMAQ_L and wdsmk_12, significant underprediction occurs in the afternoons when the SOA concentration is low. However, during early morning period overprediction is a problem such as on 7/5, 7/8, 7/9, 7/10

and 7/11 for the coarse grid prediction and on 7/5 and 7/11 for fine grid prediction. Even so, throughout the whole simulation period, CMAQ_L and wdsmk_12 on both grids still tend to slightly underpredict the ambient SOA concentrations. The predicted mean SOA observations and predictions from the 3 sets of simulations are shown in Table 4.3. The percent underpredictions in the mean predictions for the coarse grid simulation and fine grid simulation are 24% and 37% for CMAQ_L and 20% and 32% for wdsmk_12, respectively. Underpredictions from diesel_12, in terms of mean predictions, are much larger than those from CMAQ_L and wdsmk_12, with 67% for coarse grid simulation and 79% for fine grid simulation. Overall, compared with CMAQ_L, wdsmk_12 predicts a little bit higher SOA concentrations with an increase in the mean prediction of 5.6% at JST for coarse grid simulation and of 6.8% for fine grid simulation; and diesel_12 decreases the mean predictions by 57% and 68% for coarse grid and fine grid predictions, respectively.

Figure 4.6 (a) and (b) presents 24-hr average simulated SOA concentration in $PM_{2.5}$ from the three sets of simulations in this study along with the observations from SEARCH for JST 32km domain and 8km domain, respectively. For other monitoring sites selected for this study, no continuous/semi-continuous OC and EC sample data are available to do the EC tracer analysis. At JST no observations are available on 7/7, 7/8, 7/9 and 7/10. diesel_12 significantly underpredicts the daily average SOA concentrations on all the days. Predictions from CMAQ_L and wdsmk_12 are much higher but still underpredict the concentration of SOA at JST during the whole simulation period except on 7/5. As the mean observations and predictions shown in Table 4.3, the percent underpredictions in the mean predictions for the coarse grid simulation and fine grid
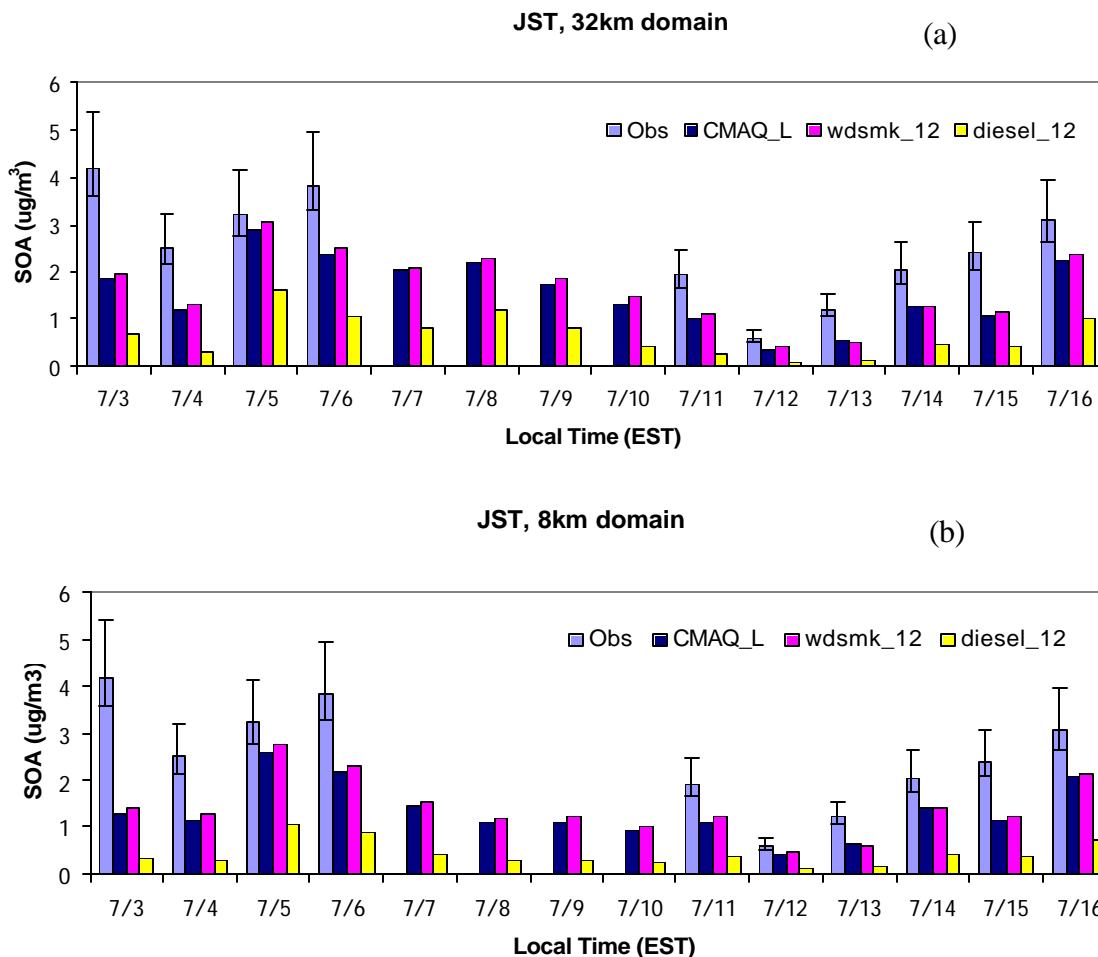
Figure 4.6. 24-hr average simulated SOA concentrations compared with observations for JST, with horizontal resolution of (a) 32km; (b) 8km. The observations were calculated using a value of 1.05 for the primary OC/EC ratio and a factor of 1.4 for conversion between the concentrations of observed secondary carbon and secondary organic aerosol. The error bars represent a range of 1.2 to 1.8 to convert the concentration of secondary OC to that of secondary organic aerosol.

simulation are 41% and 44% for CMAQ_L, 37% and 40% for wdsmk_12, and 76% and

81% for diesel_12. It can be seen that incorporation of composition effects as POA

represented as diesel soot significantly lowers the SOA predictions. In other words,

theoretically, if POA at the location of interest is mainly diesel soot, CMAQ_L, with the

assumption of ideal behavior in SOA production, greatly overpredicts the ambient SOA concentration; if wood smoke makes up most of POA, CMAQ_L slightly underpredicts the SOA concentration. However, the actual situation is that predictions from CMAQ_L and wdsmk_12 probably would also be under the ambient concentrations due to the insufficiencies in the other aspects of the models such as no treatment of SOA formation from some potential SOA precursors. Based on the source identification of Zheng et al. (2002), diesel soot made more contribution than wood smoke to the POA concentration at JST during July, 1999, so it is expected that the SOA prediction from diesel_12 is more likely to represent the actual SOA concentrations. The underprediction is probably due to the reasons analyzed in Chapter III such as no treatment of SOA formation from sesquiterpenes and isoprene in CMAQ modeling system, uncertainties in deriving SOA concentration from OC/EC data, and other required data adjustments.

3.1.3 Comparison of hourly organic aerosol concentrations in $PM_{2.5}$ ($OM_{2.5}$) predictions against measurements at Jefferson Street (JST), Atlanta, GA

Figure 4.7 presents the time series of measured and predicted $OM_{2.5}$ at JST. $OM_{2.5}$ includes both SOA and POA. POA concentrations from the three sets of simulations at the same monitoring site are very close but not exactly the same due to the different diagnostic parameters for aitken and accumulation modes, which result in slightly different fractions of each mode fitting into $PM_{2.5}$ particles. However, the difference between the simulated POA concentrations from CMAQ_L, wdsmk_12 and diesel_12 is far less than 0.1 ug/m^3, which can be ignored without interference with data interpretation. So the difference in the predicted $OM_{2.5}$ concentration is almost totally caused by the different amount of SOA concentrations predicted by the 3 sets of
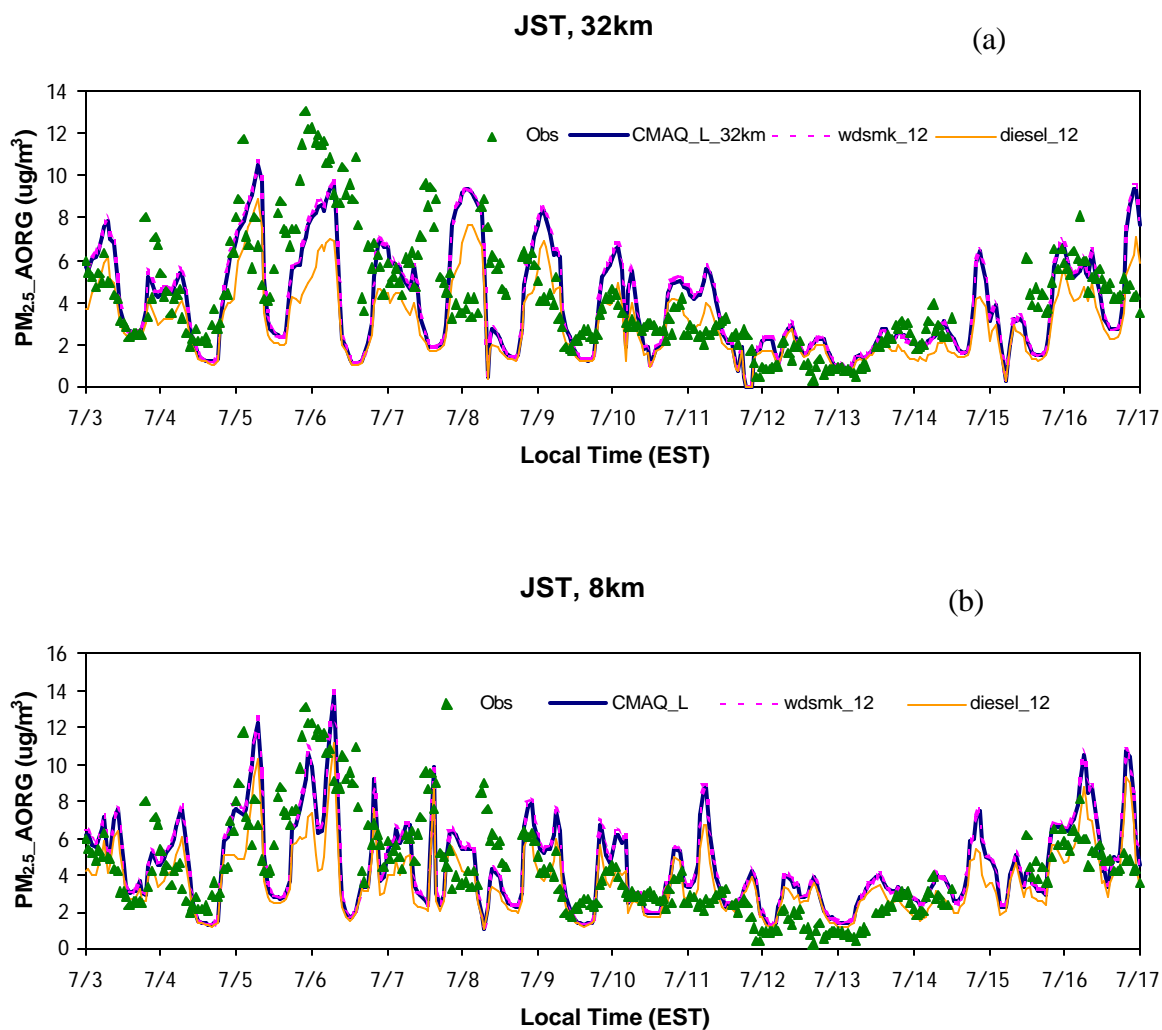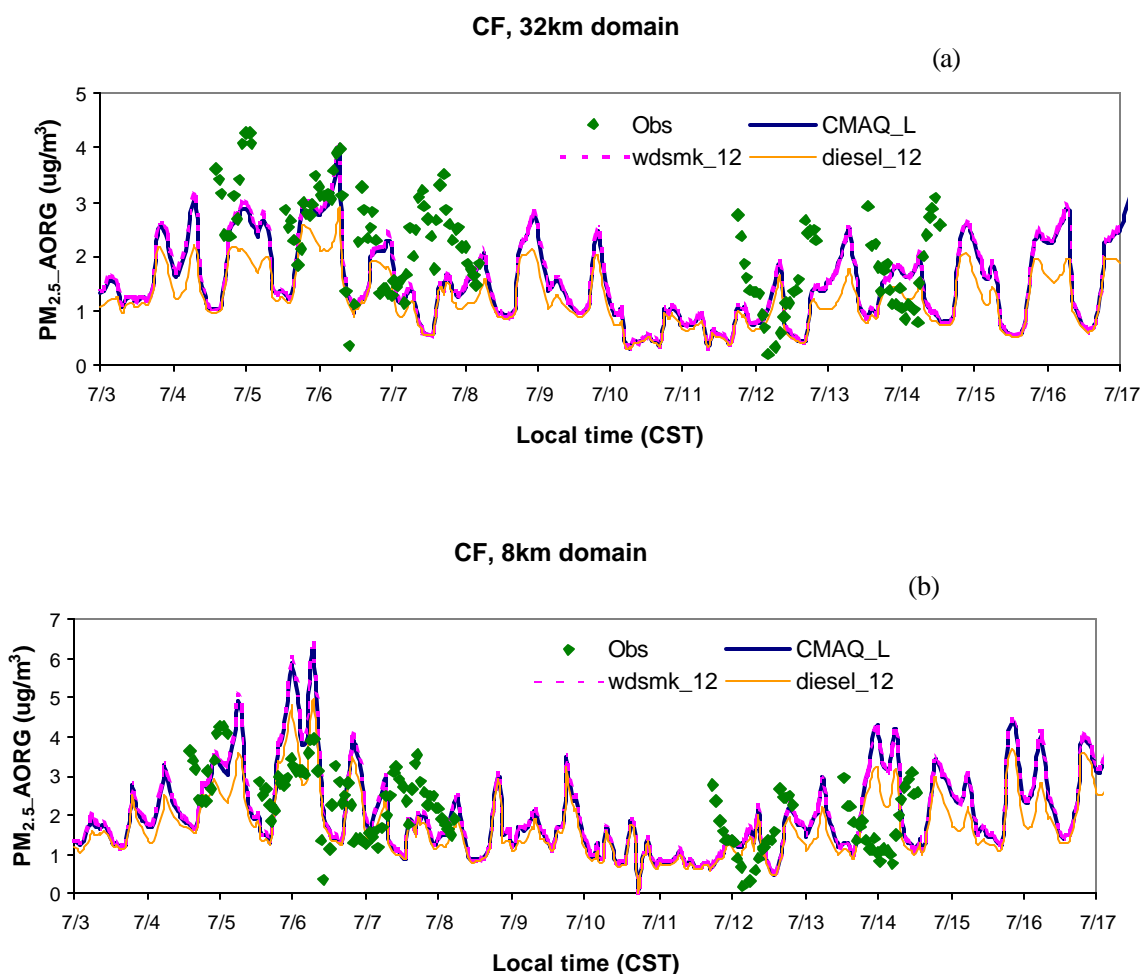
Figure 4.7. Temporal distribution of simulated organic aerosol concentration against hourly observations at JST, with horizontal resolution of (a) 32km; (b) 8km.

simulations. However, just as discussed previously, due to the absence of direct method to distinguish SOA from POA, uncertainties are involved in deriving SOA from OA concentrations, for example, the (OC/EC) $_{pri}$ ratio in EC tracer method. Comparing the hourly OM$_{2.5}$ predictions against hourly measurements excludes such kind of uncertainty and the results are more reliable. Figure 4.7 shows that simulations on both grids

reproduce very well the $OM_{2.5}$ temporal variation during the simulation period except on 7/7 and 7/8 for coarse-grid simulation and 7/8 and 7/11 for fine-grid simulation. CMAQ_L and wdsmk_12 predict very close $OM_{2.5}$ concentrations on both grids while diesel_12 predicts much lower $OM_{2.5}$ concentrations than CMAQ_L and wdsmk_12 at the points with daily maximum due to the composition effects on SOA production as detailed in section 3.1.1.

Table 4.3 shows the predicted mean $OM_{2.5}$ concentrations at JST during the period from 7/3/99 to 7/16/99 using the paired predictions and measurement data for the three sets of simulations performed in this study. The mean predictions from CMAQ_L and wdsmk_12 reproduce the mean observation quite well while diesel_12 presents a slight underprediction with 29% for simulation on coarse-grid domain and 17% on fine-grid domain. Scatter plots of $OM_{2.5}$ predictions from fine-grid simulations versus observations (Figure 4.8 (c) and (d)) show that vast majority of the data points fall within a factor of two of the observations and the correlation coefficients (~0.49) are increased dramatically compared with those between SOA predictions and ambient SOA concentrations (~0.26). The difference in data distribution suggests that the uncertainties involved in deriving SOA concentrations are notable. The distinct different between Figure 4.8 (b) and (d) suggest that some of the "observed" SOA should really be classified as POA or the POA is overpredicted. The models probably do not underpredict SOA concentration to the same extent as indicated in section 3.1.2.
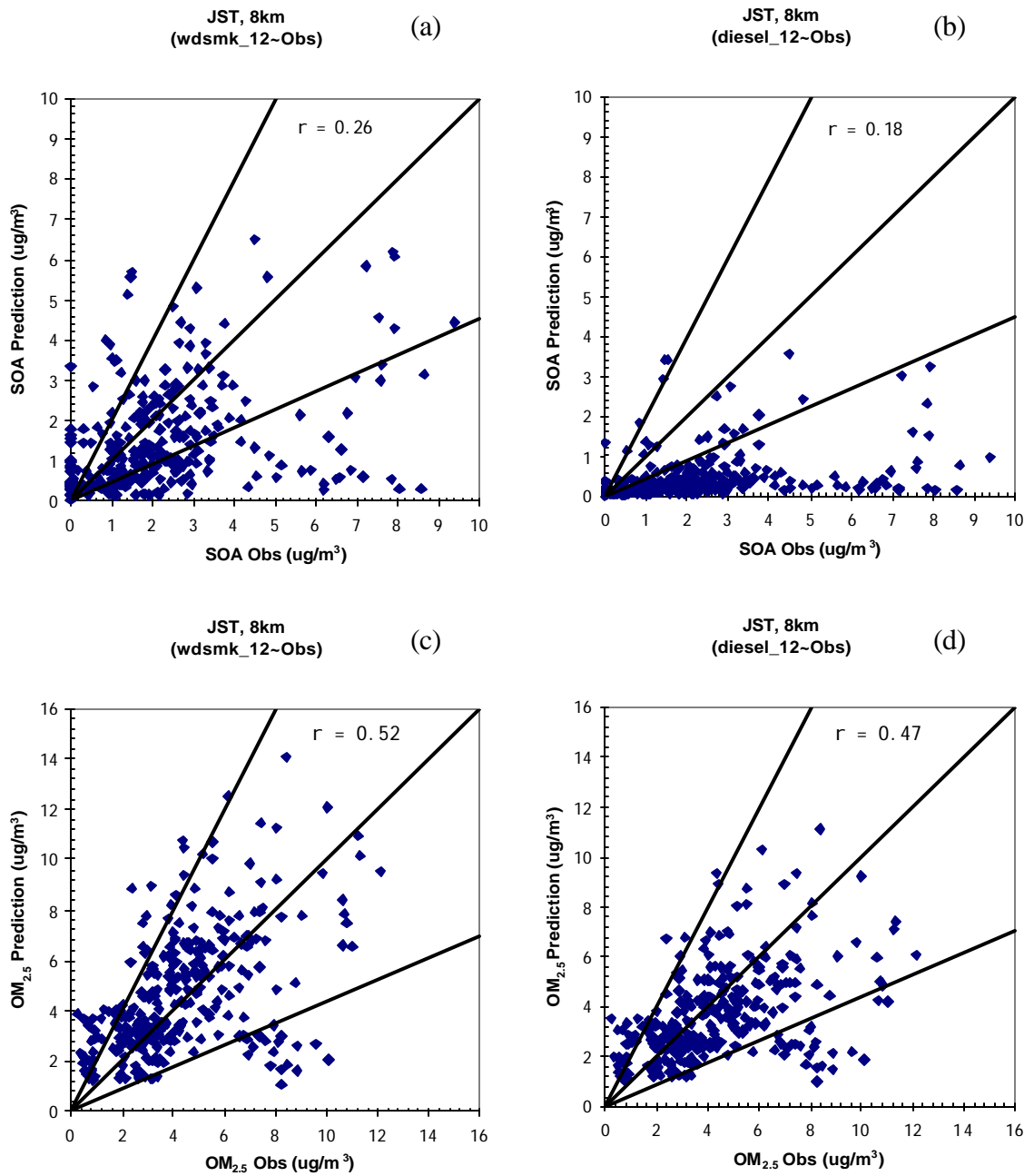
Figure 4.8. Scatter plots of hourly SOA and OM$_{2.5}$ coarse-grid predictions from wdsmk_12 and diesel_12 (abscissa) versus observations (ordinate). 1:1, 1:2 and 2:1 lines are provided for reference.

114

3.1.4 Comparison of hourly OM$_{2.5}$ predictions against measurements at Cornelia Fort (CF), Nashville, TN

The temporal distribution of predicted and measured OM$_{2.5}$ concentration data at CF is presented in Figure 4.11. CMAQ_L and wdsmk_12 predict similar OM$_{2.5}$ concentrations on both grids all the time. Generally speaking, diesel_12 predicts lower OM$_{2.5}$ concentration than CMAQ_L and wdsmk_12. However, during some periods such as on 7/10, 7/11, 7/12, diesel_12 predicts almost the same amount of OM$_{2.5}$ as CMAQ_L and wdsmk_12 on both grids, which means that on those days little SOA was formed at CF and OM$_{2.5}$ are almost completely composed of POA. It is unlikely to quantify the model performance on OM$_{2.5}$ due to the limited amount of the hourly ambient data. However, the simulations on coarse grid reproduce well the temporal variation of OM$_{2.5}$ at CF from the evening, July 5, to the morning, July 6 while the fine-grid simulation predicts reasonably well the time series of OM$_{2.5}$ concentration from evening, July 5 to the early morning of July 8, when reasonably long continuous ambient data were measured and the temporal variation trend of the predicted and measured OM$_{2.5}$ data can be compared.

CF, 32km domain

(a)

CF, 8km domain

(b)

Figure 4.9. Temporal distribution of simulated organic aerosol concentration against hourly observations at CF, with horizontal resolution of (a) 32km; (b) 8km. The factor of 1.4 was used to obtain the concentration of organic aerosols from the concentration of observed organic carbon.

3.1.5 Comparison of daily average OM$_{2.5}$ predictions against measurements at JST and YRK

Figure 4.12 and 4.13 compare the daily average OM$_{2.5}$ predictions against ambient data at JST and YRK, respectively. At both sites, during the selected simulation period, diesel_12 predicts less OM$_{2.5}$ than CMAQ_L and wdsmk_12 all the time.

CMAQ_L and wdsmk_12 predict very close daily average $OM_{2.5}$ concentrations with a little higher prediction from wdsmk_12 most of the time. For simulations on both grids, wdsmk_12 increases the mean prediction from CMAQ_L by ~ 2.7% at YRK; and ~ 2.1% at JST. diesel_12 decreases the mean predictions of CMAQ_L by ~ 24% at YRK; ~22% at JST.

When compared with the ambient data, at JST much of the time the predictions from diesel_12 are below the lower limit of the variations (1.2×OC) caused by the conversion between the observed OC concentration and the calculated OA concentration. For CMAQ_L and wdsmk_12, however, for most of the days the simulated daily average $OM_{2.5}$ concentrations are within the variations of the observations except the underpredictions on 07/14 and 07/15 for coarse grid simulation and the overprediction on 07/11 for fine grid domain simulation. The mean predictions from CMAQ_L and wdsmk_12 on both grids at JST agree very well with the mean observation, with only ~13% underprediction for the coarse grid simulation and ~7% overprediction for fine grid simulation. The percent underpredictions in mean predictions for diesel_12 at JST are 35% and 15% for coarse grid and fine grid simulations, respectively.

At YRK, as indicated by Figure 4.11, CMAQ_L, wdsmk_12 and diesel_12 all tend to underpredict the daily average aerosol concentrations, especially for the fine grid domain. The percent underpredictions in the mean predictions from fine-grid simulations for CMAQ_L, wdsmk_12 and diesel_12 are 48%, 46% and 60%, respectively. The discrepancy may be attributed to the underprediction of SOA, the uncertainties in the emission of primary $OM_{2.5}$ and probably the uncertainties in the ambient data. Overall the simulations on coarse grids give better results than those on fine grids at YRK.

117
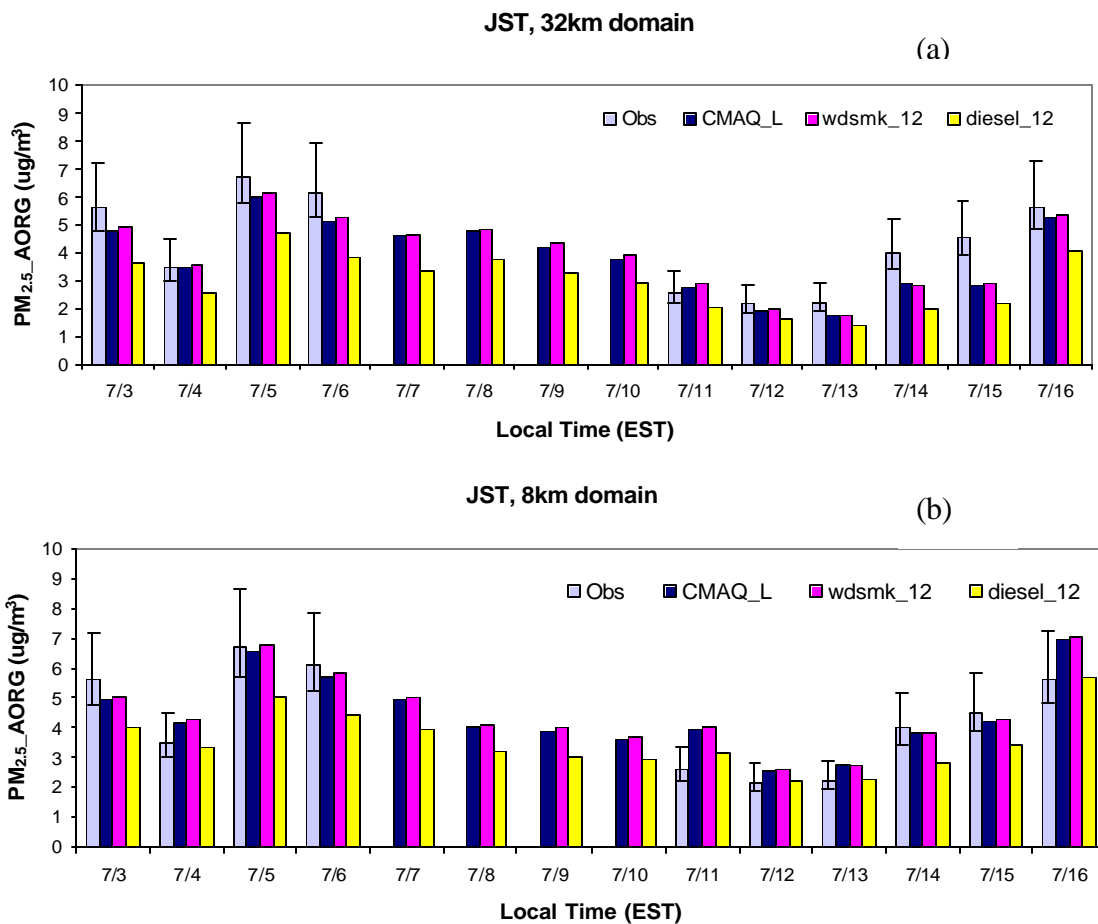
Figure 4.10. 24-hr average simulated organic aerosol concentrations compared with observations for JST, with horizontal resolution of (a) 32km; (b) 8km. The factor of 1.4 was used to obtain the concentration of organic aerosols from the concentration of observed organic carbon. The error bars represent a range of 1.2 to 1.8 to convert the concentration of observed OC to that of $OM_{2.5}$.
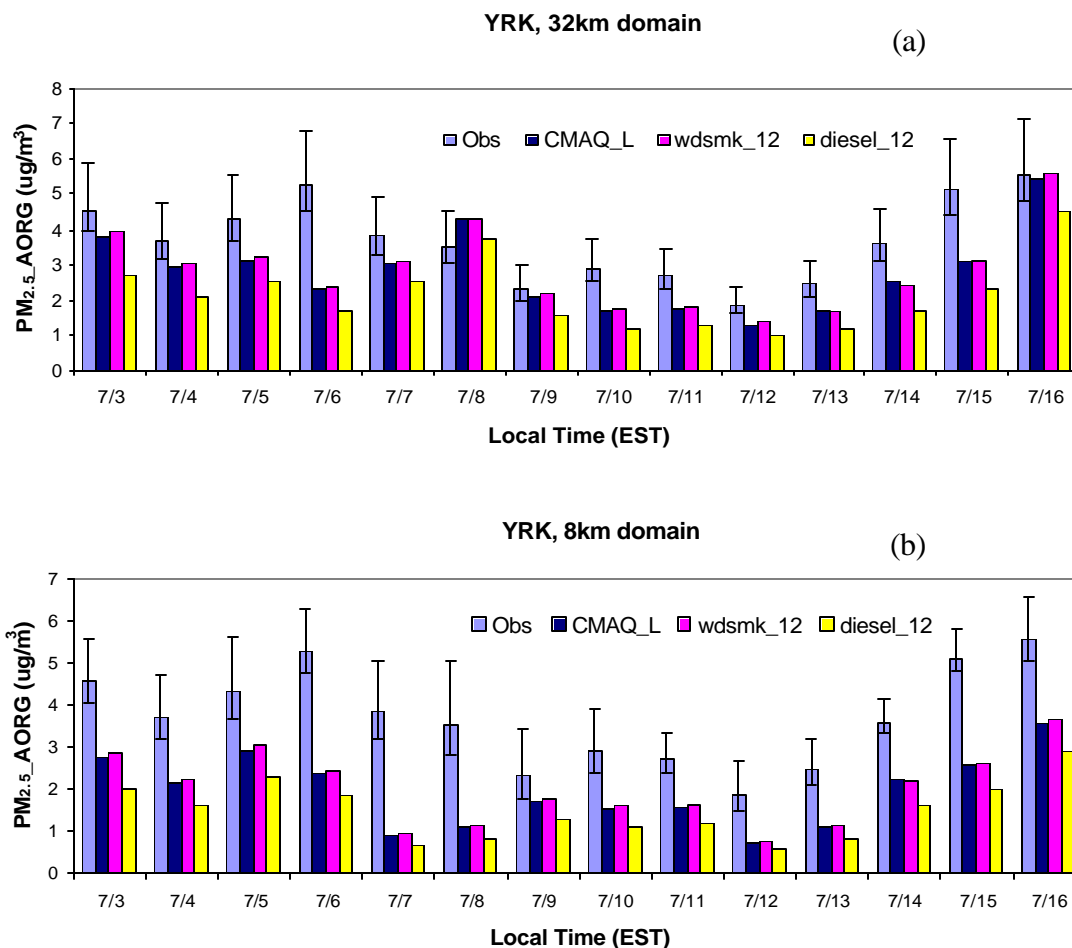
Figure 4.11. 24-hr average simulated organic aerosol concentrations compared with observations for YRK, with horizontal resolution of (a) 32km; (b) 8km. The factor of 1.4 was used to obtain the concentration of organic aerosols from the concentration of observed organic carbon. The error bars represent a range of 1.2 to 1.8 to convert the concentration of observed OC to that of $OM_{2.5}$.

3.2 Statistical Performance Evaluation

In this study, the traditional model evaluation metrics, mean error (ME), mean bias (MB), mean normalized error (MNE), mean normalized bias (MNB), normalized mean error (NME), normalized mean bias (NMB), mean fractional error (MFE) and mean fractional bias (MFB), are used to evaluate the models performance on daily average

OM$_{2.5}$ at the 11 monitoring sites across the sub-grid domain over the simulation period from July 3 to 16, 1999. The advantage and disadvantage of each model performance evaluation metrics can be found in Boylan et al. (2006) and Boylan and Russell (2006). Normalized measures such as NME and NMB (normalized by the sum of observations), MFE and MFB (normalized by the sum of observations and corresponding predictions) are more reliable than MNE and MNB, which may inflate when applied to small concentrations. Mean bias and mean errors provides the actual measures of the model performance but they are difficult to interpret if not accompanied by observations for evaluation.

The analysis results are presented in Table 4.4. CMAQ_L, wdsmk_12 and diesel_12 all tend to underpredict the mean OM$_{2.5}$ concentrations for both grid simulations. The percent underpredictions in the mean predictions for both grids are ~44% for CMAQ_L and wdsmk_12 while ~ 57% for diesel_12. As indicated by the values of MNB, NMB and MFB in table 4.2, CMAQ_L and wdsmk_12 present similar predictions, with approximately 15% higher OM$_{2.5}$ predictions than diesel_12. Overall, predictions on both grids have no distinct difference.

The difference in the statistical values between wdsmk_12 and diesel_12 indicates that the representation of POA has significant effects on OM$_{2.5}$ predictions. Compared with CMAQ_L, no matter what grids are applied, wdsmk_12 predicts a little bit higher OM$_{2.5}$ concentrations with an increase in the mean prediction of ~2.7%; diesel_12 decreases the mean predictions of CMAQ_L by ~22%. The incorporation of composition effects, therefore, slightly enhances the SOA production when POA represented as wood

Table 4.4. Performance statistics for daily average $OM_{2.5}$ concentration.

Mean Observation (ug/m³)	Data Pair	Simulations	Simulations	Mean predictions (ug/m³)	ME[2]	MB[3]	MNE[4] (%)	MNB[5] (%)	NME[6] (%)	NMB[7] (%)	MFE[8] (%)	MFB[9] (%)
4.53	78[1]	32km	CMAQ_L	2.46	2.26	-2.07	45.8	-37.6	49.9	-45.7	65.7	-59.2
			wdsmk_12	2.53	2.22	-2.00	45.2	-35.8	49.1	-44.2	64.3	-56.9
			diesel_12	1.90	2.67	-2.64	54.1	-51.9	59.0	-58.2	82.1	-80.2
		8km	CMAQ_L	2.54	2.18	-1.99	46.3	-37.0	48.2	-43.9	65.7	-59.0
			wdsmk_12	2.61	2.15	-1.91	45.7	-35.2	47.4	-42.4	64.3	-56.7
			diesel_12	1.99	2.60	-2.54	54.5	-50.6	57.3	-56.0	81.7	-78.9

Table 4.5. Performance statistics for SEARCH daily average $OM_{2.5}$ concentration.

Mean Observation (ug/m³)	Data Pair	Simulations	Simulations	Mean predictions (ug/m³)	ME[2]	MB[3]	MNE[4] (%)	MNB[5] (%)	NME[6] (%)	NMB[7] (%)	MFE[8] (%)	MFB[9] (%)
4.36	52[1]	32km	CMAQ_L	3.12	1.52	-1.23	32.8	-20.3	34.8	-28.3	39.9	-30.1
			wdsmk_12	3.21	1.47	-1.14	32.2	-18.0	33.8	-26.3	38.6	-27.5
			diesel_12	2.40	2.01	-1.96	42.1	-38.7	46.1	-44.9	57.2	-54.4
		8km	CMAQ_L	3.17	1.48	-1.18	35.6	-21.7	33.9	-27.1	44.2	-34.1
			wdsmk_12	3.26	1.44	-1.10	35.2	-19.5	33.0	-25.2	42.9	-31.5
			diesel_12	2.48	1.97	-1.88	44.8	-38.9	45.2	-43.2	61.1	-56.8

Table 4.6. Performance statistics for IMPROVE daily average $OM_{2.5}$ concentration.

Mean Observation (ug/m³)	Data Pair	Simulations	Simulations	Mean predictions (ug/m³)	ME[2]	MB[3]	MNE[4] (%)	MNB[5] (%)	NME[6] (%)	NMB[7] (%)	MFE[8] (%)	MFB[9] (%)
2.84	13[1]	32km	CMAQ_L	0.87	1.97	-1.97	67.6	-67.6	69.5	-69.5	107	-107
			wdsmk_12	0.89	1.94	-1.94	66.6	-66.6	68.5	-68.5	107	-105
			diesel_12	0.65	2.19	-2.19	75.5	-75.5	77.1	-77.1	125	-125
		8km	CMAQ_L	1.00	1.83	-1.83	62.8	-62.8	64.7	-64.7	96.9	-96.9
			wdsmk_12	1.03	1.81	-1.81	61.7	-61.7	63.7	-63.7	94.8	-94.8
			diesel_12	0.77	2.07	-2.07	71.4	-71.4	72.9	-72.9	115	-115

Table 4.7. Performance statistics for SOS99-Nashville daily average $OM_{2.5}$ concentration.

Mean Observation (ug/m³)	Data Pair	Simulations	Simulations	Mean predictions (ug/m³)	ME[2]	MB[3]	MNE[4] (%)	MNB[5] (%)	NME[6] (%)	NMB[7] (%)	MFE[8] (%)	MFB[9] (%)
6.93	13[1]	32km	CMAQ_L	1.40	5.53	-5.53	76.4	-76.4	79.8	-79.8	128	-128
			wdsmk_12	1.43	5.50	-5.50	75.9	-75.9	79.4	-79.4	127	-127
			diesel_12	1.12	5.81	-5.81	80.9	-80.9	83.8	-83.8	139	-139
		8km	CMAQ_L	1.57	5.36	-5.36	72.2	-72.2	77.4	-77.4	121	-121
			wdsmk_12	1.60	5.33	-5.33	71.7	-71.7	76.9	-76.9	119	-119
			diesel_12	1.29	5.63	-5.63	76.8	-76.8	81.3	-81.3	131	-131

[1]The statistics are calculated by using the simulation~observation data pairs with the observed organic aerosol concentration > 0.5 μg/m³.

[2]Mean Error: $ME = \dfrac{1}{N}\sum\limits_{1}^{N}\left|Model - Obs\right|$

[3]Mean Normalized Gross Error: $MNE = \dfrac{1}{N}\sum\limits_{1}^{N}\left(\dfrac{\left|Model - Obs\right|}{Obs}\right)\bullet 100\%$

[4]Mean Bias: $MB = \dfrac{1}{N}\sum\limits_{1}^{N}(Model - Obs)$

[5]Mean Normalized Bias: $MNB = \dfrac{1}{N}\sum\limits_{1}^{N}\left(\dfrac{Model - Obs}{Obs}\right)\bullet 100\%$

[6]Normalized Mean Error: $NME = \dfrac{\sum\limits_{1}^{N}|Model - Obs|}{\sum\limits_{1}^{N}Obs}\bullet 100\%$

[7]Normalized Mean Bias: $NMB = \dfrac{\sum\limits_{1}^{N}(Model - Obs)}{\sum\limits_{1}^{N}Obs}$

[8]Mean Fractional Error: $FE = \dfrac{2}{N}\sum\limits_{1}^{N}\left|\dfrac{Model - Obs}{Model + Obs}\right|$

[9]Mean Fractional Bias: $FB = \dfrac{2}{N}\sum\limits_{1}^{N}\left(\dfrac{Model - Obs}{Model + Obs}\right)$

smoke particles while considerably lowered the model predictions and enlarged the discrepancies when POA represented as diesel soot.

Based on the performance goals recommended by EPA (EPA, 2001) in terms of MNB ($\leq$ 15%) and MNE ($\leq$ 30%) for a good performance of PM, CMAQ_L, wdsmk_12 and diesel_12 all present a relatively poor prediction of $OM_{2.5}$. However, simulation of $OM_{2.5}$, a mixture of hundreds of components, is much more complicated than single pollutant, for example O3. Based on the model performance criteria on $OM_{2.5}$ proposed in Boylan and Russell (2006) of $\pm75\%$ and $\pm60\%$ as in MFE and MFB, respectively, for the simulation of $OM_{2.5}$, the performance of CMAQ_L and wdsmk_12 should be considered acceptable.

As in Chapter III, the evaluation statistics are also calculated separately for each individual data set as shown in table 4.5, 4.6 and 4.7. Model performance on each of the individual data sets indicates that the model performance varies with different data sources. Based on Boylan and Russell (2006), CMAQ_L and wdsmk_12 produces excellent simulations of $OM_{2.5}$, while diesel_12 also performs very well, on SEARCH data. The percent underpredictions in the mean predictions are ~ 26% for CMAQ_L and wdsmk_12 and 44% for diesel_12. Large underpredictions exist for $OM_{2.5}$ at IMPROVE and SOS99-Nashville monitoring sites. For IMPROVE data set, the percent underpredictions for CMAQ_L and wdsmk_12 in the mean predictions are ~ 65%; for diesel_12, ~ 75%. The worst case is with SOS99 data set. The percent underpredictions in the mean predictions are ~78% for CMAQ_L and wdsmk_12 and ~82% for diesel_12. The values of MFE and MFB indicate an unacceptable model performance on $OM_{2.5}$ at IMPROVE and SOS99-Nashville monitoring sites based on Boylan and Russell (2006).

The number of data pairs is pretty small applied to evaluate the model performance on IMPROVE and SOS99-Nashville data sets, which is constrained by the fine-grid simulation domain. A model performance evaluation, using the coarse-grid predictions, on all the appropriate sites from IMPROVE is recommended.

The underlying reasons for the underpredictions have been analyzed in Chapter III. Briefly stated, the uncertainties in the OC emission inventories, no simulation of some potential SOA precursors such as sesquiterpenes and isoprene, and the inadequacy in the smog chamber data to represent the SOA formation under real atmosphere conditions, as well as the assumption of reversible absorption in SOA production may all contribute to the discrepancy between the predictions and ambient $OM_{2.5}$ data.

4. Conclusions

In this study, the organic aerosol module in CMAQ was modified to incorporate the composition effects on SOA production. The online calculation of ζ_i, the activity coefficient of the lumped group i, and $C_{sat,i}^*$, the effective saturation concentration of pure species i, is incorporated into the module and accounts for the composition effects on SOA production.

Simulation results indicate that the composition effects on SOA production depend closely on the POA composition representation. Wood smoke and diesel soot, the two largest contributors to ambient aerosols in southeastern US in summer, has been respectively used to represent POA in this study. The simulation results indicate that the polarity difference between wood smoke and diesel soot has a dramatic effect on the amount of SOA produced. Compared with the SOA production with no composition

effects accounted for, the simulations with POA represented as wood smoke slightly enhances the SOA production while the simulation with POA as diesel soot considerably lowered the model predictions and enlarged the discrepancies between the modeled values and ambient data. The similar polarity of wood smoke particles and SOA10 and SOA12, the lumped groups corresponding to biogenic sources and the two largest contributors to the SOA mass production, makes the aerosol mixture made up of SOA products and POA represented as wood smoke actually form a quasi-ideal solution as shown by the predicted activity coefficients of the aerosol components. The unit activity assumption is a good approximation in such a case to speed up the simulation. For the assumption of POA as diesel soot, the apparent difference in simulated SOA concentrations with/without consideration of composition effects makes the unit activity coefficient assumption unjustified. The nonideality in the solution composed of diesel soot (POA) and the SOA products greatly lowers the concentration of SOA. The simulation results indicate that at JST due to incorporation of composition effects, the predicted mean SOA concentration over the simulation period were lowered by ~60% when POA is represented as diesel soot. Diesel soot is a significant POA contributor in urban areas, especially in summer (Zheng et al., 2002; Fraser et al., 2003), composition effects on SOA production in these areas should be accounted for.

Compared against ambient daily average $OM_{2.5}$ data, underprediction is the common trend. The MNB, NMB and MFB for the predictions over the southeastern U.S. domain with horizontal resolution of 8 km are, respectively, -35, -42 and –57 for POA as wood smoke and –51, -56 and –79 for POA as diesel soot compared with –37, -44 and –59 when no composition effects are considered. Similar results are obtained for the 32 km

domain. However, the model performance differs a lot on different data sources. This may indicate some uncertainties in the measurement data.

Incorporation of partitioning composition effects into air quality models is one step towards more accurate descriptions of SOA production. Due to the fact that our understanding of SOA production is not complete, the simulation results on $OM_{2.5}$ are not unexpected. Model predictions will improve with the development of the state-of-the-science concerning carbonaceous aerosols as well as the availability of additional experimental data.

CHAPTER V

COMPOSITION- AND TEMPERATURE- DEPENDENT SECONDARY ORGANIC AEROSOL (SOA) PARTITIONING: UNCERTAINTIES IN THE SIMULATION RESULTS

1. Introduction

Air quality models are very important tools to study the formation and evolution of air pollutants in the atmosphere (Russell and Dennis, 2000). However, accurate simulation of secondary organic aerosol (SOA) presents many challenges because of the inadequate knowledge on their formation pathways and sparse data on their thermodynamic properties which are needed to determine their partitioning parameters. Lack of experimental data contributes to the uncertainties in input data, which subsequently propagates to the outputs. It's important to note that for every input to the model, some degree of uncertainty exists. However, some inputs have greater uncertainties than others due to the lack of enough information to make accurate estimation, for example, for the enthalpy of vaporization for the individual SOA components before lumping. If the uncertainty for an input is relatively large and model results are sensitive to that input, a change in the assigned value would produce a notable difference in the result, and it may be worthwhile to try to reduce the level of uncertainty in that input. So the simulations described in this chapter are designed to identify some of these critical gaps in our knowledge where further research efforts will be able to improve SOA simulation.

Due to the fact that we do not know enough about the SOA products and their thermodynamic properties, in formulating lumped groups for composition- and temperature- dependent SOA partitioning, some of the most important sources of uncertainties are the assigned values of enthalpy of vaporization for the individual SOA components and the lumping criteria applied to convert individual components into lumped groups. The enthalpy of vaporization for the SOA components directly affects the temperature dependence of the partitioning behavior of the lumped groups. Different lumped groups formulated by different lumping criteria may have different structure and partitioning parameters. In addition, including the organics-related water in the simulation system may also affect a lot the SOA mass production. The following uncertainties, therefore, were investigated in this study: the enthalpy of vaporization of the modeled species, the inclusion of organics-related water, and the adopted lumping criteria. The Community Multiscale Air Quality model (CMAQ) incorporated with the revised aerosol module (with composition effects accounted for as elaborated in Chapter IV) is used as test bed to do the simulation.

2. Factors of Uncertainty

In this study, simulation results from wdsmk_12 in Chapter IV are used as base case to quantify the influence of investigated uncertainty factors on SOA production. In wdsmk_12, 12 lumped groups are used to represent SOA products and the pre-existing primary organic aerosol (POA) was represented as wood smoke particles. No treatment of the aerosol phase organics-related water is addressed in the simulation system. Vaporization enthalpy of 156KJ/mol is assigned to each individual SOA products to

represent the temperature dependence of their partitioning behavior. Thus, the key uncertainty factors investigated in this study are temperature dependence, the organics-related water, lumping criteria adopted to lump the individual products. The effect of POA representation on SOA production has been studied and analyzed in Chapter IV.

2.1 Vaporization Enthalpy

As described in Chapter II, the gas/particle partitioning process in CMAQ is simulated as an absorptive process, which follows the model proposed by Pankow (1994a, 1994b). If the aerosol phase is assumed to form a pseudo ideal solution as demonstrated by laboratory studies (Odum et al, 1996, 1997b), the effective saturation concentration $C_{sat,i}^*$ (μg/m^3) of pure species i can be expressed as (Strader et al., 1999; Schell et al., 2001),

$$C_{sat,i}^* = \frac{\mathbf{z}_i p_i^0 MW_i 10^6}{RT}$$
(5.1)

where, $\mathbf{z}i$ is the activity coefficient in the absorbing aerosol phase; p_i^0 (torr) is the sub-cooled liquid vapor pressure; MW_i (g/mol) is the molecular weight; R is the gas constant (8.314Jmol^{-1}k^{-1}), T (K) is the temperature.

Temperature dependence of $C_{sat,i}^*$ mainly reflect through the relationship between saturation vapor pressure and temperature as indicated by Clasusius-Clapeyron equation as follows,

$$P_i^0 = C_i \exp(\frac{-H_i}{RT})$$
(5.2)

where C_i is the pre-exponential constant of product i (atm); H_i is the enthalpy of vaporization of product i (kcal/mol).

Substitute (5.2) into equation (5.1), the following equation is obtained for the temperature dependence of $C_{sat,i}^*$,

$$C_{sat,i}^* = \frac{MW_i V_i C_i 10^6}{RT} \exp(\frac{-B_i}{T})$$ (5.3)

where B_i is equal to H_i/R.

If the $C_{sat,i}^*$ value at a reference temperature ($C_{sat,T_{ref}}^*$) is known and the vaporization enthalpy of the compound can be assumed to be constant during the temperature range of interest, then the relationship between $C_{sat,T_{ref}}^*$ and $C_{sat,T}^*$, the value of $C_{sat,i}^*$ at any other temperature T, is,

$$\frac{C_{sat,T}^*}{C_{sat,T_{ref}}^*} = \frac{T_{ref}}{T} \exp\left(-B_i(\frac{1}{T} - \frac{1}{T_{ref}})\right)$$ (5.4)

Then if ideal behavior is assumed, at temperature T the ratio between the $C_{sat,i}^*$ values for the same lumped group with different formulated B values is,

$$\frac{C_{sat,B1}^*}{C_{sat,B2}^*} = \exp[(\frac{1}{T} - \frac{1}{T_{ref}})(-B1 + B2)]$$ (5.5)

where T_{ref} is the reference temperature, referred to the smog chamber experimental temperature in this study when appropriate. If no specific smog chamber experiment is available for formulating the lumped groups corresponding to certain precursor such as ALK5, $T_{ref} = 308K$; B1 and B2 are the corresponding B values in different simulations.

Equation (5.5) indicates that for the same lumped group, when the ambient temperature is lower than T_{ref}, higher B value will result in lower $C^*_{sat,i}$ value.

Sheehan and Bowman (2001) investigated the SOA production dependence on temperature by using a box model and the simulation results indicate that the predicted SOA concentrations may vary a lot depending on the vaporization enthalpy used to reflect the extent of temperature dependence. The expected range of the vaporization enthalpy suggested in Sheehan and Bowman (2001) is 42 – 105 kJ/mol and the enthalpy values that have been used in different model studies are 42 kJ/mol (Chung and Seinfeld, 2002), 79 kJ/mol (Andersson-Sköld and Simpson, 2001; Pun et al., 2003; Tsigaridis and Kanakidou 2003), 156 kJ/mol (Strader et al., 1999; Schell et al., 2001). The current SOA module in CMAQ is developed on the basis of Schnell et al. (2001) and inherited the enthalpy value 156 kJ/mol to account for the temperature dependence of saturation vapor pressures of the semi-volatiles that can partition into the aerosol phase. The base case simulation wdsmk_12 adopted this value, too, while wdsmk_LB used an alternative lower enthalpy value 83 kJ/mol, the mid point of the enthalpy range suggested in Sheehan and Bowman (2001), for all the individual aerosol components used to formulate the lumped products. The disparity in the simulation results from wdsmk_12 and wdsmk_LB can illustrate the influence of temperature dependence on SOA production.

2.2 Organics-related water

The water absorbed into the aerosol phase can affect the amount of SOA produced via changing the activity coefficient ζ and lowering the mean molecular weight

of the absorbing phase. Seinfeld et al (2001) theoretically analyzed the humidity effect on $K_{ab,i}$, the inverse of equivalent $C_{sat,i}^{*}$. The complicated humidity effects on activity coefficient makes it difficult to predict its effects on final SOA produced. For hydrophilic components, more water in the absorbents surely favors their partitioning into aerosol phase; for hydrophobic ones, however, it may or may not be such a case.

In this study, the water associated with the organics was modeled as another semivolatile product in the SOA production process. Organics and inorganics are treated separately and no interaction between the organics and inorganics is accounted for (ZSR relationship is assumed). This approach has been tested to be a good first-order approximation for the water uptake by the internally mixed inorganic-organic particle (within 20%) (Virkkula et al., 1999; Cruz and Pandis, 2000). However, when the organics present affect the hygroscopic behavior of the inorganic components, this approach may not be appropriate.

At the beginning of each time step the saturation vapor pressure of water, $p_{H_2O(T)}^{*}$ (Pa), at ambient temperature T (K) was calculated using the following equation from Appendix of Kulmala et al. (1998)

$$p_{H_2O_{(T)}}^{*}(P_a) = \exp(77.34491296 - 7235.424651/T - 8.2 \times \ln(T) + T \times 5.7113 \times 10^{-03}) \quad (5.6)$$

Then combined with the corresponding activity coefficient from UNIFAC and the molecular weight of water, MW_{H_2O}, as well as the universal ideal gas constant R, the saturation concentration of water in aerosol phase at ambient temperature T, C_{sat,H_2O}^{*} ($\mu g/m^3$), was calculated by equation (5.1). The total amount of water $Ctot_{H_2O,t}$ ($\mu g/m^3$) in both gas phase and aerosol phase is determined by equation (5.7)

using $p^*_{H_2O(T)}$, the ambient relative humidity *AIRRH*, and both I and J mode organics-related water, *CBLK(VH2OOI)* and *CBLK(VH2OOJ)*, in aerosol phase from last time step,

$$Ctot_{H_2O,t} = \frac{MW_{H_2O}P^*_{H_2O}}{RT} \times AIRRH + CBLK(VH2OOI) + CBLK(VH2OOJ) \quad (5.7)$$

Then the set of 13 equations (12 for semi-volatile organics and 1 for water) defined by equation (4.5) were solved to get aerosol phase concentrations of each species, $C_{aer,i,t}$.

After the condensation process, the water associated with organic aerosol was then split into I and J mode proportionally to total organic aerosol (POA+SOA) in each mode at the end of the last time step, the same approach adopted in CMAQ for anthropogenic and biogenic organic aerosol.

2.3 Lumping Criteria

In consideration of the impossibility and no need to individually track and model each of the large number of products identified corresponding to each SOA precursor, lumped species are formulated for modeling purpose. For each precursor 2 or 3 lumped groups are used to represent the partitioning characteristics of the whole product mixture. In this study, structure and partitioning parameters formulated by the lumping method developed by Bian and Bowman (2002, 2005) was used to provide necessary calculation parameters, such as the number and type of functional groups as well as the vapor pressures for the lumped products, etc.

Different lumping criteria may affect the partitioning characteristics of the lumped groups due to the differences in structure and partitioning properties such as α and B values. In the base case simulation (wdsmk_12), 12 lumped groups were formulated

based on the vapor pressures of the individual products at 308 K, with 10^{-5} torr and 10^{-9} torr as dividing lines. ALK5 and TRP1 each has 3 lumped products and ARO1, ARO2, and OLE2 each has 2 products. In order to study the effects of different lumping criteria on SOA simulation results, wdsmk_10 was conducted using 10 lumped products to simulate the SOA production, with 2 lumped groups formulated for each precursor (as indicated in Table 5.3) using 1.5×10^{-5} torr as diving line. Coincidently, the lumped groups for ARO1, ARO2, and OLE2 are all the same from these two different lumping criteria and only ALK5 and TRP1 are affected. Note that basically the same lumping procedure presented in Bian and Bowman (2002 & 2005) was used to get the lumped groups except that mole-based, instead of mass-based, coefficients were used to determine the molecular weight and the structure of the lumped products.

3. Simulation results and analysis

3.1 The simulations

In addition to the base case simulation wdsmk_12, 3 more sets of simulations are performed for evaluating the uncertainties in the simulation results caused by 1) the assigned enthalpy of vaporization for the individual SOA components before lumping (wdsmk_LB); 2) inclusion of organics-related water in the simulation (wdsmk_13); and 3) different lumping criteria to convert individual products to lumped groups (wdsmk_10). Table 5.1 shows the overall descriptions of the SOA modules in different simulations.

Table 5.1. Overview of the organic aerosol module in the 4 sets of simulations.

Model version	wdsmk_12	wdsmk_LB	wdsmk_13	wdsmk_10
# of products	12	12	12	10
Simulation includes organics-related water	No	No	Yes	No
enthalpy value for the individual products before lumping	156 kJ/mol	83 kJ/mol	156 kJ/mol	156 kJ/mol
activity coefficients	Calculated using UNIFAC as a function of x_i, s_{ji}, and T			
POA	Simulated as wood smoke particles			

Table 5.2. Partitioning properties of lumped groups for simulation wdsmk_LB.

Lumped Group	Model Name	α	p^{o*} (torr)[a,b]	MW	B (K)[b]
TRP1					
a	SOA9	0.330	**5.54×10^{-4}**	163.7	**9863**
b	SOA10	0.346	**1.48×10^{-6}**	179.0	**9422**
c	SOA12	0.013	**3.36×10^{-13}**	184.0	**10000**
ARO1					
a	SOA7	0.255	**1.71×10^{-4}**	136.0	**9601**
b	SOA8	0.170	**2.54×10^{-6}**	148.0	**6498**
ARO2					
a	SOA5	0.144	**8.43×10^{-5}**	170.1	**9763**
b	SOA5	0.144	**5.26×10^{-6}**	201.5	**8024**
OLE2					
a	SOA3	0.645	**7.02×10^{-5}**	111.1	**9753**
b	SOA4	0.102	**1.16×10^{-6}**	133.4	**5427**
ALK5					
a	SOA1	0.099	**9.18×10^{-5}**	198.7	**9875**
b	SOA2	0.099	**9.33×10^{-7}**	279.1	**5429**
c	SOA11	0.022	**1.67×10^{-9}**	422.2	**9922**

[a] p^{o*} is corresponding to 298K, which is the reference temperature in CMAQ.
[b] The values of p^{o*} and B highlighted in bold are different from those in base case simulation wdsmk_12.

As stated in section 2.1, in the simulation wdsmk_LB, the enthalpy value of 83kJ/mol, instead of 156kJ/mol, are assumed for all the individual products. The effect of

this change is only on the B values for the lumped groups, i.e., the temperature dependence of the lumped groups is decreased when compared with the base case. The structure information and the α values of the lumped groups is identical as those in wdsmk_12, which can be found in Tables 3.5 and 3.6 in Chapter III. Table 5.2 presents the vapor pressures at 298K and B values of the lumped groups in simulation wdsmk_LB. In wdsmk_13, organics-related water was added in the simulation and was modeled in the same way as other 12 organic semi-volatiles, which are all the same as those applied in wdsmk_12. In wdsmk_10, 2 products are formulated for each precursor. The affected precursors are TRP1 and ALK5. For ARO1, ARO2 and OLE2, identical lumped groups as those for wdsmk_12 are applied. The partitioning properties and the structure information of the lumped groups for wdsmk_10 are presented in table 5.3 and table 5.4.

Table 5.3. Partitioning properties of lumped groups for simulation wdsmk_10.

Lumped Group	Model Name	α	p^{o*} (torr)[a]	MW	B (K)
TRP1					
a	SOA9	0.330	2.41×10^{-4}	163.7	17492
b	**SOA10**[b]	**0.359**	**8.25×10^{-7}**	**179.1**	**13385**
ARO1					
a	SOA7	0.255	8.49×10^{-5}	136.0	15999
b	SOA8	0.170	1.06×10^{-6}	148.0	14537
ARO2					
a	SOA5	0.144	3.78×10^{-5}	170.1	15949
b	SOA6	0.144	1.79×10^{-6}	201.5	16320
OLE2					
a	SOA3	0.645	7.02×10^{-5}	111.1	17812
b	SOA4	0.102	1.16×10^{-6}	133.4	13304
ALK5					
a	**SOA1**[b]	**0.132**	**1.69×10^{-5}**	**202.5**	**16922**
b	**SOA2**[b]	**0.088**	**1.21×10^{-7}**	**347.6**	**12757**

[a] p^{o*} is corresponding to 298K, which is the reference temperature in CMAQ.
[b] The lumped groups highlighted in bold are different from those in wdsmk_12.

Table 5.4. UNIFAC structural properties of lumped groups for simulation wdsmk_10.

Precursor	Lumped Group	UNIFAC functional groups ID#												
		CH3	CH2	CH	C	ACH	AC	ACCH3	OH	ACOH	CH3CO	CH2CO	CHO	COOH
TRP1	a	2	1.83	1.77	1.38				0.53			0.55	0.45	0.48	0.07
	b*	**2**	**1.40**	**2.11**	**1**				**0.18**			**0.52**	**0.073**	**0.11**	**1.30**
ARO1	a			0.68		2.65	0.66	0.33	0.68	0.33			0.34	1
	b			2					2		1			1
ARO2	a					5.31	2.75	0.76						1.06
	b					7.98	4.51	0.37						0.75
OLE2	a	1	2.25	0.02					0.08				0.54	1.37
	b		2.15	0.44					0.44					2
ALK5	a*	**0.65**	**9.54**											**1.35**
	b*	**1**	**20.54**											**1**

*The molecular structure of the lumped groups highlighted in bold is different from those in wdsmk_12.

3.2 Simulation results

The simulations were performed on the same modeling domains as in Chapters III and IV. Same emission files and meteorological data were applied for all simulations. The direct outputs for aerosol components from the models in I and J modes are post processed in order to make comparison against ambient data. The data processing procedure is detailed in section 3.1.1 in Chapter III. The final predictions, which represent the predicted values corresponding to $PM_{2.5}$, are presented here for comparisons against each other and against ambient data. The predicted SOA concentrations from the simulations are presented first because they are of the most concern considering the modifications incorporated into the organic aerosol module. Comparison with field data follows.

In each figure, different predicted values are indicated by the name of the corresponding model version. The coarse-grid simulation results at JST are presented to illustrate the effects of each uncertainty on predictions. Figure 5.1 presents the time series of the predicted SOA concentrations (even for wdsmk_13, no water include but only SOA concentrations) against hourly observations; The daily average SOA concentration in $PM_{2.5}$, along with the observations, are presented in Figure 5.6; For the organic aerosol concentration in $PM_{2.5}$ ($OM_{2.5}$), Figure 5.7 compares hourly $OM_{2.5}$ predictions against measurements and Figure 5.8 shows the comparisons between daily $OM_{2.5}$ predictions against observations.

JST, 32km
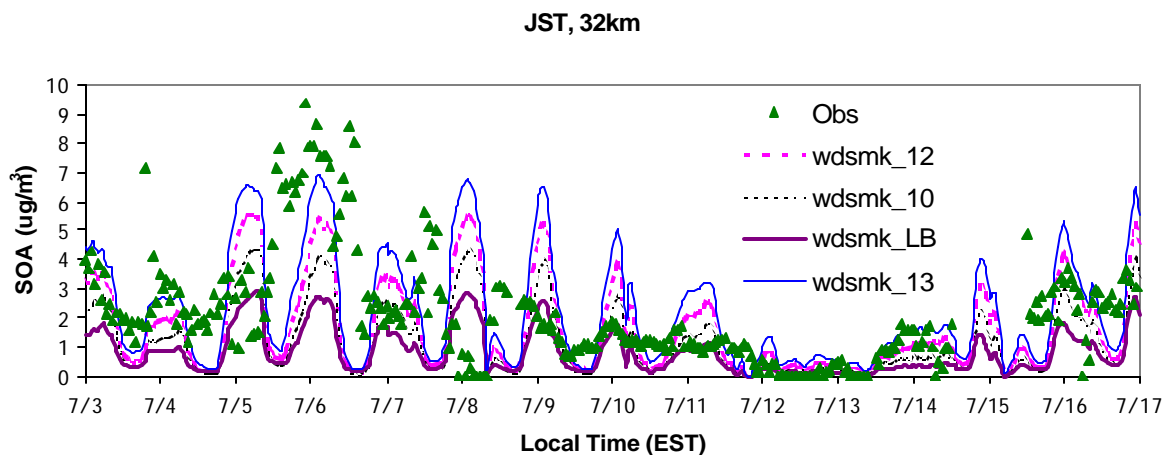
Figure 5.1. Temporal distribution of coarse-grid SOA predictions against hourly observations at JST from different model versions.

3.2.1 Effect of Different Vaporization Enthalpy

As indicated in equation (5.2), vaporization enthalpy assumed for the products have great effects on the vapor pressure calculation, and subsequently on the saturation concentration of the species, when temperature changes. This effect has been shown in Figure 5.1 by the simulated SOA concentrations from wdsmk_12 and wdsmk_LB. As shown in Figure 5.1, the low temperature dependence of the saturation concentrations of the model species in wdsmk_LB significantly lowers the SOA predictions especially at the daily maximum due to the low ambient temperature at these points. The mean SOA prediction from wdsmk_LB is 51% less than that from wdsmk_12.

The lumped groups in wdsmk_12 and wdsmk_LB have the same $C^*_{sat,i}$ values at the reference temperature (T_{ref}). When the temperature is lower than T_{ref}, however, the lumped groups in wdsmk_LB will have higher $C^*_{sat,i}$ values than the corresponding

140

values in wdsmk_12 due to their lower B values. The reference temperature T_{ref} for TRP1 is 308K and for ARO1, ARO2 and ALK5 is 310 K. The typical daily temperature variation at JST throughout the simulation period is from 295 K to 303 K. At 295 K, according to equation (5.4), the ratio of the $C_{sat,i}^*$ values between wdsmk_12 and wdsmk_LB is 0.29 for SOA10, which is the largest contributor to the SOA mass production; however, at 303 K, the ratio is 0.63. This means that the lower the ambient temperature than T_{ref}, the larger the temperature effect.

For the same lumped group, wdsmk_12 and wdsmk_LB predict very similar activity coefficients. The discrepancy between the simulated SOA concentrations is mainly caused by the different temperature dependence of $C_{sat,i}^*$.

3.2.2 Effect of Organic-Related Water

When organics-related water is added into the simulation, the water uptake into the aerosol phase influences the partitioning behavior of the semi-volatiles. As shown in Figure 5.1, due to water absorbing into aerosol phase, the predicted daily maximum SOA concentrations are approximately 20% higher than those from wdsmk_12. When compared with the mean prediction from wdsmk_12, wdsmk_13 increases the SOA average concentration prediction by 35%.

The amount of water absorbing into aerosol phase is shown in Figure 5.2. Basically water uptake varies with the variability of relative humidity (RH). However, the actual amount of water absorbed into the aerosol phase, in the range from ~0 to ~2 $\mu g/m^3$, is also limited by the amount of aerosol present. The predicted activity coefficients for the individual lumped groups and water are shown in Figure 5.3. The activity coefficient for

water is in a pretty narrow range from 1.19 to 1.54, which renders water makes up a large

portion of the aerosol phase on mole basis considering the high RH at JST.

JST, 32km
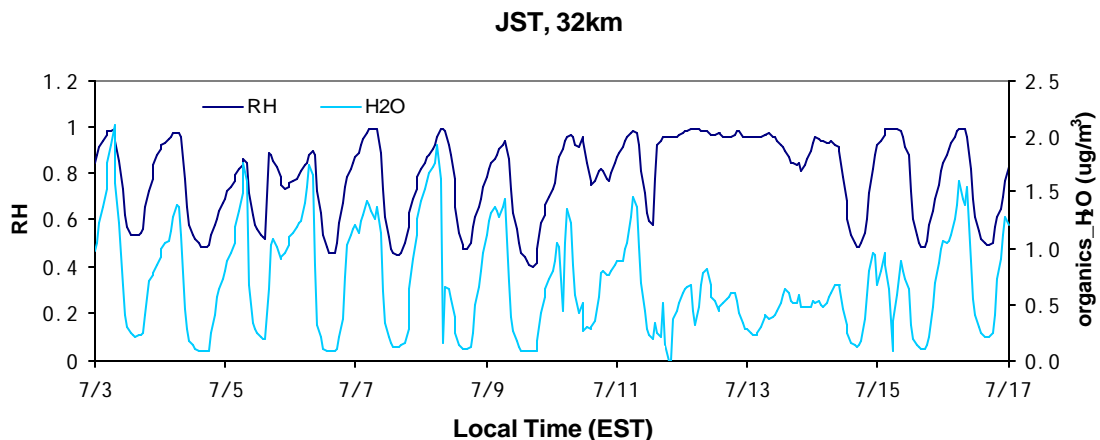
Figure 5.2. Temporal distribution of coarse-grid predicted organics-related water concentration at JST.

Compared with the activity coefficients predicted in wdsmk_12 for the SOA

components in Figure 4.4 (b) in Chapter IV, the activity coefficients for all the lumped

groups but SOA7 and SOA8 are increased by different extents. The biggest elevation

occurs to SOA11, the highly hydrophobic 3rd lumped group corresponding to ALK5, with

its predicted activity coefficient varying in the range of 41 to 2027, compared with 15 to

31 predicted in wdsmk_12. The activity coefficients for SOA10 and SOA12, the two

biggest contributors to the SOA mass production, go up slightly and are in the range of

0.91-1.43 and of 0.95 to 1.94, respectively, compared with the range of 1.0-1.1 and of

0.84-0.98 predicted in wdsmk_12. For other groups, moderate increases of a couple of

times are predicted. For SOA7 and SOA8, the lumped groups formulated to represent the

aerosol mixtures from ARO1, their predicted activity coefficients in wdsmk_13 decrease

from 1.6-2.1 in wdsmk_12 to 0.88-1.5 and from 1.0-4.7 in wdsmk_12 to 0.18 - 1.1, respectively.

Generally speaking for the same lumped group the activity coefficient predicted in wdsmk_13 varies in a wider range than the predictions from wdsmk_12 especially SOA11, SOA2 and SOA6. The greater variability of the predicted activity coefficients in wdsmk_13 indicates a greater non-ideality in the system. The temporal variations of the predicted activity coefficients for the lumped groups, except SOA7 and SOA8, in wdsmk_13 follow the variability of predicted water fractions in aerosol phase. This pattern indicates that all the lumped groups but SOA7 and SOA8 are hydrophobic. However, for SOA10 and SOA12, the slight changes of their activity coefficients with the aerosol water fraction indicate that these two lumped groups are not that hydrophobic as other groups.

The predicted activity coefficients for POA components, except POA1, from wdsmk_13 are all lower than those from wdsmk_12. The temporal variations of the activity coefficients for POA components shows that POA1 is hydrophobic while other components are more hydrophilic. The net effect of these aerosol-water interactions is the water absorbing into aerosol phase. With water contributing to the absorbing aerosol phase, the partitioning of more hydrophilic groups SOA1, SOA5, SOA7, SOA8, SOA9 and SOA10 is enhanced while the partitioning of other, more hydrophobic, groups such as SOA2, SOA6, SOA11 and SOA12 is weakened compared with that when no water presents. The net result is that the total amount of SOA is increased.
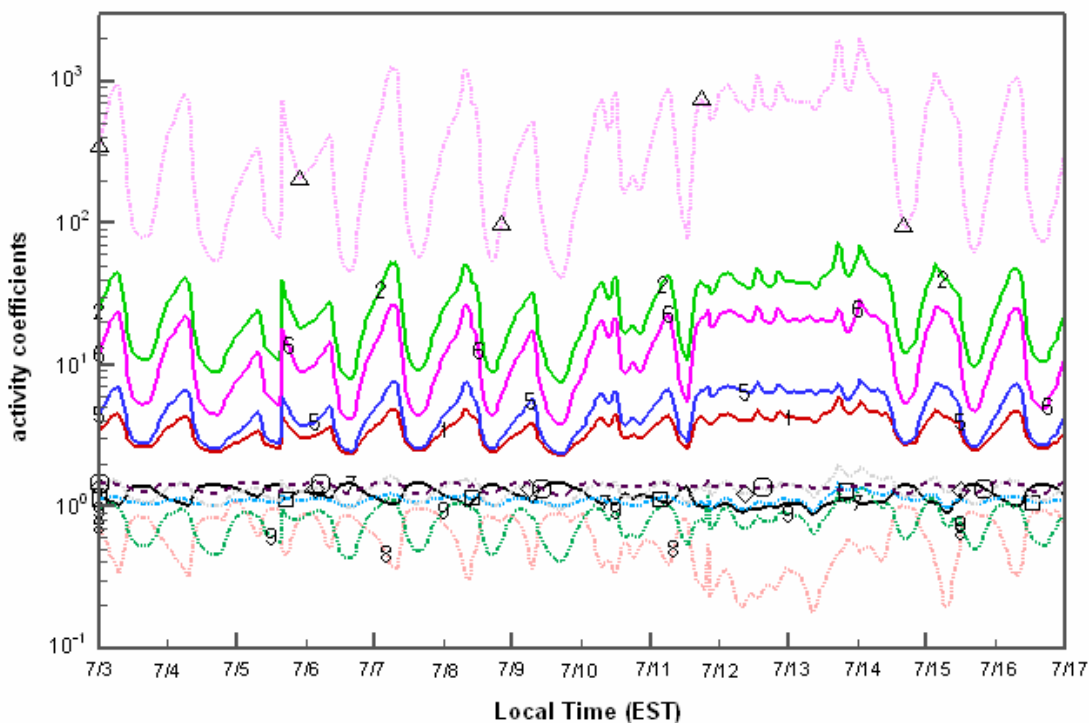
Figure 5.3. Predicted activity coefficients for SOA components and water at JST from coarse-grid simulation.

3.2.3 Effect of Different Lumped Groups

The effect of different lumped groups on SOA production is indicated by the predictions from wdsmk_12 and wdsmk_10. Figure 5.1 shows that the SOA predictions from wdsmk_10 is always lower than those from wdsmk_12, with ~25% lower at daily maximum. wdsmk_10 predicts on average 27% less anthropogenic SOA and 38% less biogenic SOA than wdsmk_12. In wdsmk_12, SOA12, the 3rd lump group corresponding to TRP1, has very low vapor pressure. It is expected to readily partition into aerosol phase. In wdsmk_10, however, the aerosol components used to formulate SOA10 and

SOA12 in wdsmk_12 are lumped together into a single group, SOA10. This new averaged group has a higher vapor pressure than SOA12 and its partitioning behavior is not affected by temperature as that much as either SOA10's or SOA12's. The net result is that the new averaged group partitions less to the aerosol phase. Similarly, the aerosol mixtures corresponding to ALK5 are also reformulated using the new vapor pressure diving criteria. The individual products lumped to get SOA2 in wdsmk_12 are unequally divided into two groups by the new diving line. The first part was lumped together with the components for formulating SOA1 in wdsmk_12 to get the new averaged group SOA1 in wdsmk_10; the second part lumped together with the products for formulating SOA11 to get the new lumped group SOA2 in wdsmk_10. The net effect of the vapor pressures and B values changes of SOA1 and SOA2 due to the reformulation is the lowered SOA prediction from wdsmk_10.

The predicted activity coefficients for individual lumped groups in wdsmk_10 are similar as those in wdsmk_12. SOA2 is most incompatible with wood smoke with predicted activity coefficients from 9 to 14. SOA9 has the lowest activity coefficients with variation from 0.2 to 0.5. Similar activity coefficients are predicted for SOA5, SOA6, SOA7 and SOA8 as in wdsmk_12. Although SOA10, the dominator of the SOA mass production, also has activity coefficients around 1 as in wdsmk_12, the differences in the vapor pressures and B values applied in these two sets of simulations play an important role in the SOA production. The combined effects of composition and partitioning parameters are the lowered SOA production predicted by wdsmk_10 when compared with wdsmk_12.

3.2.4 Comparison of hourly and daily average SOA predictions against measurements at Jefferson Street (JST), Atlanta, GA.

Figure 5.1 indicates that same temporal distributions of SOA are predicted by all simulations but with different magnitude. So when compared with hourly measurement data, the models performance on reproducing the temporal variation of SOA concentration are the same as that detailed in Chapter IV for the coarse-grid prediction. Overall, the simulations reproduce well the temporal variations of SOA concentrations throughout the whole simulation period except the apparent fail in the period from the noon on 7/7 to 7/8. The common trend is the underprediction in afternoons except on 7/12 and 7/13 when the SOA concentration is very low. wdsmk_13 tends to overpredict the SOA concentration in early mornings except on 7/4 and 7/6 while wdsmk_LB underpredicts the SOA concentration all the time except on 7/12.

Throughout the simulation period, wdsmk_13 predicts the highest SOA concentrations and wdsmk_LB the lowest. Scatter plots of the predictions against observations depicts a large scatter with correlation coefficients around 0.28 (Figure 5.4). wdsmk_LB and wdsmk_10 obviously underpredict the SOA concentrations, by 61% and 43%, respectively, in terms of mean predictions and mean observations. The mean SOA concentration predicted by wdsmk_13 (2.34 $\mu g/m^3$), however, reproduce well the mean observation (2.18 $\mu g/m^3$) but with poor correlation ($r = 0.29$). Compared with the base case simulation, allowing water partitioning into the absorbing phase improves the model performance on SOA prediction at JST.
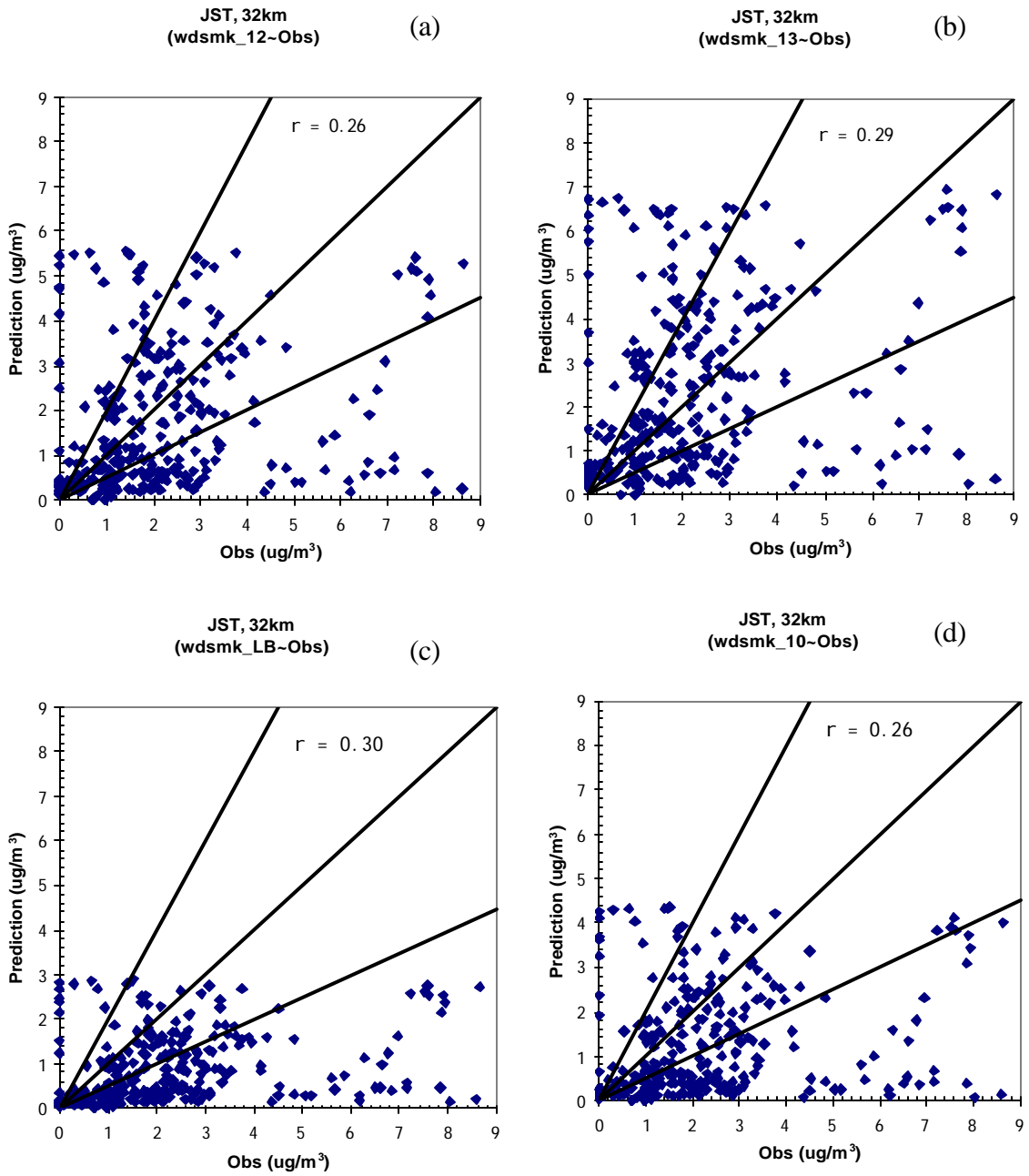
Figure 5.4. Scatter plots of hourly SOA predictions (abscissa) versus observations (ordinate) from different model versions: (a) wdsmk_12; (b) wdsmk_13; (c) wdsmk_LB; (d) wdsmk_10. 1:1, 1:2 and 2:1 lines are provided for reference.

147

JST, 32km domain
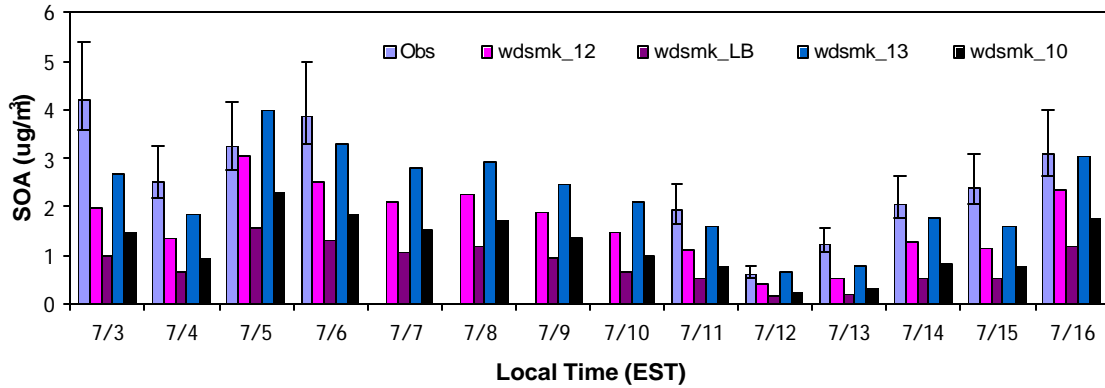
Figure 5.5. 24-hr average simulated SOA concentrations compared with observations for JST with horizontal resolution of 32km. The observations were calculated using a value of 1.05 for the primary OC/EC ratio and a factor of 1.4 for conversion between the concentrations of observed secondary carbon and secondary organic aerosol. The error bars represent a range of 1.2 to 1.8 to convert the concentration of secondary OC to that of secondary organic aerosol.

When compared with daily average SOA measurements (Figure 5.5), wdsmk_13 reproduces the observations much better than wdsmk_LB and wdsmk_10. It also gives better predictions than wdsmk_12 on all the days. Overall, the enhanced SOA partitioning due to water absorption into aerosol phase improves the model prediction on SOA concentration at JST. The significant underprediction from wdsmk_LB indicates the strong temperature effects on SOA production. The different SOA concentrations predicted from wdsmk_12 and wdsmk_10 suggests that the lumping criteria have appreciable effects on SOA production as well.

3.2.5 Comparison of hourly and daily average OM$_{2.5}$ predictions against measurements at Jefferson Street (JST), Atlanta, GA

The SOA data comparison presented in section 3.2.4 involves the uncertainties in deriving the SOA concentrations. Due to the fact no direct method is available to distinguish SOA from POA, the ratio between primary organic carbon (POC) and elementary carbon (EC) in EC tracer method is somewhat uncertain considering the limitations of the method itself and different OC/EC operation procedures applied to get the OC and EC concentrations in Lim and Turpin (2002) and the SEARCH data. In this section, therefore, the hourly model predicted OM$_{2.5}$ data, which include both POA and SOA, are compared against hourly measurements to exclude these uncertainties.
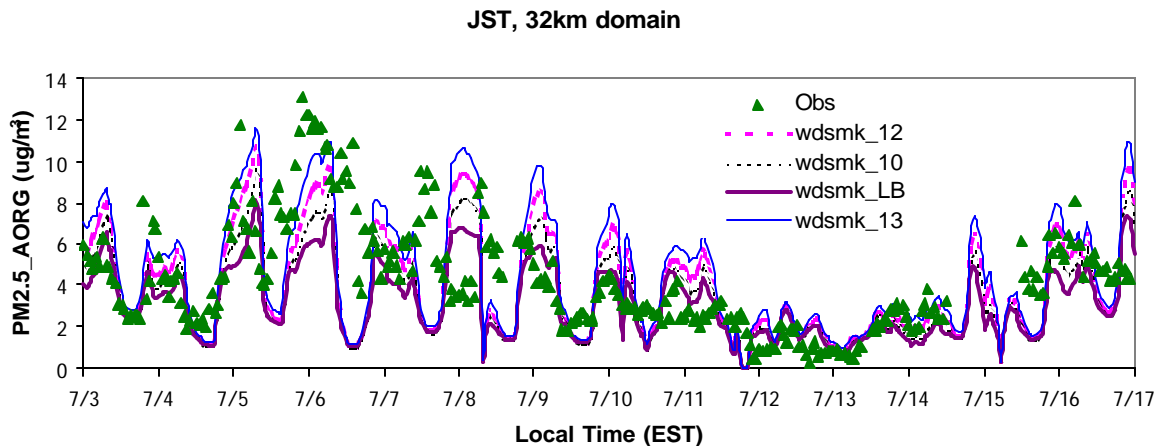
Figure 5.6. Temporal distribution of simulated organic aerosol concentration against hourly observations at JST with horizontal resolution of 32km.

Figure 5.6 presents the temporal distribution of the simulation results, along with hourly observations, from different model versions. Same temporal distributions are predicted and as in Figure 5.1, wdsmk_13 gives the highest and wdsmk_LB the lowest

149
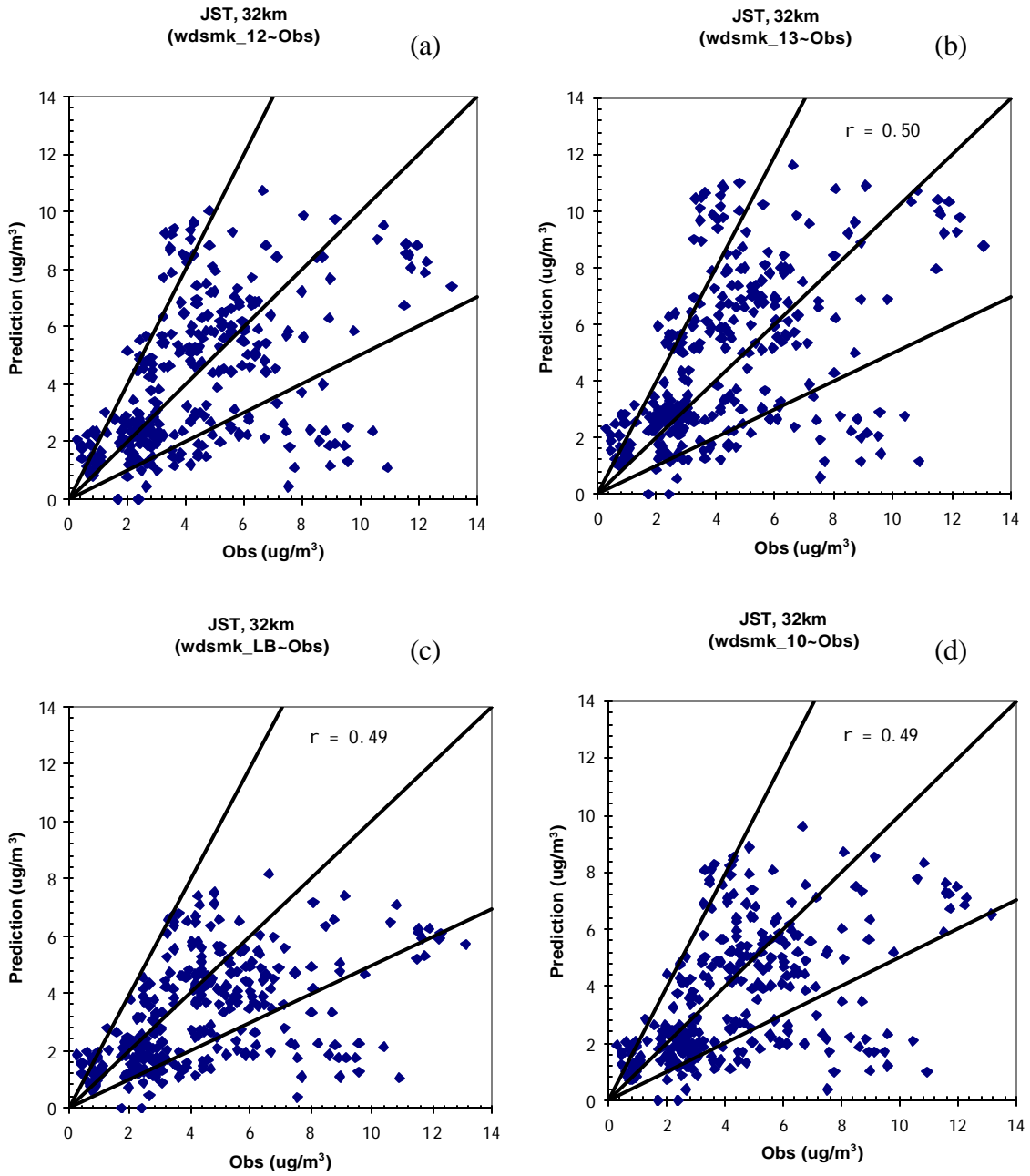
Figure 5.7. Scatter plots of hourly OM$_{2.5}$ predictions (abscissa) versus observations (ordinate) from different model versions: (a) wdsmk_12; (b) wdsmk_13; (c) wdsmk_LB; (d) wdsmk_10. 1:1, 1:2 and 2:1 lines are provided for reference.

150

predictions all the time due to the different SOA predictions from different model versions. Except the period from the noon on 7/7 to 7/8, predictions from all the model versions agree reasonably well with the ambient data. Scatter plots of the $OM_{2.5}$ predictions versus observations (Figure 5.7) show that no matter which model version is applied, vast majority of the predictions fall within a factor of two of the observations and the correlation coefficients (~0.50) are all increased dramatically compared with those between SOA predictions and ambient SOA concentrations (~0.28). The mean predictions, calculated by excluding the data points without corresponding measured data, from wdsmk_13 (4.71 $\mu g/m^3$), wdsmk_12 (4.11 $\mu g/m^3$) and wdsmk_10 (3.62 $\mu g/m^3$) all reproduce well the mean observation (4.33 $\mu g/m^3$). wdsmk_LB predicts a little lower mean value of 3.23 $\mu g/m^3$.

As pointed out in Chapters III and IV, the different data distribution indicated by Figures 5.4 and 5.7 suggests that uncertainty in data interpreting and deriving SOA concentrations using EC tracer method is notable. The ratio between POC and EC is probably not always the same throughout the simulation period.

Figure 5.8 compares the daily average $OM_{2.5}$ predictions from different model versions against measurements at JST. wdsmk_10 and wdsmk_LB underpredict the mean observation by 23% and 31%, respectively. Surprisingly the mean prediction from wdsmk_13, calculated for the dates when ambient data are available, exactly reproduces the mean observation (4.33 ug/m^3). When compared with wdsmk_12, wdsmk_13 increases the mean prediction by 14% while wdsmk_10 and wdsmk_LB, respectively, decrease the mean prediction by 12% and 21%.

JST, 32km domain
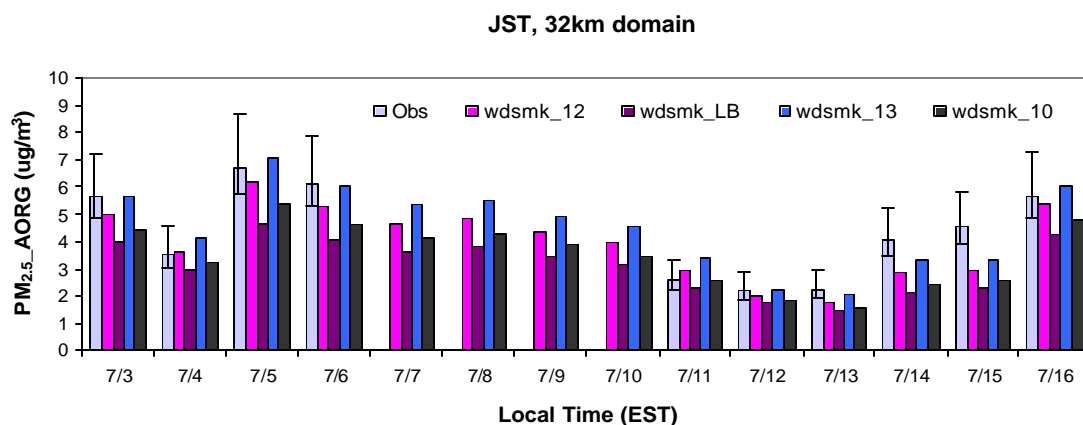
Figure 5.8. 24-hr average simulated organic aerosol concentrations compared with observations at JST with horizontal resolution of 32km. The factor of 1.4 was used to obtain the concentration of organic aerosols from the concentration of observed organic carbon. The error bars represent a range of 1.2 to 1.8 to convert the OC concentration to organic aerosol concentration.

3.2.6 Statistical performance evaluation

For all the monitoring sites located in the sub-domain, the predicted daily average $OM_{2.5}$ concentrations are plotted against the daily observations in Figure 5.9. The data from SEARCH, IMPROVE, and SOS99-Nashville are plotted in the same plot for each model version. Vast majority of the predictions on IMPROVE and SOS99-Nashville data fall below the 1:2 reference line, which means that significant underpredictions occur to the SOS99-Nashville data and IMPROVE data corresponding to the sites located in the subdomain. However, as indicated in Chapter III, the model performance on IMPROVE sites is not always so poor as on the sites used for this study. Except wdsmk_13, other three model versions, especially wdsmk_LB and wdsmk_10, also tend to underpredict the SEARCH data.
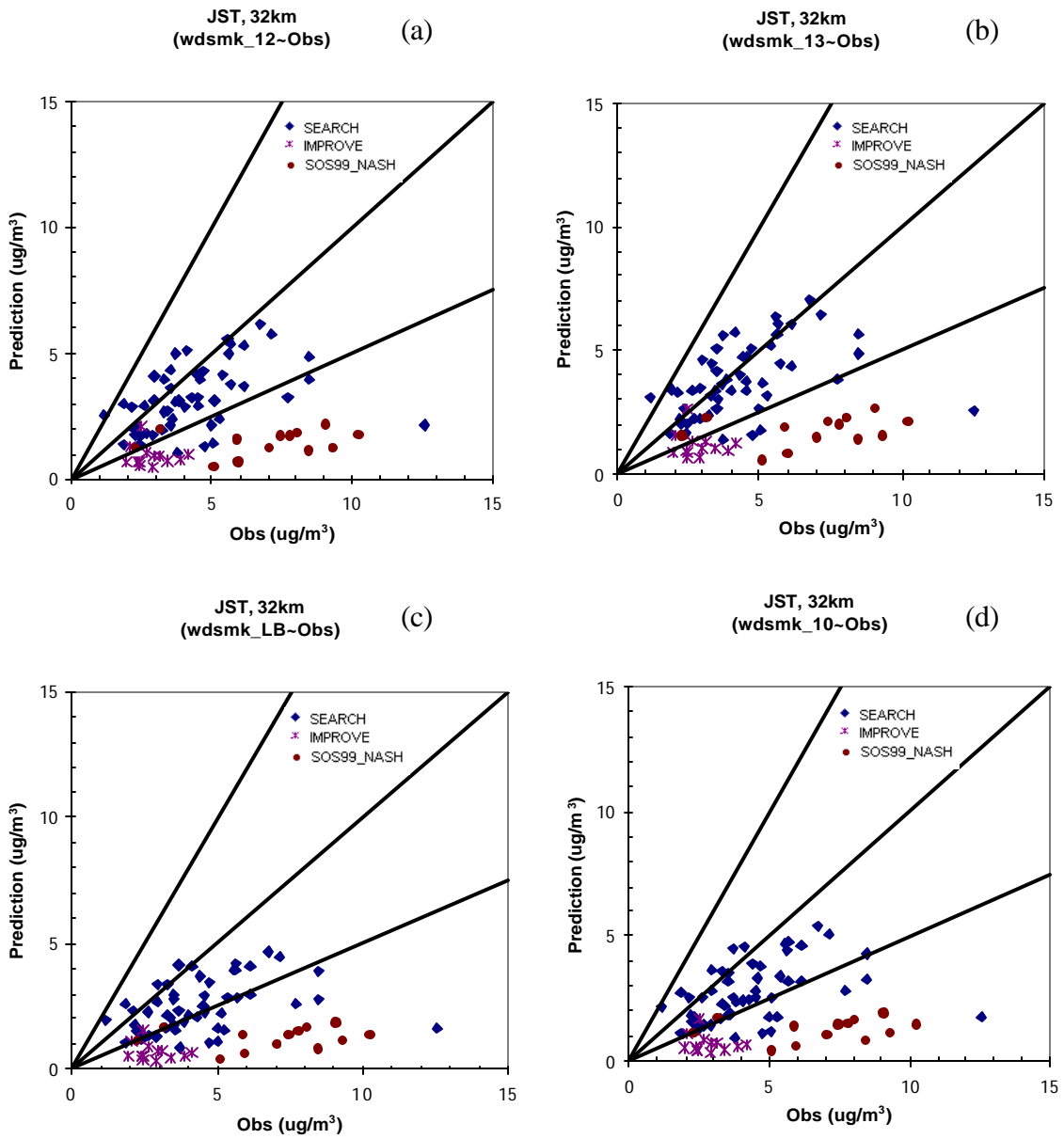
Figure 5.9. Scatter plots of daily OM$_{2.5}$ predictions from coarse-grid simulation (abscissa) versus observations (ordinate) for different model versions: (a) wdsmk_12; (b) wdsmk_13; (c) wdsmk_LB; (d) wdsmk_10. 1:1, 1:2 and 2:1 reference lines are provided.

Table 5.5 compares the mean predictions of $OM_{2.5}$ from different model versions against mean observations averaged over the 11 monitoring sites located across the sub-domain. Again, wdsmk_13 presents the best prediction in terms of mean prediction. The models performance evaluated statistically on SEARCH data is summarized in table 5.6. Very good prediction is shown by wdsmk_13 with relatively small error (NME = 28% and MFE = 30%) and slightly negative bias (NMB = -13% and MFB = -11%). wdsmk_13 achieves the performance goals recommended both by EPA (EPA, 2001) in terms of MNB (≤ 15%) and MNE (≤ 30%) and by Boylan and Russell (2006) in terms of MFE (±50%) and MFB (±30%), which suggests that wdsmk_13 provides an excellent prediction on daily average $OM_{2.5}$ concentration at SEARCH sites used for this study. The performance of wdsmk_12 is also pretty good while wdsmk_10 and wdsmk_LB have pretty large error and bias but their performance is also acceptable based on the performance criteria proposed by Boylan and Russell (2006).

Table 5.5. Coarse-grid mean predictions of $OM_{2.5}$ from different model versions averaged over the 11 monitoring sites located across the sub-domain.

Model version	Mean prediction ($\mu g/m^3$)	Discrepancy (%)	
		from mean observation (4.53 $\mu g/m^3$)	from wdsmk_12
wdsmk_12	2.53	-44	
wdsmk_13	3.00	-34	19
wdsmk_10	2.16	-52	-15
wdsmk_LB	1.97	-57	-22

Table 5.6. Summary statistics for coarse-grid models performance on SEARCH daily average $OM_{2.5}$ concentration.

Model version	Mean observation $(\mu g/m^3)$	Mean prediction $(\mu g/m^3)$	ME	MB	MNE (%)	MNB (%)	NME (%)	NMB (%)	MFE (%)	MFB (%)
wdsmk_12		3.21	1.5	-1.1	32	-18	34	-26	39	-28
wdsmk_13	4.36	3.78	1.2	-0.58	28	-3.4	28	-13	30	-11
wdsmk_10		2.77	1.8	-1.6	38	-29	41	-36	49	-42
wdsmk_LB		2.48	2.0	-1.9	42	-36	45	-43	56	-51

4. Conclusions

With the determined set of products selected for each precursor, 3 kinds of uncertainties in implementing the composition effects on SOA production in air quality models are investigated in this study. When compared to the base case simulation results, the predicted daily maximum SOA concentration might be increased by 20% from wdsmk_13 or decreased by 25% and 50%, respectively, from wdsmk_10 and wdsmk_LB. The simulation results indicate that all the uncertainties investigated in this study have appreciable effects on the SOA predictions especially the enthalpy of vaporization (H_i) assumed for the individual SOA components. It is absolutely worthwhile to reduce the level of uncertainty in determining the individual H_i values for SOA components. The lumping criteria applied in formulating the lumped groups also need attention to get robust predictions. The inclusion of organics-related water in the simulation improves the simulation results in this study due to the enhanced partitioning of the organic semivolatiles with water absorbing into the aerosol phase, though the CPU time for the system to converge is significantly increased (by ~ 8 times compared to the base case simulation). However, model performance should be evaluated in other regions to get a

complete vision of the model's capability in reproducing the ambient data temporally and spatially.

This study highlights some of the research areas that need more research efforts such as the measurement and accurate estimation of the vaporization enthalpy values for the SOA components and the treatment of the effects of aerosol water, maybe both organics- and inorganics- related, on organic partitioning. The great effects of organics-related water on the predicted SOA concentrations in this study suggests that significant different SOA mass may be predicted by the different representation of the effects of aerosol water on the organic partitioning process.

CHAPTER VI

SUMMARY AND CONCLUSIONS

1. Overview of work performed

A new organic aerosol module was developed in this study for studying and quantifying the composition effects on SOA production. An updated set of SOA precursors and corresponding products were formulated in order to appropriately represent the real varieties of atmospheric volatile organic compounds (VOCs) capable of producing SOA and the major identified SOA components. The new SOA representation is formulated based on real identified SOA components. Partitioning parameters used to describe the SOA production process were developed reflecting detailed experimental information about the individual SOA products. The new SOA representation not only can reproduce the SOA prediction capability of the current aerosol module in CMAQ but also defines the molecular structure of the SOA mixture, allowing composition dependent partitioning to be incorporated. The new organic aerosol module was incorporated into CMAQ to evaluate the composition effects on SOA production in Southeastern United States. Simulation results from the updated CMAQ were compared against field measurements, from two monitoring networks –IMPROVE and SEARCH and one field study - Southern Oxidants Study (SOS99), in the Nashville region during the summer of 1999. Simulations were also conducted to study the relative importance of model parameters and to identify parameters that need to be determined more accurately. This

new module is not only suitable for CMAQ, but also can be incorporated into other air quality models.

2. Summary of results and conclusions

In this study the composition effects on SOA production were successfully quantified and systematically investigated using different POA representations, different enthalpies of vaporization for the individual SOA components before lumping, different number of lumped groups, and inclusion of organics-related water in the simulation. Critical findings of this study are that

1) composition effects on SOA production closely depend on POA representation, and

2) uncertainties in formulating lumped groups as well as in defining the simulation system have appreciable effects on quantifying these effects.

These and additional research findings are described in more detail below.

2.1 Formulation and Evaluation of new SOA representation

Exploration of aerosol composition effects on SOA production requires chemical structure information for the aerosol phase. In Chapter III, lumped groups, whose partitioning parameters and structure information were calculated directly from the corresponding properties of the individual SOA products, were formulated. The new SOA representation was evaluated and validated using data from both experimental and atmospheric systems. Key results from this evaluation were:

- *Similar SOA predictions*

The new lumped groups successfully reproduce the prediction capability of model species whose partitioning parameters are derived by fitting smog chamber experimental data.

- *Feasible and applicable for composition effects simulations*

  The chemical structure information formulated in the new SOA representation enables the current study on the composition effects on SOA production, as well as future simulations, to be conducted.

- *More complete description of the composition effects on SOA production*

  Compared with the composition dependent partitioning implemented in other models by using surrogate compounds, the new SOA representation formulated in this study presents a better account for the composition effects on SOA production. The reduced uncertainty in defining the chemical structure of the SOA mixtures renders the simulation results more reliable. In addition, it is easy to keep the SOA parameters updated with the most recent experimental results.

- *Typical PM modeling accuracy*

  Due to the complexity in simulating PM, which is a mixture of hundreds of components, CMAQ (the modeling framework incorporated with the original aerosol module) and CMAQ_L (the modeling framework incorporated with the revised aerosol module but with no composition effects accounted for) represent the typical model performance on $OM_{2.5}$ of current air quality models. The uncertainties in OC emission inventory and OC measurements, the incommensurability uncertainty due to the way to compare predictions and ambient data, as well as the treatment of SOA production process all contribute to

the discrepancy between modeled and observed organic aerosol (OM$_{2.5}$) concentrations.

2.2 Composition effects quantification

In Chapter IV, the lumped groups formulated in Chapter III were used to quantify the effects of aerosol composition on SOA production with POA represented as wood smoke and diesel soot, respectively. Key conclusions from this study were:

- *Strong dependence on POA representation*

  As indicated by the simulation results, POA composition representation has great effects on SOA formation. Compared with the amount of SOA produced when no composition effects are accounted for, representing the pre-existing absorbing phase as wood smoke slightly enhanced SOA concentrations (~ 5% at JST) while representing it as diesel soot appreciably lowered the predictions (~ 60% at JST) and enlarged the discrepancies between the modeled values and ambient data.

- *Discrepancies between SOA predictions and measurements*

  The SOA prediction with POA represented as diesel soot particles should provide the best representation of the actual SOA concentration at JST, due to the fact that POA at this location is composed of more diesel soot than wood smoke during the simulation period (Zheng et al., 2002), but it significantly underpredicted measured SOA levels. Discrepancy in the predictions and measurements may be due to the insufficiency of CMAQ in representing SOA precursors and the uncertainties in deriving SOA concentrations as well as additional uncertainties introduced from other required data adjustments.

- *Composition effects need to be included in atmospheric applications*

  Predicted activity coefficients of the individual aerosol components indicate that the aerosol mixture composed of wood smoke and SOA components form a quasi-ideal solution and $\zeta_i = 1$ is a good approximation to speed up the simulation. However, the case is not that simple for POA represented as diesel soot. The nonideality in the solution consisting of diesel soot and SOA products considerably lessens SOA production and the ideal behavior assumption would greatly overpredict the SOA concentration in areas where diesel soot makes significant contribution to the POA concentration.

2.3 Effects of uncertainty factors

In Chapter V, uncertainties involved in implementing composition effects on SOA formation in air quality models were investigated. A number of simulations were performed in order to quantify the effects of these uncertainties on the simulation results. POA was represented as polar wood smoke particles in all the simulations. Key findings from these simulations were:

- *Significant effects of vaporization enthalpy*

  A decrease of 50% in the simulated mean SOA concentration was predicted when individual SOA product vaporization enthalpies were varied from 156 kJ/mol to 83 KJ/mol, representing current high and midrange estimates for vaporization enthalpies. The large difference in the simulated SOA concentrations highlights the needs of more research efforts to reduce the high uncertainty involved in assigning the enthalpy of vaporization for SOA components.

- *Appreciable effects of organics-related water*

   Allowing water to partition into the absorbing organic aerosol phase increased the predicted mean SOA concentration by 35% when compared to the base case simulation. The increase is caused by the combining effects of aerosol-phase water on the predicted activity coefficients and on the mean molecular weight of the absorbing phase. Despite the assumption that no interaction exists between organics and inorganics, the simulation results still demonstrate the effect of aerosol water on SOA production and indicate a noticeable increase in the predicted SOA concentration.

- *Appreciable effects of applied lumping criteria*

   The effects of lumping criteria applied to convert individual SOA products into lumped groups on SOA prediction can not be ignored either. The partitioning parameters of the lumped groups, particularly their vapor pressures and the temperature dependence of their effective saturation concentration are sensitive to the lumping criteria adopted. The number of products used to represent SOA production in atmospheric application needs to be carefully determined to get the most reasonable results.

3. Recommendations for future research

This work systematically investigated the composition effects on SOA production. While the results obtained in this study contribute significantly to our understanding of the composition effects on SOA production, this study also revealed some important future research needs, including the composition representation of ambient POA,

extended model evaluation, and more appropriate treatment of organic partitioning. It is also very important to keep the SOA parameters updated with the latest experimental data.

3.1 Composition representation of ambient POA

The POA representation in this work, either as wood smoke or as diesel soot, is somewhat simplified due to the fact that POA, as SOA, is a mixture of hundreds of products, which are released from different sources. In addition, the POA composition may differ significantly from location to location, which means that the composition of POA is closely related to the local emissions while at the same time, however, it may also be affected by the particles transported from adjacent areas. As indicated by this work, the ambient POA composition has great effects on gas/particle partitioning. Thus, the POA composition representation certainly deserves great research efforts in the future.

3.2 Model evaluation over a wider range of meteorological conditions and geographical areas

As revealed in this study, when compared with ambient data from different sources, different conclusions may be drawn about the new model's performance. This highlights the difficulties in accurately simulating atmospheric organic aerosol and may be also an indication of the uncertainties in the measurement data. The model evaluation in this study focuses only on an area of the Southeastern United States. And all the simulations were conducted over a pretty short simulation period from July 3 to July 17, 1999. In order to get a comprehensive evaluation of the model's performance, model

performance evaluation carried out over a wider range of meteorological conditions and geographical areas are definitely necessary.

3.3 Update SOA parameters as more experimental data becomes available

This study uses the latest experimentally identified SOA compositions to formulate the lumped groups for modeling purpose. However, identification of SOA products as well as measurements of their thermodynamic properties will definitely continue to progress. It is very important to keep the partitioning parameters of the model species aligned with the advancement in experimental data. It is pretty easy to update the SOA parameters in the lumping procedure as well as to incorporate the updates in the new organic aerosol module.

3.4 Extension of organic partitioning to both organic and aqueous phases

In this study, except in wdsmk_13, the SOCs, hydrophilic or hydrophobic, are only allowed to partition into the organic phase. Even in wdsmk_13, it is assumed that no interactions exist between the organics and inorganics. The water related to the inorganic aerosol has no effects on the organic partitioning. However, the hydrophilic SOCs are expected to partition more easily into the aqueous phase than into the organic phase. Even for the more hydrophobic compounds, they can partition into the aqueous phase as well but maybe to a less extent than the hydrophilic ones. So extending the partitioning of SOCs to both organic and aqueous phases is a good research direction to further improve the description of SOA formation included in this new aerosol module.

APPENDIX A: IDENTIFIED SOA COMPONENTS

Biogenic Precursors

Table A1. SOA products (**a-pinene**) [1,2,3,4,5,6,7,8,9,10]

Pinonaldehyde		1-Hydroxypinonaldehyde	
Norpinonaldehyde		10-Hydroxypinonaldehyde	
Pinic acid		4-Oxopinonic acid	
Pinonic acid		4-Oxopinonaldehyde	
Norpinic acid		10-Oxopinonic acid	
Norpinonic acid		10-Hydroxypinonic acid	
Pinalic-4-acid		2-Hydroxy-3-pinanone	
a-Campholenal			

166

Table A2. SOA products (**b**-Pinene) [3,5,6,8,11]
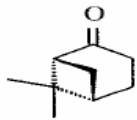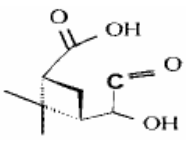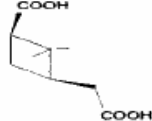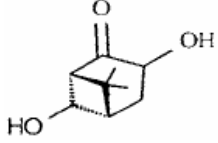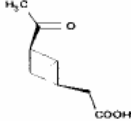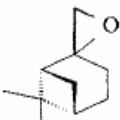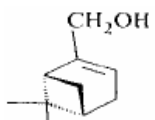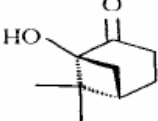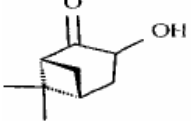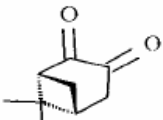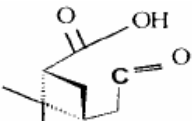
Nopinone		4-hydroxypinalic-3-acid	
Pinic acid		3,7-dihydroxynopinone	
Pinonic acid		Myrtanal	
b -pinene oxide		Myrtenol	
1-hydroxynopinone			
3-hydroxynopinone			
10-hydroxypinonic acid			
3-oxonopinone			
Pinalic-3-acid			

Table A3. SOA products (**D^3-Carene**)[2,3,5,6,8]

cis-3-caric acid (cis-2,2-dimethyl-1,3-cyclopropyldiethanoic acid) (C9H12O4)	
cis-nor-3-caric acid (3-carboxy-2,2-dimethylcyclopropanylethanoic acid) (C8H12O4)	
cis-3-caronic acid (2,2-dimethyl-3-(2-oxopropyl)cyclopropanylethanoic acid) (C10H16O3)	
cis-nor-3-caronic acid (2,2-dimethyl-3-(2-oxopropyl)cyclopropanylmethanoic acid) and isomers (C9H14O3)	
Pinic acid	
(cis-10-)hydroxy-3-caronic acid (cis-2,2-dimethyl-3-(hydroxy-2-oxopropyl)-cyclopropanylethanoic acid)	
C8H12O2	

Table A4. SOA products (**Sabine**)[3,5,6,8]

cis-sabinic acid (2-carboxyl-1-isopropylcyclopropylethanoic acid) (C9H14O4)	
cis-norsabinonic acid (2-carboxy-1-isopropylcyclopropylmethanoic acid) and its isomers(C9H14O3)	
Sabina ketone (5-isopropylbicyclo[3.1.0]hexan-2-one) (C9H14O)	
hydroxy-sabina ketone (3-hydroxy-5-isopropylbicyclo[3.1.0[hexan-2-one) (C9H14O2)	
3-oxo-sabina ketone (C9H12O2)	
Pinic acid	
2-(2-isopropyl)-2-formyl-cyclopropyl-methanoic acid (C8H12O3)	
C8H12O4 (norsabinic acid)	
C10H16O4	
C6H8O3	
10-hydroxysabinonic acid	

Table A5. SOA products (**Limonene**)[5,6,8]

Limonic acid (3-isopropenylhexanedioic acid) (C9H14O4)		ketolimonalic acid (3-formylmethyl-2-oxohexanoic acid) (C8H12O4)	
keto-limonic acid (3-acetylhexanedioic acid) (C8H12O5)		7-hydroxy-limononic acid (7-hydroxy-3-isopropenyl-6-oxoheptanoic acid) (C10H16O4)	
norlimonic acid (2-isopropenylpentanedioic acid) (C8H12O4)		7-hydroxyketolimononic acid (3-acetyl-7-hydroxy-6-oxoheptanoic acid) (C9H14O5)	
limononic acid (3-isopropenyl-6-oxoheptanoic acid) (C10H16O3)		7-hydroxylimononaldehyde (7-hydroxy-3-isopropenyl-6-oxoheptanal) (C10H18O3)	
ketolimononic acid (3-acetyl-6-oxoheptanoic acid) (C9H14O4)		7-hydroxyketolimononaldehyde (3-acetyl-7-hydroxy-6-oxoheptanal) (C9H16O4)	
limona ketone (4-acetyl-1-methylcyclohexene) (C9H14O)			
limononaldehyde (3-isopropenyl-6-oxo-heptanal) (C10H18O2)			
ketolimonaldehyde (3-acetyl-6-oxoheptanal) (C9H16O3)		**Table A6**. SOA products(**Terpinolene**)[8]	
norlimononic acid (2-isopropenyl-5-oxo-hexanoic acid) (C9H14O2)		Terpinolic acid (C7H10O4)	
limonalic acid (3-formylmethyl-2-methylenylhexanoic acid) (C9H14O3)		C7H10O3	

169
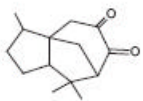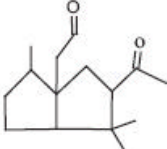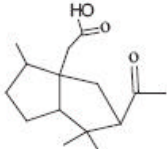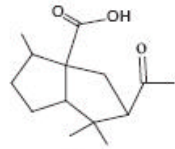
Table A7. SOA products (*b* -Caryophyllene)[13]
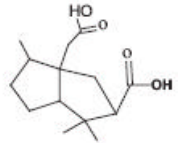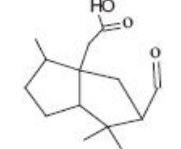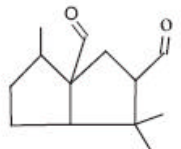
b -nocaryophyllone (*b* -caryophylla ketone) (8-oxo-4,11,11-trimethylbicyclo[7.2.0]undec-4-ene)		*b* -14-hydroxycaryophyllone aldehyde (3,3-dimethyl- *g* -methylene-2-(3-oxobutanol)-cyclobutanal)	
b -caryophyllene oxide (*b* -caryophyllene-3-oxide) (9-methylene-4,12,12-trimethyl-5-oxatricyclo[8.2.0.0^{4,6}]dodecane		*b* -14-hydroxycaryophyllonic acid (3,3-dimethyl- *g* -methylene-2-(3-oxobutanol)-cyclobutanoic acid)	
b -caryophyllene aldehyde (3,3-dimethyl- *g* -methylene-2-(3-oxobutyl)-cyclobutanebutanal)		*b* -14-hydroxynocaryophyllonic acid (3,3-dimethyl- *g* -methylene-2-(3-oxobutanol)-cyclobutanoic acid)	
b -norcaryophyllone aldehyde (3,3-dimethyl- *g* -methylene-2-(3-oxobutyl)-cyclobutanepropanal)		3,3-dimethyl-2-(3-oxobutyl)-cyclobutane-methanal	
b -caryophyllinic acid (3,3-dimethyl- *g* -methylene-2-(3-propanoic acid)-cyclobutanebutaoic acid)		3,3-dimethyl-2-ethanal-cyclobutane-methanal	
b -nocaryophyllonic acid (3,3-dimethyl- *g* -oxo-2-(3-oxobutyl)-cyclobutanebutaonic acid)			
b -caryophyllonic acid (3,3-dimethyl- *g* -methylene-2-(3-oxobutyl)-cyclobutanebutanoic acid)			
b -nocaryophyllone aldehyde (3,3-dimethyl- *g* -oxo-2-(3-oxobutyl)-cyclobutanebutanal)			
b -nornocaryophyllone aldehyde (3,3-dimethyl- *g* -oxo-2-(3-oxopropyl)-cyclobutanebutanal)			
b -norcaryophyllonic acid (3,3-dimethyl- *g* -methylene-2-(3-oxobutyl)-cyclobutanepropanoic acid)			

Table A8. SOA products (*a*-**Humulene**)[12]

3-seco-*a*-humulone aldehyde (3,3,7-trimethyl-11-one-dodec-4,7-dien-1-aldehyde)		*a*-humulalic 10-acid (3,7,10,10-tetramethyl-11-formyl-dec-3,7-dien-1-oic acid)	
7-seco-*a*-humulone aldehyde (4,7,7-trimethyl-11-one-dodec-4,8-dien-1-aldehyde)		*a*-humulalic 11-acid (2,2,5,9-tetramethyl-10-formyl-dec-4,8-dien-1-oic acid)	
a-humulal aldehyde (2,2,5,9-tetramethyl-10-formyl-dec-4,8-dien-1-aldehyde)		*a*-humuladionic acid (2,2,5,9-tetramethyl-undec-4,8-dien-dicarboxylic acid)	
a-humulene 10-oxide (2,6,6,9-tetramethyl-4,5-epoxy-1,8-cycloundecadiene)		3-seco-*a*-14-hydroxyhumulone aldehyde (3,3,7-trimethyl-11-onedodec-4,7-dien-1-aldehyde)	
a-humulene 3-oxide (2,6,6,9-tetramethyl-8,9-epoxy-1,4-cycloundecadiene)		3-seco-*a*-norhumulone aldehyde (2,2,6-trimethyl-10-one-undec-3,6-dien-1-aldehyde)	
a-humulene 7-oxide (2,6,6,9-tetramethyl-1,2-epoxy-4,8-cycloundecadiene)		*a*-norhumulal aldehyde (2,2,5,9-tetramethyl-10-formyl-dec-4,8-dien-1-aldehyde)	
3-seco-*a*-humulaic-3-acid (3,3,7-trimethyl-11-one-dodec-4,7-dien-1-oic acid)		3,3-dimethyl-7-one-oct-4-ene-1-aldehyde	
3-seco-*a*-humulaic-7-acid (4,7,7-trimethyl-11-one-dodec-4,8-dien-1-oic acid)			

Table A9. SOA products (*a* -cedrene)[14]

9-Oxo-*a*-nocedranone	
a -Cedronaldehyde	
a -Cedronic acid	
a -Norcedronic acid	

a -Cedrinic-acid	
a -Cedralic-10-acid	
a -Cedral aldehyde	

1. Glasius, et al., 1999.
2. Yu et al., 1998.
3. Yu, et al., 1999.
4. Jang and Kamens, 1999.
5. Glasius et al., 2000.
6. Larsen, et al., 2001.
7. Hoffmann, et al., 1998.
8. Koch, et al., 2000.
9. Christoffersen, et al., 1998.
10. Jaoui and Kamens, 2001.
11. Jaoui and Kamens, 2003b.
12. Jaoui and Kamens, 2003c.
13. Jaoui et al., 2003.
14. Jaoui et al., 2004.

Anthropogenic Precursors

Table A10. SOA products **(Toluene)** [1,2,3,4,8,9]
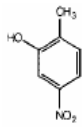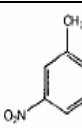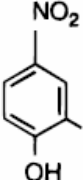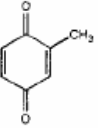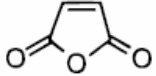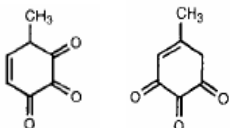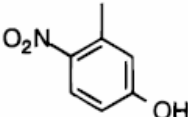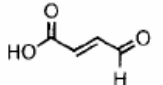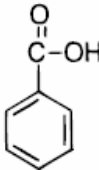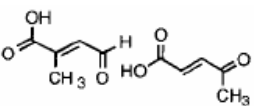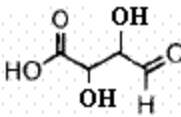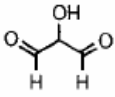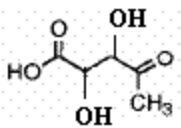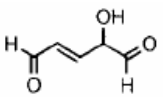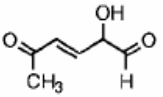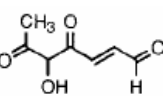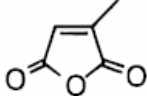
2-methyl-5-nitrophenol		dihydro-2,5-furandione	
2-methyl-4,6-dinitrophenol		2-methyl-4-nitrophenol	
2-methyl-benzoquinone		2,5-furandione	
methyl-cyclohexene tricarbonyls		3-methyl-4-nitrophenol	
4-oxo-2-butenoic acid		benzonic acid	
4-oxo-2-pentenoic acid/2-methyl-4-oxo-2-butenoic acid			
2-hydroxy-1,3-propandial/3-hydroxy-2-oxo-propanal/2,3-dihydroxy-2-propenal		2,3-dihydroxy-4-oxobutanoic acid	
2-hydroxy-3-penten-1,5-dial		2,3-dihydroxy-4-oxopentanoic acid	
2-hydroxy-5-oxo-3-hexen-5-al			
5-hydroxy-4,6-dioxo-2-heptenal			
3-methyl-2,5-furandione			

173

Table A11. SOA products (*m*-Xylene)[2,7]
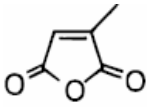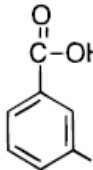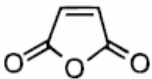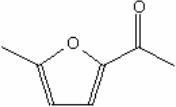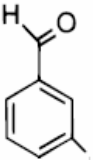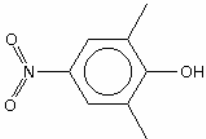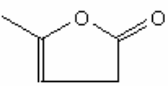
3-methyl-2,5-furandione	
m-toluic acid	
2,5-furandione	
2-acetyl-5-methylfuran	
m-tolualdehyde	
2,6-dimethyl-4-nitrophenol	
5-methyl-2(3*H*)-furanone	

Table A12. SOA products (*p*-Xylene)[2,7]
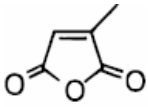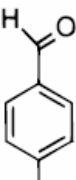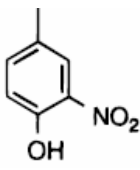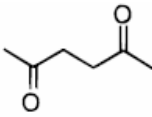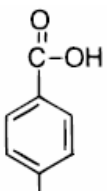
3-methyl-2,5-furandione	
p-tolualdehyde	
4-methyl-2-nitrophenol	
2,5-hexanedione	
dihydro-2,5-furandione	
p-toluic acid	

174

Table A13. SOA products **(1,2,4-trimethylbenzene)**[2,7]
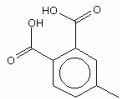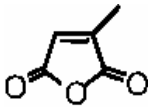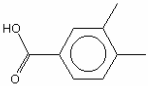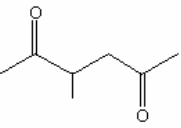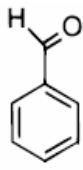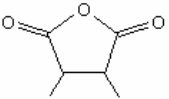
4-methylphthalic acid	
3-methyl-2,5-furandione	
3,4-dimethylbenzoic acid	
3-methyl-2,5-hexanedione	
2,5-furandione	
benzaldehyde	
3,4-dimethylfurandione	

Table A14. SOA products **(Ethylbenzene)**[2]
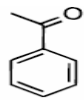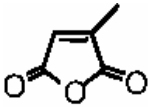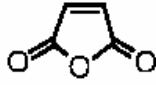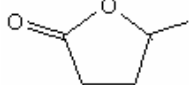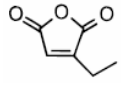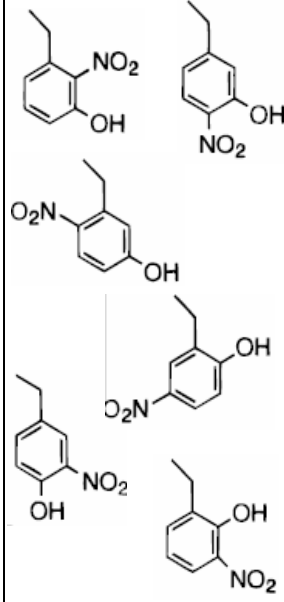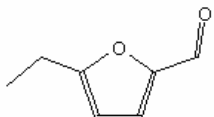
acetophenone	
3-methyl-2,5-furandione	
2,5-furandione	
dihydro-5-methyl-2-furanone	
benzaldehyde	
3-ethyl-2,5-furandione	
ethyl nitrophenol	
5-ethyl-2-furaldehyde	

175

Table A15. SOA products (*m*-ethyltoluene)[2]
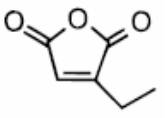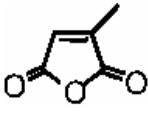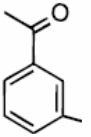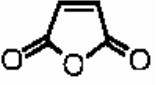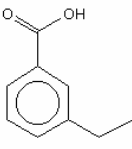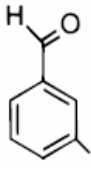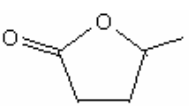
3-ethyl-2,5-furandione	
3-methyl-2,5-furandione	
3'-methylacetophenone	
2,5-furandione	
3-ethylbenzoic acid	
m-tolualdehyde	
dihydro-2,5-furandione	
dihydro-5-methyl-2-furanone*	

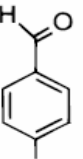**Table A16**. SOA products (*p*-ethyltoluene)[2]
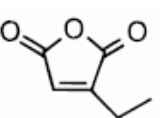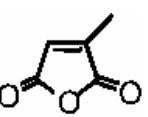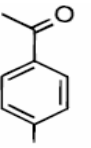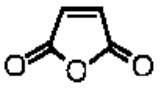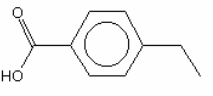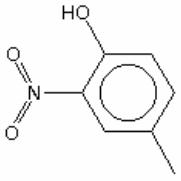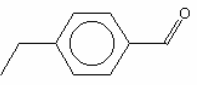
3-ethyl-2,5-furandione	
3-methyl-2,5-furandione	
4'-methylacetophenone	
p-tolualdehyde	
2,5-furandione	
4-ethylbenzoic acid	
4-methyl-2-nitrophenol	
4-ethylbenzaldehyde	

176

Table A17. SOA products (**Cyclohexene**)[6]
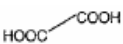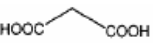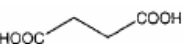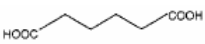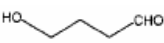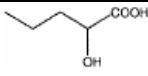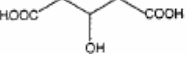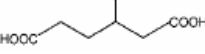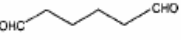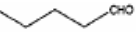
oxalic acid	HOOC–COOH
malonic acid	HOOC–COOH
succinic acid	HOOC–COOH
glutaric acid	HOOC–COOH
adipic acid	HOOC–COOH
4-hydroxy-1-butanal	HO–CHO
2-hydroxy pentanoic acid	COOH, OH
3-hydroxy glutaric acid	HOOC–COOH, OH
3-hydroxy adipic acid	OH, HOOC–COOH
4-oxo-butanoic acid	OHC–COOH
5-oxo-pentanoic acid	OHC–COOH
6-oxo-hexanoic acid	OHC–COOH
1,4-butanedial	OHC–CHO
1,5-pentanedial	OHC–CHO
1,6-hexanedial	OHC–CHO
pentanal	CHO
5-oxo-pentyl formate	OHC–O–CHO

Table A18. SOA products (**1-Octene**)[5]

heptanal	C3H7 ... O
heptanoic acid	C3H7 ... OH, O
dihydro-5-propyl-2(3H)-furanone	C3H7 ... O=O

Table A19. SOA products (**1-Decene**)[5]

nonanal	C5H9 ... O
nonanoic acid	C5H9 ... OH, O
dihydro-5-pentyl-2(3H)-furanone	C5H9 ... O=O

1. Jang and Kamens, 2001a.
2. Forstner, et al., 1997a.
3. Yu, et al., 1997.
4. Smith et al., 1998.
5. Forstner, et al., 1997b.
6. Kalberer, et al., 2000.
7. Smith et al., 1999.
8. Hamilton et al., 2005.
9. Kleindienst et al., 2004.

REFERENCES

Alves, C.A., Pio, C.A., 2005. Secondary organic compounds in atmospheric aerosols: speciation and formation mechanisms. *Journal of the Brazilian Chemical Society* 16 (5), 1017-1029.

Andersson-Sköld, Y. and Simpson, D., 2001. Secondary organic aerosol formation in Northern Europe: A model study. *J. Geophys. Res.* 106, 7357-7374.

Andreae, M.O. and Crutzen, P.J., 1997. Atmospheric aerosols: Biogeochemical sources and role in atmospheric chemistry. *Science* 276, 1052-1058.

Ansari, A.A., Pandis, S.N., 2000. Water absorption by secondary organic aerosol and its effect on inorganic aerosol behavior. *Environmental Science and Technology* 34, 71-77.

Arey, J., A.M. Winer, R. Atkinson, S.M. Aschmann, W.D. Long, and C.L. Morrison, 1991a. The emission of (Z)-3-hexen-1-ol, (Z)-3-hexenylacetete, and other oxygenated hydrocarbons from agriculture plant species. *Atmospheric Environment*, 25, 1063-1075.

Bahreini, R., Keywood, M.D., NG, N.L., Varutbangkul, V., Gao, S., Flagan, R.C., Seinfeld, J.H., Worsnop, D.R., Jimenez, J.L., 2005. Measurements of secondary organic aerosol from oxidation of cycloalkenes, terpenes, and *m*-xylene using an aerodyne aerosol mass spectrometer. *Environmental Science and Technology* 39, 5674-5688.

Baltensperger, U., Kalberer, M., Dommen, J., Paulsen, D., Alfarra, M.R., Coe, H., Fisseha, R., Gascho, A., Gysel, M., Nyeki, S., Sax, M., Steinbacher, M., Prevot, A.S.H., Sjögren, S., Weingartner, E., Zenobi, R., 2005. Secondary organic aerosol from anthropogenic and biogenic precursors. *Faraday Discussions* 130, 265-278.

Barthelmie, R.J., Pryor, S.C., 1999. A model mechanism to describe oxidation of monoterpenes leading to secondary organic aerosol: a-pinene and ß-pinene. *Journal of Geophysical Research* 104, 23,657-23,669.

Bian, F. and Bowman, F.M., 2002. Theoretical method for lumping multicomponent secondary organic aerosol mixtures. *Environmental Science and Technology* 36, 2491-2497.

Bian, F. and Bowman, F.M., 2005. A lumping model for composition- and temperature-dependent partitioning of secondary organic aerosols. *Atmospheric Environment,* 39, 1263-1274.

Binkowski, F.S., 1999. Aerosols in Models-3 CMAQ, in *Science Algorithms of the EPA Models-3 Community Multiscale Air Quality (CMAQ) Modeling System*, chap. 10, *EPA/600/R-99/030*, Off. Of Res. And Dev., U.S. Environ. Prot. Agency, Washington, D.C.

Binkowski, F.S., and Roselle, S.J., 2003. Models-3 community multiscale air quality (CMAQ) model aerosol component, 1, Model description. *Journal of Geophysical Research* 108 (D6), 4183, doi:10.1029/2001JD001409.

Binkowski, F.S., and Shankar, U., 1995. The regional particulate model, 1, Model description and preliminary results. *Journal of Geophysical Research* 100, 26,191-26,209.

Blando, J.D., Porcja, R.J., Li, T-H, Bowman, D., Lioy, P.J. and Turpin, B.J., 1998. Secondary formation and the Smoky Mountain organic aerosol: an examination of aerosol polarity and functional group composition during SEAVS. *Environmental Science and Technology*, 32, 604-613.

Bowman, F.M, and Karamalegos, A.M., 2002. Estimated effects of composition on secondary organic aerosol mass concentrations. *Environmental Science and Technology* 36, 2701-2707.

Bowman, F.M., Odum, J.R., Seinfield, J.H. and Pandis, S.N., 1997. Mathematical model for gas-particle partitioning of secondary organic aerosols. *Atmospheric Environment*, 31, 3921-3931.

Boylan, J.W., Odman, M.T., Wilkinson, J.G., Russell, 2006. Integrated assessment modeling of atmospheric pollutants in the Southern Appalachian Mountains: Part II. Fine particulate matter and visibility. *Journal of the Air & Waste Management Association* 56, 12-22.

Boylan, J.W., Russell, A.G., 2006. PM and light extinction model performance metrics, goals, and criteria for three-dimensional air quality models. Atmospheric Environment, in press.

Byun, D.W., Ching, J.K.S., 1999. Science algorithms of the EPA Models-3 community multiscale air quality (CMAQ) modeling system. EPA/600/R-99/030. U.S. Environmental Protection Agency: Research Triangle Park, NC. (Available at http://www.epa.gov/asmdnerl/CMAQ/CMAQscienceDoc.html).

Cabada, J.C., Pandis, S.N., Robinson, A.L., 2002. Sources of atmospheric carbonaceous particulate matter in Pittsburgh, Pennsylvania. *Journal of the Air & Waste Management Association* 52, 732-741.

Cabada, J.C., Pandis, S.N., Subranmanian, R., Robinson, A.L, Polidori, A., Turpin, B., 2004. Estimating the secondary organic aerosol contribution to PM$_{2.5}$ using the EC tracer method. *Aerosol Science and Techonology* 38(S1), 140-155.

Carter, W.P.L., 1990. A detailed mechanism for the gas-phase atmospheric reactions of organic compounds. *Atmos. Envion.* 24A, 481-515.

Carter, W.P.L., 2000a. Documentation of the SAPRC-99 chemical mechanism for VOC reactivity assessment. Final report to California Air Resources Board, Contract 92-329 and 95-308. (Report available on internet by anonymous FTP site at ftp://ftp.cert.ucr.edu/pub/carter/pubs/s99txt.pdf).

Carter, W.P.L., 2000b. Implementation of the SAPRC-99 chemical mechanism into the models-3 frame work. Report to the United States Environmental Protection Agency. (Report is available on internet by anonymous FTP site at: ftp://ftp.cert.ucr.edu/pub/carter/pubs/s99mod3.pdf).

Castro, L.M., Pio, C.A., Harrison, R.M., Smith, D.J.T., 1999. Carbonaceous aerosol in urban and rural European atmospheres: estimation of secondary organic carbon concentrations. *Atmospheric Environment* 33, 2771-2781.

Chandramouli, B., Jang, M., Kamens, R.M., 2003. Gas-particle partitioning of semi-volatile organics on organic aerosols using a predictive activity coefficient model: analysis of the effects of parameter choices on model performance. *Atmospheric Environment* 37, 853-864.

Chen, J., Griffin, R.J., 2005. Modeling secondary organic aerosol formation from oxidation of *a*-pinene, *b*-pinene, and *d*-limonene. *Atmospheric Environment* 39, 7731-7744.

Choi, M.Y., and Chan, C.K., 2002. The effects of organic species on the hygroscopic behaviors of inorganic aerosols. *Environmental Science and Technology* 36, 2422-2428.

Chow, J.C., Watson, J.G., Crow, D., Lowenthal, D.H., Merrifield, T., 2001. Comparison of IMPROVE and NIOSH carbon measurements. *Aerosol Science and Technology* 34, 23-34.

Christoffersen, T.S., Hjorth, J., Horie, O., Jensen, N.R., Kotzias, D., Molander, L.L., Neeb, P., Ruppert, L., Winterhalter, R., Virkkula, A., Wirtz, K., Larsen, B.R., 1998. cis-Pinic acid, a possible precursor for organic aerosol formation from ozonolysis of α-pinene. *Atmospheric Environment* 32, 1657-1661.

Chung, S.H., Seinfeld, J.H. 2002. Global distribution and climate forcing of carbonaceous aerosols. *Journal of Geophysical Research* 107, 4407, doi:10.1029/2001JD001397.

Claeys, M., Graham, B., Vas, G.,Wang,W., Vermeylen, R., Pashynska, V., Cafmeyer, J., Guyon, P., Andreae, M. O., Artaxo, P., and Maenhaut, W., 2004a. Formation of secondary organic aerosols through photooxidation of isoprene, Science, 303, 1173–1176.

Claeys, M., Wang, W., Ion, A. C., Kourtchev, I., Gelencser, A., and Maenhaut, W., 2004b. Formation of secondary organic aerosols from isoprene and its gas-phase oxidation products through reaction with hydrogen peroxide, Atmos. Environ., 38, 4093–4098.

Cocker III, D.R., Clegg, S.L., Flagan, R.C., Seinfeld, J.H., 2001a. The effect of water on gas-particle partitioning of secondary organic aerosol. Part I: α-pinene/ozone system. *Atmospheric Environment* 35, 6049-6073.

Cocker III, D.R., Mader, B.T., Kalberer, M., Flagan, R.C., Seinfeld, J.H., 2001b. The effect of water on gas-particle partitioning of secondary organic aerosol: II. m-xylene and 1,3,5-trimethylbenzene photooxidatiion systems. *Atmospheric Environment* 35, 6073-6085.

Cruz C.N., Pandis, S.N., 2000. Deliquescence and hygroscopic growth of mixed inorganic-organic atmospheric aerosol. *Environmental Science and Technology* 34, 4313-4319.

Czoschke, N.M., Jang, M., Kamens, R.M., 2003. Effect of acidic seed on biogenic secondary organic aerosol growth. *Atmospheric Environment* 37, 4287-4299.

Demou, E., Visram, H., Donaldson, D.J., Makar, P.A., 2003. Uptake of water by organic films: the dependence on the film oxidation state. *Atmospheric Environment* 37, 3529-3537.

Derwent, R.G., Collins, W.J., Jenkin, M.E., Johnson, C.E., Stevenson, D.S. 2003. The global distribution of secondary organic particulate matter in a 3-D Lagrangian chemistry transport model. *Journal of Atmospheric Chemistry* 44, 57-95.

Dick, W.D., Saxena, P., and McMurry, P.H., 2000. Estimation of water uptake by organic compounds in submicron aerosol measured during the southeastern aerosol and visibility study. *Journal of Geophysical Research* 105 (D1), 1471-1479.

Docherty, K., Ziemann, P., 2003. Effects of stabilized criegee intermediate and OH radical scavengers on aerosol formation from reactions of β-pinene with O3. *Aerosol Science and Technology* 37, 877-891.

Dodge, M.C., 2000. Chemical oxidant mechanisms for air quality modeling: critical review. *Atmospheric Environment* 34, 2103-2130.

Donaldson, K., Li X.Y. and MacNee, W., 1998. Ultrafine (Nanometre) particle mediated lung injury. *Journal of Aerosol Science* 29, 553-560.

Eder, B., Yu, SC, 2006. A performance evaluation of the 2004 release of Models-3 CMAQ. *Atmospheric environment*, *in press.*

Edney, E.O., Driscloo, D.J., Speer, R.E., Weather, W.S., Kleindienst, T.E., Li, W., Smith, D.F., 2000. Impact of aerosol liquid water on secondary organic aerosol yields of irradiated toluend/propylene/NO_x/$(NH_4)_2SO_4$/air mixtures. *Atmospheric environment* 34, 3907-3919.

Edney, E.O., Kleindienst, T.E., Conver, T.S., McIver, C.D., Corse, E.W., Weathers, W.S., 2003. Polar organic oxygenates in $PM_{2.5}$ at a southeastern site in the United States. *Atmospheric Environment* 37, 3947-3965.

Edney, E.O., Kleindienst, T.E., Jaoui, M., Lewandowski, M., Offenberg, J.H., Wang, W., Claeys M., 2005. Formation of 2-methyl tetrols and 2-methylglyceric acid in secondary organic aerosol from laboratory irradiated isoprene/NO_x/SO_2/air mixtures and their detection in ambient PM2.5 samples collected in the eastern United States. *Atmospheric Environment* 39, 5281-5289.

Environ, 2003. Development of an advanced photochemical model for particulate matter: PMCAMx. Final Report CRC project A-30, Environ.

EPA, 2001. Draft guidance for demonstrating attainment of air quality goals for PM2.5 and regional haze. U.S. Evironmental Protection Agency, Office of Air Quality Planning and Standards. Research Triangle Park, NC, 2001.

EPA, 2003. Release notes on CMAQv4.3. (Available at http://www.cmascenter.org/help/model_docs/cmaq/4.3/RELEASE_NOTES.txt)

EPA, 2006. Release notes on CMAQ. (Available at http://www.epa.gov/asmdnerl/CMAQ/CMAQscienceDoc.html).

Fehsenfeld, F., Calver, J., Fall, R., Goldan, P., Guenther, A.B., Hewitt, C.N., Lamb, B., Liu, S., Trainer, M., Westberg, H., and Zimmerman, P., 1992: Emissions of volatile organic compounds from vegetation and the implications for atmospheric chemistry. *Global Biogeochem. Cycles* 6, 389-430.

Fisseha, R., Dommen, J., Sax, M., Paulsen, D., Kalberer, M., Maurer, R., Hofler, F., Weingartner, E., Baltensperger, U., 2004. Identification of organic acids in secondary organic aerosol and the corresponding gas phase from chamber experiments. Analytical Chemistry 76, 6535-6540.

Forstner, H.J.L., Flagan, R.C., Seinfeld, J.H., 1997a. Secondary organic aerosol from the photooxidation of aromatic hydrocarbons: molecular composition. *Environmental Science and Technology* 31, 1346-1358.

Forstner, H.J.L., Flagan, R.C., Seinfeld, J.H., 1997b. Molecular speciation of secondary organic aerosols from photooxidation of the higher alkenes: 1-Octene and 1-Decene. *Atmospheric Environment* 31(13), 1953-1964.

Fraser, M.P., Yue, Z.W., Buzcu, B., 2003. Source apportionment of fine particulate matter in Hourston, TX, using organic molecular markers. *Atmospheric Environment* 37, 2117-2123.

Fredenslund, A., Gmehling, J. and Rasmussen, P., 1977. Vapor-liquid equilibrium using UNIFAC: a group-contribution method, Elsevier Scientific Publishing Company, Amsterdam.

Gao, S., Ng, N.L., Keywood, M., Varutbangkul, V., Bahreini, R., Nenes, A., Je, J., Yoo, K.Y., Beauchamp, J.L., Hodyss, R.P., Flagan, R.C., and Seinfeld, J.H, 2004a. Particle phase acidity and oligomer formation in secondary organic aerosol. *Environmental Science and Technology* 38, 6582-6589.

Gao, S., Keywood, M., Ng, N.L., Surratt, J., Varutbangkul, V., Bahreini, R., Flagan, R.C., Seinfeld, J.H., 2004b. Low-molecular-weight and oligomeric components in secondary organic aerosol from the ozonolysis of cycloalkenes and α-pinene. *The Journal of Physical Chemistry A* 108(46), 10147-10164.

Gery M.W., Whitten G.Z., Killus J.P. and Dodge M.C., 1989. A photochemical kinetics mechanism for urban and regional scale computer modeling. *J. geophys. Res.* 94, 12,925-12,9556.

Gipson, G.L. and Young, J.O., 1999. Gas-phase chemistry, in *Science Algorithms of the EPA Models-3 Community Multiscale Air Quality (CMAQ) Modeling System*, chap. 8, EPA/600/R-99/030, U.S. Environ. Prot. Agency, Washington, D.C.

Glasius, M., Duane, M., Larsen, B.R., 1999. Determination of polar terpene oxidation products in aerosols by liquid chromatography-ion trap mass spectrometry. *Journal of Chromatography* A 833, 121-135.

Glasius, M., Lahaniati, M., Calogirou, A., Bella, D.D., Jensen, N.R., Hjorth, J., Kotzias, D., and Larsen, B.R., 2000. Carboxylic acids in secondary aerosols from oxidation of cyclic monoterpenes by ozone. *Environ. Sci. Technol.* 34, 1001-1010.

Gong, H., Matsunaga, A., Ziemann, P.J., 2005. Products and mechanism of secondary organic aerosol formation from reactions of linear alkenes with NO3 radicals. *Journal of Pysical Chemistry* 109, 4312-4324.

Griffin, R.J., Cocker III, D.R., Flagan, R.C., Seinfeld, J.H., 1999. Organic aerosol formation from the oxidation of biogenic hydrocarbons. *Journal of Geophysical Research* 104, 3555-3567.

Griffin, R.J., Cocker III, D.R., Seinfeld J.H., 1999a. Estimate of global atmospheric organic aerosol formation from oxidation of biogenic hydrocarbons. *Geophysical Research Letter*, 26, 2721-2724.

Griffin, R.J., Dabdub, D., Kleeman, M.J., Fraser, M.P., Cass, G.R., Seinfeld, J.H., 2002a. Secondary organic aerosol 3. Urban/regional scale model of size-and composition-resolved aerosol. *Journal of Geophysical Research* 107 (D17), 4334, doi:10.1029/2001JD000544.

Griffin, R.J., Dabdub, D., Seinfeld, J.H., 2002b. Secondary organic aerosol-1. Atmospheric chemical mechanism for production of molecular constituents. *Journal of Geophysical Research* 107 (D17), 4332, doi:10.1029/2001JD000541.

Griffin, R.J., Nguyen, K., Dabdub, D., and Seinfeld, J.H., 2003. A coupled hydrophobic-hydrophilic model for predicting secondary organic aerosol formation. *Journal of atmospheric chemistry* 44, 171-190.

Gross, A., and Stockwell, W.R., 2003. Comparison of the EMEP, RADM2 and RACM mechanisms. *Journal of Atmospheric Chemistry* 44, 151-170.

Guenther, A., Geron, C., Pierce, T., Lamb, B., Harley, P., Fall, R., 2000. Natural emission of non-methane volatile organic compounds, carbon monoxide, and oxides of nitrogen from North America. *Atmospheric Environment* 34, 2205-2230.

Guenther, A., Hewitt, C.N., Erickson, D., Fall, R., Geron, C., Graedel, T., Harley, P., Klinger, L., Lerdau, M., McKay, W.A., Pierce, T., Scholes, B., Steinbrecher, R., Tallamraju, R., Taylor, J., and Zimmerman, P., 1995. A global model of natural volatile organic compound emission. *Journal of Geophysical Research* 100, 8873-8892.

Hamilton, J.F., Webb, P.J., Lewis, A.C., Reviejo, M.M., 2005. Quantifying small molecules in secondary organic aerosol formed during the photo-oxidation of toluene with hydroxyl radicals. *Atmospheric Environment* 35, 7263-7275.

Harner, T., Bidleman, T.F., 1998. Octanol-air partition coefficient for describing particle/gas partitioning of aromatic compounds in urban air. *Environmental Science and Technology*, 32, 1494-4502.

Hinds, W.C., 1999. Aerosol technology, Wiley-Interscience, New York.

Hoffmann, T., Bandur, R., Marggraf, U., and Linscheid, M., 1998. Molecular composition of organic aerosols formed in the α-pinene/O3 reaction: Implication

for new particle formation processes. *Journal of Geophysical Research* 103, 25569-25578.

Hoffmann, T.P.W., Odum, J.R., Bowman, F., Collins, D.R., Klockow, D., Flagan, R.C., Seinfeld, J.H., 1997. Formation of organic aerosols from the oxidation of biogenic hydrocarbons. *Journal of Atmospheric Chemistry* 26, 189-222.

Hough, A.M. and Johson, C.E., 1991. Modeling the role of nitrogen oxides, hydrocarbons and carbon monoxide in the global formation of tropospheric oxidants. *Atmospheric Environment* 25A, 1819-1835.

Hurley, M.D., Sokolov, O., Wallington, T.J., Takekawa, H., Karasawa, M., Klotz, B., Barnes, I., Becker, K.H., 2001. Organic aerosol formation during the atmospheric degradation of toulene. *Environmental Science and Technology* 35, 1358-1366.

Iinuma, Y., Böge, O., Gnauk, T., Herrmann, H., 2004. Aerosol-chamber study of the α-pinene/O_3 reaction: influence of particle acidity on aerosol yields and products. *Atmospheric Environment* 38(5), 761-773.

Iinuma, Y., Böge, O., Miao, Y.-K., Sierau, B., Gnauk, T., and Herrmann, H., 2005. Laboratory studies on secondary organic aerosol formation from terpenes. *Faraday Discussions* 130, 279-294.

Izumi, K., Fukuyama, T., 1990. Photochemical aerosol formation from aromatic hydrocarbons in the presence of NO_x. *Atmospheric Environment* 24A, 1433-1441.

Jang M., Kamens, R.M., Leach, K.B., Strommen, M.R., 1997. A thermodynamic approach using group contribution methods to model the partitioning of semivolatile organic compounds on atmospheric particulate matter. *Environmental Science and Technology* 31, 2805-2811.

Jang, M., Kamens, R.M., 1998. A thermodynamic approach for modeling partitioning of semi-volatile organic compounds on atmospheric particulate matter: humidity effects. *Environmental Science and Technology* 32, 1237-1243.

Jang, M., Kamens, R.M., 1999. Newly characterized products and composition of secondary aerosols from the reaction of α-pinene with ozone. *Atmospheric Environment* 33, 459-474.

Jang, M., Kamens, R.M., 2001a. Characterization of secondary aerosol from the photooxidation of toluene in the presence of NO_x and 1-propene. *Environmental Science and Technology*, 35, 3626-3639.

Jang, M. and Kamens, R.M., 2001b. Atmospheric secondary organic aerosol formation by heterogeneous reactions of aldehydes in the presence of a sulfuric acid aerosol catalyst. *Environmental Science and Technology* 35, 4758-4766.

Jang, M., Czoschke, N.M., Lee, S., Kamens, R.M., 2002. Heterogeneous atmospheric aerosol formation by acid-catalyzed paticle phase reactions. *Science* 298, 814-817.

Jang, M., Czoschke, N. M., Northcross, A. L., 2005. Semiempirical model for organic aerosol growth by acid-catalyzed heterogeneous reactions of organic carbonyls. *Environmental Science and Technology* 39, 164-174.

Jang, M., Lee, S., Kamens, R.M., 2003a. Organic aerosol growth by acid-catalyzed heterogeneous reactions of octanal in a flow reactor. *Atmospheric Environment* 37, 2125-2138.

Jang, M.S., Carroll, B., Chandramouli, B., Kamens, R.M., 2003b. Particle growth by acid-catalyzed heterogeneous reactions of organic carbonyls on preexisting aerosols. Environmental Science and Technology 37, 3828–3837.

Janson, R., Rosman, L., Karlsson, A., and Hansson, H.-C., 2001. Biogenic emissions and gaseous precursors to forest aerosols. *Tellus* 53B, 423-440.

Jaoui, M. and Kamens, R.M., 2001. Mass balance of gaseous and particulate product analysis from α-pinene/NO$_x$/air in the presence of natural sunlight. *Journal of Geophysical Research* 106 (D12), 12,541-12,558.

Jaoui, M. and Kamens R.M., 2003a. Gaseous and particulate oxidation products analysis of a mixture of a-pinene + ß-pinene/O3/air in the absence of light and a-pinene + ß-pinene/NOx/air in the presence of natural sunlight. *Journal of Atmospheric Chemistry*, 44, 259-297.

Jaoui, M. and Kamens, R.M., 2003b. Mass balance of gaseous and particulate products from β-pinene/O$_3$/air in the absence of light and β-pinene/NO$_x$/air in the presence of natural light. *Journal of Atmospheric Chemistry* 43, 101-141.

Jaoui, M. and Kamens, R.M., 2003c. Gas and particulate distribution from the photooxidation of α-humulene in the presence of NO$_x$, natural atmospheric air and sunlight. *Journal of Atmospheric Chemistry* 46, 29-54.

Jaoui, M., Leungsakul, S., and Kamens, R.M., 2003. Gas and particle products distribution from the reaction of β-caryophyllene with ozone. *Journal of Atmospheric Chemistry* 45, 261-287.

Jaoui, M., Sexton, K.G., Kamens, R.M., 2004. Reaction of α-cedrene with ozone: mechanism, gas and particulate products distribution. *Atmospheric Environment* 38, 2709-2725.

Jaoui, M., Kleindienst, T.E., Lewandowski, M., Offenberg, J.H., Edney, E.O., 2005. Identification and quantification of aerosol polar oxygenated compounds bearing

carboxylic or hydroxyl groups. 2. Organic tracer compounds from monoterpenes. *Environmental Science and Technology* 39, 5661-5673.

Jenkin, M.E., Shallcross, D.E., Harvery, J.N., 2000. Development and application of a possible mechanism for the generation of *cis*-pinic acid from the ozonolysis of *a*- and *ß*-pinene. *Atmospheric Environment* 34, 2837-2850.

Jenkin, M.E., 2004. Modelling the formation and composition of secondary organic aerosol from a- and ß-pinene ozonolysis using MCM v3. *Atmospheric Chemistry and Physics* 4, 1741-1757.

Jiang, W., Smyth, S., Giroux, É., Roth, H., Yin, D., 2006. Differences between CMAQ fine mode particle and PM2.5 concentrations and their impact on model performance evaluation in the lower Fraser valley. *Atmospheric Environment, in press.*

Johnson, D., Jenkin, M.E., Wirtz, K., Martin-Reviejo, M., 2004. Simulating the formation of secondary organic aerosol from the photooxidation of toluene. *Evironmental Chemistry* 1, 150-165.

Johnson, D., Jenkin, M.E., Wirtz, K., Martin-Reviejo, M., 2005. Simulating the formation of secondary organic aerosol from the photooxidation of aromatic hydrocarbon. *Evironmental Chemistry* 2, 35-48.

Kalberer, M., Yu, J., Cocker, D.R., Flagan, R.C., and Seinfeld, J.H., 2000. Aerosol formation in the cyclohexene-ozone system. *Environmental Science and Technology* 34, 4894-4901.

Kamens, R., Jang, M., Chien, C.-J., and Leach, K., 1999. Aerosol formation from the reaction of a-pinene and ozone using a gas-phase kinetics-aerosol partitioning model. *Environmental Science and Technology* 33, 1430-1438.

Kamens, R.M, Jaoui, M., 2001. Modeling aerosol formation from a-pinene +NOx in the presence of natural sunlight using gas-phase kinetics and gas-particle partitioning theory. *Environmental Science and Technology* 35, 1394-1405.

Kanakidou, M., Tsigaridis, K., Dentener, F.J., and Crutzen, P.J. 2000. Human-activity-enhanced formation of organic aerosols by biogenic hydrocarbon oxidation. *Journal of Geophysical Research* 105, 9243-9254.

Kaupp, H. and McLachlan, M.S., 1999. Gas/particle partitioning of PCDD/Fs, PCBs, PCNs and PAHs. *Chemosphere*, 38(14), 3411-3421.

Kavouras, I.G., and Stephanou, E.G., 2002. Direct evidence of atmospheric secondary organic aerosol formation in forest atmosphere through heteromolecular nucleation. *Environ. Sci. Technol.* 36, 5083-5091.

Kavouras, I.G., Mihalopoulos, N., and Stephanou, E.G., 1998. Formation of atmospheric particles from organic acids produced by forests. *Nature* 395, 683-686.

Kavouras, I.G., Mihalopoulos, N., Stephanou, E.G., 1999. Formation of gas/particle partitioning of monoterpenes photo-oxidation products over forests. *Geophysical Research Letter* 26 (1), 55-58.

Kavouras, I.G., Mihalopoulos, N., and Stephanou, E.G., 1999a. Secondary organic aerosol formation vs primary organic aerosol emission: In situ evidence for the chemical coupling between monoterpene acidic photooxidation products and new particle formation over forests. *Environmental Science and Technology* 33, 1028-1037.

Keywood, M.D., Kroll, J.H., Varutbangkul, V., Bahreini, R., Flagan, R.C., and Seinfeld, J.H., 2004. Secondary organic aerosol formation from cyclohexene ozonolysis: Effect of OH scavenger and the role of radical chemistry. *Environmental Science and Technology* 38, 3343-3350.

Kleindienst, T.E., Smith, D.F., Li, W., Edney, E.O., Driscoll, D.J., Speer, R.E., Weathers, W.S., 1999. Secondary organic aerosol formation from the oxidation of aromatic hydrocarbons in the presence of dry submicron ammonium sulfate aerosol. *Atmospheric Environment* 33, 3669-3681.

Kleindients, T.E., Corse, E.W., Li, W., McIver, C.D., Conver, T.S., Edney, E.O., Driscoll, D.J., Speer, R.E., Weathers, W.S., and Tejada, S.B., 2000. Secondary organic aerosol formation from the irradiation of simulated automobile exhaust. Journal of the Air & Waste Management Association 52, 259-272.

Kleindienst, T.E., Conver, T.S., McIver, C.D., and Edney, E.O., 2004. Determination of secondary organic aerosol products from the photooxidation of toluene and their implications in ambient $PM_{2.5}$. *Journal of Atmospheric Chemistry* 47, 79-100.

König, G., M. Brunda, H. Puxbaum, C.N. Hewitt, S.C. Duckham and J. Rudolph, 1995. Relative contribution of oxygenated hydrocarbons to the total biogenic VOC emissions of selected mid-European agricultural and natural plant species. *Atmospheric Environment*, 29, 861-874.

Koch, S., Winterhalter, R., Uherek, E., Kolloff, A., Neeb, P, Moortgat, G.K., 2000. Formation of new particles in the gas-phase ozonolysis of monoterpenes. *Atmospheric Environment* 34, 4031-4042.

Kourtchev, I., Ruuskanen, T., Waenhaut, W., Kulmala, M., Claeys, M., 2005. Observation of 2-methyltetrols and related photo-oxidation products of isoprene in boreal forest aerosol from Hyytiälä, Finland. *Atmospheric Chemistry and Physics* 5, 2761-2770.

Larsen, B.R., Bella, D.D., Glasius, M., Winterhalter, R., Jensen, N.R., and Hjorth, J., 2001. Gas-phase OH oxidation of monoterpenes: gaseous and particulate products. *Journal of Atmospheric Chemistry*, 38, 231-276.

Leach, K.B., Kamens, R.M., Strommen, M.R. and Jang, M., 1999. Partitioning of semivolatile organic compounds in the presence of a secondary organic aerosol in a controlled atmosphere. *Journal of Atomspheric Chemistry*, 33, 241-264.

Leaitch, W.R., Bottenheim, J.W., Biesenthal, T.A., Li, S.-M., Liu, P.S.K., Asalian, K., Clark, H.D., Hopper, F., 1999. A case study of gas-particle conversion in an eastern Canadian forest. *Journal of Geophysical Research* 104 (D7), 8095-8111.

Leungsakul, S., Jeffries, H.E., Kamens, R.M., 2005a. A kinetic mechanism for predicting secondary organic aerosol formation from the reactions of *d*-limonene in the presence of oxides of nitrogen and natural sunlight. *Atmospheric Environment* 39, 7063-7082.

Leungsakul, S., Jaoui, M., Kamens, R.M., 2005b. Kinetic mechanism for predicting sencondary organic aerosol formation from the reaction of *d*-limonene with ozone. *Environmental Science and Technology*, 39, 9583-9594.

Lewis, C.W., Klouda, G.A., Ellenson, W.D., 2004. Radiocarbon measurement of the biogenic contribution to summertime PM-2.5 ambient aerosols in Nashville, TN. *Atmospheric Environment* 38, 6053–6061.

Liang, C., Pankow, J.F., Odum, J.R., Seinfeld, J.H., 1997. Gas/particle partitioning of semivolatile organic compounds to model inorganic, organic, and ambient smog aerosols. *Environmental Science and Technology*, 31, 3086-3092.

Lim, H.-J., and Turpin, B.J., 2002. Origins of primary and secondary organic aerosols in Atlanta: results of time-resolved measurements during the Atlanta supersite experiment. *Environmental Science and Technology* 36, 4489-4496.

Lim, Y.-B., and Ziemann, P.J. 2005. Products and mechanism of secondary organic aerosol formation from reactions of *n*-alkanes with OH radicals in the presence of NO_x. *Environmental Science and Technology* 39, 9229-9236.

Limbeck, A., Kulmala, M., and Puxbaum, H., 2003. Secondary organic aerosol formation in the atmosphere via heterogeneous reaction of gaseous isoprene on acidic particles, Geophysical Research Letter 30(19), Art. No. 1996, doi:10.1029/2003GL017738.

Mader, B.T., and Pankow, J.F., 2003. Study of the effects of particle-phase carbon on the gas/particle partitioning of semivolatile organic compoounds in the astmosphere

using controlled field experiments. *Environmental Science and Technology* 36, 5218-5228.

Martin-reviejo, M. and Wirtz, K., 2005. Is benzene a precursor for secondary organic aerosol? *Environmental Science and Technology* 39, 1045-1054.

Matsunaga, S., Mochida, M., and Kawamura, K., 2003. Growth of organic aerosols by biogenic semi-volatile carbonyls in the forestall atmosphere. *Atmospheric Environment* 37, 2045–2050.

Ming, Y., and Russell, L.M., 2002. Thermodynamic equilibrium of organic-electrolyte mixtures in aerosol particles. *AIChE Journal* 48(6), 1331-1348.

Morris, R.E., McNally, D.E., Tesche, T.W., Tonnesen, G., Boylan, J.W., Brewer, P., 2005. Preliminary evaluation of the community multiscale air quality model for 2002 over the southeastern United States. *Journal of the Air & Waste Management Association* 55, 1694-1708.

Nenes, A., Pandis, S.N., Pilinis, C., 1998. ISORROPIA : A new thermodynamic equilibrium model for multiphase multicomponent inorganic aerosols. *Aquatic Geochemistry* 4(1), 123-152.

Nenes, A., Pandis, S.N., Pilinis, C., 1999. Continued development and testing of a new thermodynamic aerosol module for urban and regional air quality models. *Atmospheric Environment* 33, 1553-1560.

Odum, J.R., Hoffmann, T., Bowman, F., Collins, D., Flagan, R.C., Seinfeld, J.H., (1996). Gas/particle partitioning and secondary organic aerosol yields. *Environmental Science and Technology* 30, 2580-2585.

Odum, J.R., Jungkamp, T.P.W., Griffin, R.J., Flagan, R.C., Seinfeld, J.H., 1997a. The atmospheric aerosol-forming potential of whole gasoline vapor. *Science* 276, 96-99.

Odum, J.R., Jungkamp, T.P.W., Griffin, R.J., Forstner, H.J.L., Flagan, R.C., Seinfeld, J.H. 1997b. Aromatics, reformulated gasoline, and atmospheric organic aerosol formation. *Environmental Science and Technology* 31, 1890-1897.

Pandis S.N., Harley, R.A., Cass, G.R., Seinfeld, J.H., 1992. Secondary organic aerosol formation and transport. *Atmospheric Environment*, 26A, 2269-2282.

Pandis, S. N., Paulson, S. E., Seinfeld, J. H., and Flagan, R. C., 1991. Aerosol formation in the photooxidation of isoprene and β-pinene. *Atmospheric Environment*, 25, 997-1008.

Pankow J.F. (1994a) An absorption model of gas-particle partitioning of organic compounds in the atmosphere. *Atmospheric Environment* 28, 185-188.

Pankow, J. F., (1994b). An absorption model of the gas/aerosol partitioning involved in the formation of the secondary organic aerosol. *Atmospheric Environment* 28, 189-193.

Pankow, J.F., 2003. Gas/particle partitioning of neutrual and ionizing compounds to single and multi-phase aerosol particles. 1. Unified modeling framework. *Atmospheric Environment* 37, 3323-3333.

Pankow, J.F., Seinfeld, J.H., Asher, W.E., and Erdakos, G.B., 2001. Modeling the formation of secondary organic aerosol. 1. Application of theoretical principles to measurements obtained in the a-pinene/, ß-pinene/, sabinene/, Δ^3-carene/, and cyclohexene/ozone systems. *Environmental Science and Technology* 35, 1164-1172.

Peng, C.-G., Chan, C.K., 2001. The water cycles of water-soluble organic salts of atmospheric importance. *Atmospheric Environment* 35, 1183-1192.

Peng, C.-G., Chan, M.N., and Chan, C.K., 2001b. The hygroscopic properties of dicarboxylic and multifunctional acids: measurements and UNIFAC predictions. *Environmental Science and Technology* 35, 4495-4501.

Peng, C.-G., Chan, M.N., Chan, C.K., 2001. The hygroscopic properties of dicarboxylic and multifunctional acids: measurements and UNIFAC predictions. *Environmental Science and Technology* 35, 4495-4501.

Peng, C.-G., Chow, A.H.L., and Chan, C.K., 2001a. Hygroscopic study of glucose, citric acid and sorbitol using an electrodynamic balance: comparison with UNIFAC predictions. *Aerosol science and technology* 35, 750-758.

Penner, J.E., Chuang, C.C., Grant, K., 1998. Climate forcing by carbonaceous and sulfate aerosols. *Climate Dynamics* 14, 839-851.

Photochemical Oxidants Review Group, 1997. Fourth Report on Ozone in the United Kingdom (D. Fowler) (CEH: Edinburgh). (Available at http://www.edinburgh.ceh.ac.uk/pollution/docs/PORGiv.htm).

Pio, C., Alves, C., Duarte, A., 2001. The organic components of aerosols in a forested area of central Greece. *Atmospheric Environment* 35(2), 389-401.

Pope, C.A., III, Thun, M.J., Namboodiri, M.M., Dockery, D.W., Evans, J.S., Speizer, F.E., and Heath Jr., C.W., 1995. Particulate air pollution as a predictor of mortality in a prospective study of U.S. adults. *American Journal of Respiratory and Critical Care Medicine* 151, 669-674.

Presto, A.A., Hartz, K.E.H., Donahue, N.M., 2005a. Secondary organic aerosol production from terpene ozonolysis. 1. Effect of UV radiation. *Environmental Science and Technology* 39, 7036-7045.

Presto, A.A., Hartz, K.E.H., Donahue, N.M., 2005b. Secondary organic aerosol production from terpene ozonolysis. 2. Effect of NO_x concentration. *Environmental Science and Technology* 39, 7046-7054.

Pun, B.K., Griffin, R.J., Seigneur, C., and Seinfeld, J.H., 2002. Secondary organic aerosol 2. Thermodynamic model for gas/particle partitioning of molecular constituents. *Journal of Geophysical Research* 107(D17), 4333, doi:10.1029/2001JD000542.

Pun, B.K., Wu, S.-Y., Seigneur, C., Seinfeld, J.H., Griffin, R.J., Pandis, S.N., 2003. Uncertainties in modeling secondary organic aerosols: three-dimensional modeling studies in Nashville/Western Tennessee. *Environmental Science and Technology* 37, 3647-3661.

Puxbaum, H., and G. König, 1997. Observation of dipropenyldisulfide and other organic sulfur compounds in the atmosphere of a beech forest with allium ursinum ground cover. *Atmospheric Environment*, 31, 291-294.

Russell, A., Dennis, R., 2000. NARSTO critical review of photochemical models and modeling. *Atmospheric Environment* 34, 2283-2324.

Ray, J., McDow, S.R., 2005. Dicarboxylic acid concentration trends and sampling artifacts. *Atmospheric Environment* 39, 7906-7919.

Sax, M., Zenobi, R., Baltensperger, U., Kalberer, M., 2005. Time resolved infrared spectroscopic analysis of aerosol formed by photo-oxidation of 1,3,5-trimethylbenzene and α-pinene. *Aerosol Science and Technology* 39, 822-830.

Saxena, P., Hildemann, L.M., 1996. Water-soluble organics in atmospheric particles: A critical review of the literature and application of thermodynamics to identify candidate compounds. *Journal of Atmospheric Chemistry*, 24, 57-109.

Saxena, P., Hildemann, L.M., 1997. Water absorption by organics: A survey of laboratory evidence and evaluation of UNIFAC for estimating water activity. *Environmental Science and Technology*, 31, 3318-3324.

Saxena, P., Hildemann, L.M., McMurry, P.H., Seinfeld, J.H., 1995. Organics alter hygroscopic behavior of atmospheric particles. *Journal of Geophysical Research* 100(D9), 18,755-18,770.

Schell, B., Ackermann, I.J., Hass, H., Binkowski, F.S., Ebel, A., 2001. Modeling the formation of secondary organic aerosol within a comprehensive air quality model system. *Journal of geophysical research* 106(D22), 28,275-28,293.

Seigneur, C., 2001. Current status of air quality models for particulate matter. *Journal of the Air & Waste Management Association* 51, 1508-1521.

Seigneur, C., Pun, B., Pai, P., et al., 2000. Guidance for the performance evaluation of three-dimensional air quality modeling systems for particulate matter and visibility. *Journal of the Air & Waste Management Association* 50, 588-599.

Seinfeld, J.H. and Pandis, S.N., 1998. Atmospheric Chemistry and Physics: From Air Pollution to Climate Change. New York John Wiley & Sons, Inc., USA.

Seinfeld, J.H., and Pankow, J.F., 2003. Organic atmospheric particulate material. *Annual Review of Physical Chemistry* 54, 121-140.

Seinfeld, J.H, Erdakos, G.B., Asher, W.E., and Pankow, J.F., 2001. Modeling the formation of secondary organic aerosol. 2. The predicted effects of relative humidity on aerosol formation in the a-pinene-, ß-pinene-, sabinene, Δ^3-carene-, and cyclohexene-ozone systems. *Environmental Science and Technology* 35, 1806-1817.

Sheehan, P.E. and Bowman, F.M., 2001. Estimated effects of temperature on secondary organic aerosol concentrations. *Environmental Science and Technology*, 35, 2129-2135.

Smith, D.F., McIver, C.D., Kleindienst, T.E., 1998. Primary product distribution from the reaction of hydroxyl radicals with toluene at ppb NO_x mixing ratios. *Journal of Atmospheric Chemistry* 30, 209-228.

Smith, D.F., Kleindienst, T.E., McIver, C.D., 1999. Primary product distributions from the reaction of OH with *m*-, *p*-xylene, 1,2,4- and 1,3,5-trimethylbenzene. *Journal of Atmospheric Chemistry* 34, 339-364.

Solomon, P.A., Chameides, W., Weber, R., Middlebrook, A., Kiang, C.S., Russell, A.G., Butler, A., Turpin, B., Mikel, D., Scheffe, R., Cowling, E., Edgerton, E., John, J.S., Jansen, J., McMurry, P., Hering, S., and Bahadori, T., 2003. Overview of the 1999 Atlanta supersite project. *Journal of Geophysical Research* 108 (D7), 8413, doi:10.1029/2001JD001458.

Spanke, J., Rannik, Ü., Forkel, R., Nigge., W., and Hoffmann, T., 2001. Emission fluxes and atmospheric degradation of monoterpenes above a boreal forest: field measurements and modelling. *Tellus* 53B, 406-422.

Speer, R.E., Edney, E.O., Kleindienst, T.E., 2003. Impact of organic compounds on the concentration of liquid water in ambient PM2.5. *Journal of Aerosol Science* 34, 63-77.

Stein, S.E., Brown, R.L., 1994. Estimation of normal boiling points from group contributions. *Journal of Chemical Information and Computer Sciences* 34, 581-587.

Stockwell W.R., Middleton P. and Chang J.S., 1990. The second generation regional acid deposition model chemical mechanism for regional air quality modeling. *J. geophys. Res.* 95, 16,343-16,367.

Strader, R., Lurmann, F., and Pandis, S.N., 1999. Evaluation of secondary organic aerosol formation in winter. *Atmospheric Environment* 33, 4849-4863.

Stroud, C.A., Makar, P.A., Michelangeli, D.V., Mozurkewich, M., Hastie, D.R., Barbu, A., Humble, J., 2004. Simulating organic aerosol formation during the photooxidation of toluene/NOx mixtures: comparing the equilibrium and kinetic assumption. *Environmental Science and Technology* 38, 1471-1479.

Takekawa, H., Minoura, H., Yamazaki, S., 2003. Temperature dependece of secondary organic aerosol formation by photo-oxidation of hydrocarbons. *Atmospheric Environment* 37, 3413-3424.

Tanner, R.L., Parkhurst, W.J., McNichol, A.P., 2004. Fossil sources of ambient aerosol carbon based on ^{14}C measurements. *Aerosol Science and Technology* 38(S1), 133-139.

Tesche, T.W., Morris, R., Tennesen, G., McNally, D., Boylan, J., Brewer, P., 2006. CMAQ/CAMx anuual 2002 performance evaluation over the eastern US. *Atmospheric Environment*, in press.

Tobias, H.J., and Ziemann, P.J., 2000. Thermal desorption mass spectrometric analysis of organic aerosol formed from reactions of 1-tetradecene and O_3 in the presence of alcohols and carboxylic acids. *Environmental Science and Technology* 34, 2105-2115.

Tobias, H.J., Docherty, K.S., Beving, D.E., and Ziemann, P.J., 2000. Effect of relative humidity on the chemical composition of secondary organic aerosol formed from reactions of 1-tetradecene and O_3. *Environmental Science and Technology* 34, 2116-2125.

Tsigaridis K. and Kanakidou M., 2003. Global modeling of secondary organic aerosol in the troposphere: a sensitivity analysis. *Atmospheric Chemistry and Physics*, 3, 1849-1869.

Turpin, B.J, Huntzicker, J.J, Larson, S.M., and Cass, G.R., 1991. Los Angeles summer midday particulate carbon – primary and secondary aerosol. *Environmental Science and Technology* 25, 1788-1793.

Turpin, B.J., Huntzicker, J.J., 1995. Identification of secondary organic aerosol episodes and quantification of primary and secondary organic aerosol concentration during SCAQS. *Atmospheric Environment* 29, 3527-3544.

Turpin, B.J., Saxena, P., Andrews, E., 2000. Measuring and simulating particulate organics in the atmosphere: problems and prospects. *Atmospheric Environment* 34, 2983-3013.

Turpin, B.J., Lim, H.-J., 2001. Species contributions to PM2.5 mass concentrations: revisiting common assumptions for estimating organic mass. *Aerosol Science and Technology* 35, 602-610.

Virkkula, A., Dingenen, R.V., Raes, F., Hjorth, J., 1999. Hygroscopic properites of aeorosol formed by oxidation of limonene, α-pinene, and β-pinene. *Journal of Geophysical Research* 104(D3), 3569-3579.

Went, F.W., 1960. Blue Hazes in the Atmosphere. *Nature* 187, 641-643.

Winterhalter, R., Van Dingenen, R., Larsen, B. R., Jensen, N. R., and Hjorth, J., 2003. LC-MS analysis of aerosol particles from the oxidation of α-pinene by ozone and OH radicals. Atmospheric Chemistry and Physics Discussion 3, 1–39, **SRef-ID: 1680-7375/acpd/2003-3-1**.

Yamasaki, H., Kuwata, K., Miyamoto, H., 1982. Effects of ambient temperature on aspects of airborne polycyclic aromatic hydrocarbons. *Environmental Science and Technology*, 16, 189-194.

Youngblood, D.A. and Kreidenweis, S.M., 1994. Further development and testing of a bimodal aerosol dynamics model. Colorado State University, Department of Atmospheric Sciences Report No.550, 1994.

Yu, J., Jeffries H.E., and Sexton, K.G., 1997. Atmospheric photooxidation of alkylbenzenes-I. Carbonyl product analysis. Atmospheric environment, 31(15), 2261-2280.

Yu J., Flagan, R.C., and Seinfeld, J.H., 1998. Identification of products containing – COOH, -OH, and –C=O in atmospheric oxidation of hydrocarbons. Environ. Sci. Tech., 32, 2357-2370.

Yu, J, Cocker III, D.R., Griffin, R.J., Flagan R.C., Seinfeld, J.H., 1999. Gas-phase oxidation of monoterpenes: gaseous and particulate products. *Journal of Atmospheric Chemistry* 34, 207-258.

Yu, J, Griffin, R.J., Cocker III, D.R., Flagan, R.C., and Seinfeld, J.H., 1999a. Observation of gaseous and particulate products of monoterpenes in forest atmosphere. *Geophysical Research Letter* 26 (8), 1145-1148.

Yu, S., Dennis, R.L., Bhave, P.V., Eder, B.K., 2004. Primary and secondary organic aerosols over the United States: estimates on the basis of observed organic carbon (OC) and elemental carbon (EC), and air quality modeled primary OC/EC ratios. *Atmospheric Environment* 38, 5257-5268.

Yu, S., Eder, B.K., Dennis, R., Chu, S.-H., Schwartz, S., 2006. New unbiased symmetric metrics for evaluation of air quality models. Atmospheric Science Letter, accepted for publication.

Ziemann, P.J., 2003. Formation of alkoxyhydroperoxy aldehydes and cyclic peroxyhemiacetals from reactions of cyclic alkenes with O_3 in the presence of alcohols. *Journal of Physical Chemistry* 107, 2048-2060.

Zhang, Y., Pun B., Vijayaraghavan, K., Wu, S.-Y., Seigneur, C., Pandis, SN, Jacobson MZ, Nenes, A., Seinfeld JH, 2004. Development and application of the model of aerosol dynamics, reaction, ionization, and dissolution (MADRID). Journal of Geophysical Research 109: Art. No. D01202.

Zhang, Y., Liu, P., Pun, B., Seigneur, C., 2006a. A comprehensive performance evaluation of MM5-CMAQ for the summer 1999 Southern Oxidant Study episode-Part I: Evaluation protocols, databases, and meteorological predictions. *Atmospheric Environment, in press.*

Zhang, Y., Liu, P., Queen, A., Misenis, C., Pun, B., Seigneur, C., Wu, S.-Y., 2006b. A comprehensive performance evaluation of MM5-CMAQ for the summer 1999 Southern Oxidant Study episode-Part II: Gas and aerosol predictions. *Atmospheric Environment, in press.*

Zhang, Y., Liu, P., Pun, B., Seigneur, C., 2006c. A comprehensive performance evaluation of MM5-CMAQ for the summer 1999 Southern Oxidant Study episode-Part III: Diagnostic and mechanistic evaluations. *Atmospheric Environment, in press.*

Zhang, Y., Pun, B., Wu, S.-Y., Vijayaraghavan, K., Seigneur, C., 2004. Application and Evaluation of two air quality models for particulate matter for a Southeastern U.S. episode. *Journal of the Air and Waste Management Association* 54, 1478-1498.

Zhang, S. Shaw, H., M., Sienfeld, J. H., and Flagan, R. C., 1992. Photochemical aerosol formation from α-pinene and β-pinene. *Journal of Geophysical Research*, 97, 20,717-20,729.